PROPERTY IMPROVEMENT OF ANTIBACTERIAL WOUND DRESSING FROM BASIL SEED (*Ocimum basilicum* L.) MUCILAGE-ZnO NANOCOMPOSITES WITH DIFFERENT CROSSLINKING AGENTS

SIRIPORN TANTIWATCHAROTHAI

A THESIS SUBMITTED IN PARTIAL FULFILLMENT OF THE REQUIREMENT

THE DEGREE OF DOCTOR OF PHILOSOPHY IN APPLIED CHEMISTRY

DEPARTMENT OF CHEMISTRY

FACULTY OF SCIENCE

KING MONGKUT'S INSTITUTE OF TECHNOLOGY LADKRABANG

2019

KMITL-2019-SC-D-010-011

PROPERTY IMPROVEMENT OF ANTIBACTERIAL WOUND DRESSING FROM BASIL SEED (*Ocimum basilicum* L.) MUCILAGE-ZnO NANOCOMPOSITES WITH DIFFERENT CROSSLINKING AGENTS

SIRIPORN TANTIWATCHAROTHAI

A THESIS SUBMITTED IN PARTIAL FULFILLMENT OF THE REQUIREMENT
THE DEGREE OF DOCTOR OF PHILOSOPHY IN APPLIED CHEMISTRY
DEPARTMENT OF CHEMISTRY
FACULTY OF SCIENCE
KING MONGKUT'S INSTITUTE OF TECHNOLOGY LADKRABANG
2019

KMITL-.....

การปรับปรุงสมบัติของวัสดุปิดแผลต้านแบคทีเรียจากเมือกแมงลัก (*Ocimum basilicum L.*) ซิงค์ออกไซด์ นาโนคอมโพสิท ด้วยสารเชื่อมโยงต่างชนิด

PROPERTY IMPROVEMENT OF ANTIBACTERIAL WOUND DRESSING FROM BASIL SEED (*Ocimum basilicum* L.) MUCILAGE-ZnO NANOCOMPOSITES WITH DIFFERENT CROSSLINKING AGENTS

ศิริพร ตันติวัชโรทัย
SIRIPORN TANTIWATCHAROTHAI

วิทยานิพนธ์นี้เป็นส่วนหนึ่งของการศึกษาตามหลักสูตร
ปริญญาวิทยาศาสตร์ดุษฎีบัณฑิต สาขาวิชาเคมีประยุกต์
ภาควิชาเคมี คณะวิทยาศาสตร์
สถาบันเทคโนโลยีพระจอมเกล้าเจ้าคุณทหารลาดกระบัง
พ.ศ. 2562

KMITL-.....

Thesis Title	Property improvement of antibacterial wound dressing from basil seed (*Ocimum basilicum L.*) mucilage-ZnO nanocomposites with different crosslinking agents
Student Name	Siriporn Tantiwatcharothai
Student ID	58605010
Degree	Doctor of Philosophy Program in Chemistry
Department	Chemistry
Year	2019
Thesis Advisor	Assoc. Prof. Dr. Jutarat Prachayawarakorn

Abstract

Due to a large water holding capacity of basil seed (*Ocimum basilicum L.*) mucilage (BSM), it could potentially produce a valuable polymer for water holding applications such as wound dressing. However, its strong hydrophilic character leads to low dimensional stability and easy degradation. The objective of this research was to prepare hydrogel sponge for wound dressing application with BSM by freeze drying technique. Moreover, various properties of BSM hydrogel sponge were improved by crosslinking with different crosslinking agents, i.e., borax and the mixture of sodium trimetaphosphate (STMP)/sodium tripolyphosphate (STPP). Zinc oxide nanoparticles (ZnONP) were incorporated as an antibacterial agent. SEM images revealed an interconnecting open-cell structure of pores in the BSM hydrogel sponge with a good distribution of ZnONP. In spite of the decrease in degree of swelling of BSM hydrogel sponge with the addition of ZnONP, water retention capacity, mechanical and thermal properties of BSM hydrogel sponge were improved. In addition, the incorporation of ZnONP resulted in an improvement of antibacterial activity against both of *S. aureus* and *E.coli*. With the addition of crosslinking agents, thickness, porosity and degree of swelling of BSM hydrogel sponges were slightly decreased. However, overall properties were improved: dimensional stability, water retention capacity (31 to 41%), stress at maximum load (2.6 to 11.4 MPa), Young's modulus (74 to 173 MPa) and strain (28 to 58%). Moreover, decomposition temperature of BSM hydrogel sponges were shifted to higher temperature after crosslinking. When considering the influence of crosslinking agents, BSM hydrogel sponge crosslinked with borax showed preferable overall properties than BSM hydrogel sponge crosslinked with STMP/STPP. Furthermore,

cytotoxicity evaluation demonstrated that crosslinked BSM hydrogel sponges-ZnO nanocomposites were not toxic to human keratinocytes cells.

Keywords: Antibacterial activity; Basil seed mucilage; Crosslinking; Hydrogel; ZnO nanoparticles

Acknowledgement

Firstly, I would like to express my sincere gratitude to my advisor Assoc. Prof. Dr. Jutarat Prachayawarakorn. Without her assistance and dedicated involvement in every step throughout the process, this thesis would have never been accomplished. I would like to thank you very much for your supporting and understanding. Moreover, I would also like to show gratitude to my committee, including Assoc. Prof. Dr. Supranee Kaewpirom, Assoc. Prof. Dr. Naratip Vittayakorn, Assist. Prof. Dr. Patchanee Charoenying and Assist. Prof. Dr. Panpailin Seeharaj for their insightful comments**.** I greatly appreciate all teachers who have instilled invaluable knowledge to me while studying at the Faculty of Science, King Mongkut's Institute of Technology Ladkrabang. I would like to express my sincere appreciation to KMITL Research Fund (Grant No. KREF 046108) for financial support. I also would like to thank KMITL research and innovation services' proofreaders, Prof. John Morris, for proofreading and editing the English in this thesis. I wish to acknowledge the supports from all staff members of the Industrial Chemistry and Polymer Technology Workshop. Last but not the least, I would like to thank my family and friends for their precious supporting me spiritually throughout writing this thesis and my life in general. This thesis stands as a testament to your unconditional love and encouragement.

Siriporn Tantiwatcharothai

Contents

Page

Contents (continued)

page

Contents (continued)

page

List of tables

page

List of tables (continue)

page

List of figures

Page

List of figures (continue)

Page

Chapter 1

Introduction

1.1 Research Motivation

Basil seeds are the seeds of the basil plant (*Ocimum basilicum* L.) which is a known aromatic herb. When basil seeds are soaked in water, outer pericarp of the basil seeds swell into mucilaginous layer called Basil Seed Mucilage (BSM) or basil seed gum. BSM is characterized as polysaccharide-rich hydrophilic hydrogel [1]. The major polysaccharide present in BSM is glucomannan (43%) with minor amount of some xylan (24%) and cellulosic polysaccharides along with 7% of uronic acid [1]. BSM is often known for a large water holding capacity since it has numerous hydroxyl groups, which could be able to form hydrogen bonds with water molecules [1]. Because of a large water holding capacity of BSM, it is an interesting source of natural material to produce polymer for water holding application such as wound dressing.

Wound dressings are important to accelerate wound healing and protect the wound from bacterial infection [2]. An ideal wound dressing should absorb wound exudates, maintain a suitable moist environment at the wound interface and protect the wound from microorganisms [2-3]. Porous hydrogel sponge wound dressings are effective, because they have large surface areas, which could absorb and retain large amounts of exudates [4]. A common technique for production of three-dimensional porous materials is freeze-drying [5-6]. Hanumant et al. reported that gum kondagogu, with gelatin, was fabricated into a porous hydrogel sponge that showed a high degree of swelling (30-65) and porosity (40-70%) [7]. Javad claimed that gelatin-starch sponge presented good swelling behavior, but poor mechanical properties [8].

Another important property of wound dressing is antibacterial activity. Bionanocomposite wound dressing is an incorporation of biopolymer and inorganic antibacterial materials such as TiO_2 and ZnO nanoparticles [9]. An addition of inorganic antibacterial nanoparticles, such as ZnO nanoparticles, in a matrix of the wound dressing, brings another important property to a wound dressing, antibacterial activity. ZnO nanaoparticles (ZnONP) have excellent antibacterial activity, are inexpensive and nontoxic to human cells [10-11]. Bio-based materials, incorporating ZnO-NP, has shown effective antibacterial activity toward *E. coli* and *S. aureus*, good thermal and mechanical properties, high fluid uptake ability and water retention [12-14].

However, the most common drawbacks of natural wound dressing are its low

dimensional stability and easy degradation into media, during swelling. Therefore, BSM hydrogel sponge wound dressings, for long-term applications, need to be improved. One effective method to overcome its drawbacks is crosslinking. Crosslinking is widely used to improve water resistantance and also mechanical and thermal properties of many hydrophilic materials, for example, starch [15- 17]. Among various crosslinking agents, borax (di-sodium tetraborate, decahydrate) and a mixture of sodium trimetaphosphate (STMP) and sodium tripolyphosphate (STPP) have potential, since they are readily available in the market and non-toxic. Moreover, there have been many reports, borax and STMP/STPP were successfully crosslinked with many polysaccharide materials, for example, starch, poly(vinyl alcohol) and gelatin, with good mechanical properties, swelling behavior and dimension stability [8, 18].

Even though, BSM has effective water holding properties and good swelling, but there is no published information showing the use of BSM as a material for wound dressing application. The aims of this research were to prepare a new natural-based antibacterial hydrogel sponge from basil seed (*Ocimum basilicum* L.) mucilage by freeze drying technique and develop properties of BSM hydrogel sponge by crosslinking, using borax and STMP/STPP. In addition, the effect of borax and STMP/STPP contents (0 to 20 wt% of dry BSM) was investigated on the morphology, thickness, porosity, degree of swelling, dimension stability, water retention capacity and mechanical and thermal properties. Furthermore, addition of ZnONP was applied to improve antibacterial properties. The effect of ZnONP was also observed.

1.2 Aims of this thesis study

1) To prepare a new natural-based antibacterial hydrogel sponge from basil seed (*Ocimum basilicum* L.) mucilage by freeze drying technique using ZnONP as a function of antibacterial agent and reinforcing filler.

2) To develop the properties of BSM hydrogel sponge by crosslinking using borax and STMP/STPP.

3) To study the effect of ZnONP and crosslinkers (borax and STMP/STPP) on the properties of BSM hydrogel sponge.

1.3 Scope of the Research

1) ZnONP (0-50 wt%) was used as functions of antibacterial agent and composite material. Borax and STMP/STPP (0-20 wt%) were used as crosslinkers.

2) Study the effect of ZnONP on the morphology, thickness, porosity, degree of swelling, dimension stability, water retention capacity and mechanical and thermal properties of BSM hydrogel sponge.

3) Study the effect of crosslinkers (borax and STMP/STPP) on the morphology, thickness, porosity, degree of swelling, dimension stability, water retention capacity and mechanical and thermal properties of BSM hydrogel sponge.

1.4 Anticipated Benefits

1) An antibacterial hydrogel sponge wound dressing, with desirable chemical and mechanical properties, was successfully prepared from basil seed mucilage.

2) The BSM hydrogel sponge could be able to use as a bio-wound dressing, instead of commercial wound dressings.

3) Basil seeds were utilized for value added product.

Chapter 2
Theory and literature reviews

2.1 Wound dressing

During the wound healing process, dressings are used for the regeneration and repairing of dermal and epidermal tissues. Wound dressing materials act as physical barriers permeable for moisture and oxygen and protect the wound mainly against microorganisms [19]. Historically, honey pastes, plant fibers, and animal fats were used as wound dressing materials. Nowadays, with new biopolymers and fabrication techniques, wound dressing material is expected to have extraordinary properties which enhance the healing process of a wound.

2.1.1 Ideal wound dressing requirements [19].

An ideal wound dressing should fulfill the following properties (Fig 2.1):

(1) Keep a moist environment around wound area
(2) Keep a local moist environment around wound
(3) Good gas transmission
(4) Biocompatible, non-toxic and non-allergic
(5) Absorb excess exudates, but do not reach to saturation on wound surface
(6) Protect the wound from contamination, infection and micro-organisms
(7) Easy to remove and change
(8) Reduce the wound surface necrosis
(9) Possess mechanical protection
(10) Reduce the pain from the wound
(11) Costly/commercially acceptable

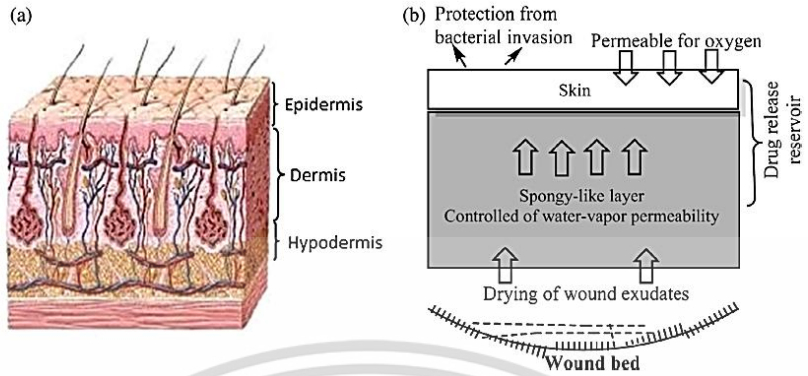

Figure 2.1 Schematic representation of (a) normal skin structure and (b) design of an ideal wound dressing [19].

2.1.2 Classification of polymeric dressing

There are many forms of polymeric wound dressing, for example, films, foams, and hydrogels [20]. The classification of polymeric wound dressing and their advantages and disadvantages are shown in Table 2.1. Biomedical material scientists suggested that hydrogel dressing meet all requirements for wound healing and suitable candidate for burn patients in the shortest time because of the following justifications: (1) hydrogels absorb the exudate and liquid from skin, (2) can maintain moist in the wound zone, and (3) possess tissue-like structure and compatibility. However, hydrogels are reported the best choice compared to other dressing forms due to they have the needed requirements for the ideal wound dressings. The disadvantage of hydrogel is its poor mechanical properties during swollen in media. The method to overcome this drawback is using ‘‘composite or hybrid hydrogel membranes” system consisting of more than one polymer in the dressing composition. Furthermore, it could be stabilized by chemical or physical interactions between the polymer chains, which are known as crosslinking. After crosslinking hydrogels have ability to retain great absorbed water in their structure [20].

Table 2.1 The types of polymeric dressing and their advantages and disadvantages [20]

Type of dressing	Advantages	Disadvantages
Films	-Good gas permeability -Easy wound monitoring through film -Transparency -Less maceration and painless	-Difficult handling -Adherence to wound bed -Non-absorbent allowing wound exudates accumulation -Easy bacterial infection
Foams	-High absorbent -Keep moist environment -non-leakage against bacterial invasion -easy to use	-Very adherent -Forming opaque layer which complicates wound monitoring -Semi-permeable for gases non-applicable for dried wounds -Poor stability
Hydrogels	-High exudates capacity -Non-adherent, -Easily removed from wound -Accelerate the healing -Easily developed and handled	-Semi-transparent -Semi-permeable to gases and water vapor -Poor bacterial barrier -Sometimes poor mechanical stability

2.2 Basil seeds

The genus *Ocimum* L. (basil) is a member of the *Lamiaceae* family. The classification of basil seeds is shown in Table 2.1 [21]. Basil seeds are an important economic and medicinal herb. Basil seeds are sacred in many Asian countries such as India, Thailand, China, Vietnam, Sri Lanka due to their excellent nutritional properties. It is used in many asian dishes such as desserts and drink. It has been part of a balanced diet in many countries for ages. It is used as a source of essential oil and flavoring agent with antimicrobial activities and antioxidative property. Some properties of different basil seeds species are summarized in Table 2.1 [1]. Basil seeds become gelatinous when soaked in water. The high mucilage content (20% wt, wet basis) of basil seeds makes it a novel source of natural hydrocolloid with invaluable functional properties, which is comparable with some other commercial gums [1].

Table 2.2 The clasiification of *Ocimum basilicum* L. seeds [21]

Classification	Name
Kingdom	*Plantae*
Order	*Lamiales*
Family	*Lamiaceae*
Genus	*Ocimum*
Species	*O. basilicum*

Table 2.3 Some physical properties of *Ocimum basilicum* L. seeds [1].

Properties	Results
Color	Black
Width	106±2.7 μm
Length	197±0.7 μm
Thickness	1.37±0.24 μm
Surface area	12.8±2.8 mm^2
Sphericity	0.62±0.04
Mass of 1,000 seeds	2.13±0.03 g
Swelling index	34-35

2.3 Basil seed mucilage

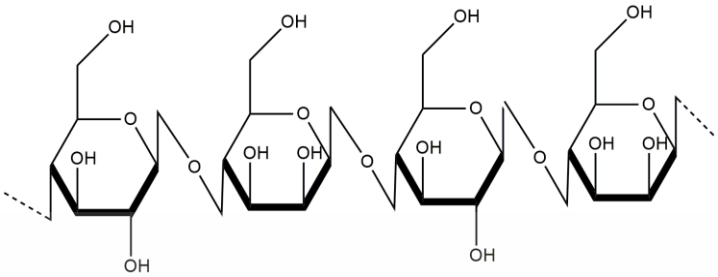

Figure 2.2 The structure of basil seed mucilage

The outer pericarp (or outer epidermis) of basil seeds, when soaks in water, swells into a gelatinous mass. The basil seed mucilage (BSM) consists mainly of high molecular weight polysaccharides (2320 kDa). Figure 2.2 shows the structure of BSM. Carbohydrate profile of basil seed is composed of starch, sugar, hemicellulose, cellulose and lignin [1]. The mucilaginous layer of the swollen seeds has two major components: glucomannan (43%) and (1, 4)-linked xylan (24%). Moreover, BSM is considered as an acidic polysaccharide, which its uronic acid value is 6.51% [1]. Chemical composition of BSM is shown in Table 2.3. For the general applications of BSM, it uses as emulsifying agent, gelling agent, disintegrant, pharmaceutical excipient, suspending agent, biodegradable film and nano delivery system.

Table 2.4 Chemical compositions of BSM [1]

Parameter	Percentage
Moisture	5.9±0.54
Ash	5.3±0.23
Protein	2.3±0.08
Total sugar	92.4±1.33
Uronic acid	6.51±0.54

2.4 Crossliking reaction

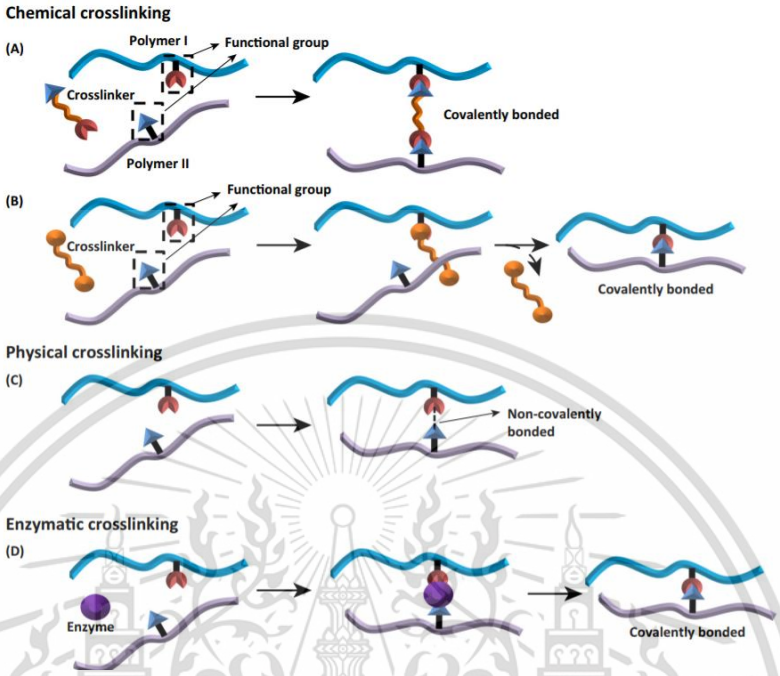

Figure 2.3 Schematic of three methods of crosslinking. (A) Chemical crosslinking with the crosslinker incorporated into the bond. (B) Chemical crosslinking with non-incorporated crosslinker into the bond. (C) Physical crosslinking. (D) Enzymatic crosslinking [22]

Crosslinking is the process of linking polymer chains by covalent or noncovalent bonds, forming tri-dimensional networks. Crosslinking is proposed to form bonds between inter- and intra- molecular of polymer chains to strengthen the material structure. Cross-linking is produced by reaction with multifunctional reagents that are efficient for forming bonds. There are three methods for crosslinking which shown in Figure 2.3. Chemical crosslinking is a result of covalent bonding between polymer chains by chemical reaction, sulfur vulcanization or irradiation; while, physical crosslinking involves non-covalent bonds, for example, hydrogen bonds or ionic bond. Crosslinking could be both intermolecular or intramolecular. It is one of the the techniques for polymer modification [23]. It is very useful, especially with biopolymer such as polysaccharide molecules because biopolymers have usually poor mechanical and barrier performance when compared to their petroleum-derived materials, limiting their applicability. The most common crosslinking agents are bifunctional compounds with reactive groups with specificity for functional groups presented on the polymer matrix. The example of materials generally used as crosslinkers is di- or poly-carboxylic acids, glutaraldehyde, genipin, borax and STMP/STPP [22].

2.4.1 Borax

Borax, sodium tetraborate decahydrate, $Na_2B_4O_7.10H_2O$, when dissolved in water, it form a boric acid-borate ion solution with a pH of about nine. Chemical structure of borax is shown in Figure 2.4. It is better formulated as $Na_2[B_4O_5(OH)_4]\cdot 8H_2O$, since borax contains the $[B_4O_5(OH)_4]^{2-}$ ion. In this structure, there are two four-coordinate boron atoms (two BO_4 tetrahedra) and two three-coordinate boron atoms (two BO_3 triangles). Borax is also easily converted to boric acid and other borates, which have many applications [24].

$$Na_2B_4O_7.10H_2O_{(s)} \rightleftharpoons 2Na^+_{(aq)} + B_4O_7^{2-}{}_{(aq)}$$

$$B_4O_7^{2-}{}_{(aq)} + 7H_2O_{(l)} \rightleftharpoons 4H_3BO_3{}_{(aq)} + 2OH^-{}_{(aq)}$$

$$H_3BO_3{}_{(aq)} + OH^-{}_{(aq)} \rightleftharpoons B(OH)_4^-{}_{(aq)}$$

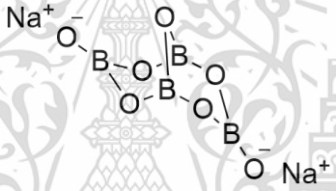

Figure 2.4 Chemical structure of borax [24]

Borax has a wide variety of uses. It is used in a component of many applications such as, crosslinking agent for biomaterials, detergents, cosmetics, and enamel glazes. It is used as a component of buffer solutions for biochemistry, food additive, as a precursor to form boron compounds, in fiberglass and fire retardant manufacture [24].

Table 2.5 Physical and chemical properties of borax [25]

Information	Identification
Name	Sodium tetraborate decahydrate
Molecular Weight	381.363 g/mol
pH	9.25 @ 20 °C (3% solution)
Physical State	solid
Color	white
Solubility in water	soluble
Melting point	62 °C
Danger hazard statement	
National Fire Protection Association	

2.4.2 Sodium Trimetaphosphate (STMP)

Sodium trimetaphosphate (STMP) is a sodium phosphate salt $(NaPO_3)_3$. The structure of STMP is shown in Fig. 2.5. It is made of repeating units of $NaPO_3$. It has three $NaPO_3$ units in its molecule. Hydrated form of STMP contains 6 or 10 molecules of water of crystallization. Production in commercial is obtained by heating $NaPO_3$ at 525 °C. The relevant properties of STMP are summarised in Table 2.2. STMP is used in starch-modified manufacturer. It is permitted as a multipurpose additive in modified food starch (not to exceed 0.04% residual phosphate). In personal care and cosmetics products, STMP is also used as an ingradient of moisturizing, skin care and bath products, makeup foundations and mascara. STMP inactivate metallic ions to prevent the deterioration of personal care products. STMP is also used as teeth polishing, help to reduce oral odor, or cleanse or the mouth and teeth [26].

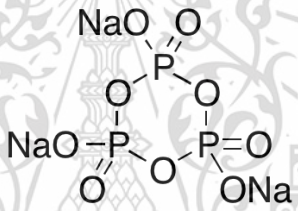

Figure 2.5 Chemical structure of sodium trimetaphosphate (STMP) [26]

Table 2.6 Physical and chemical properties of STMP [26]

Information	Identification
Name	Sodium Trimetaphosphate
Molecular Weight	305.92 g/mole
pH	7.25
Physical State	solid
Color	white
Solubility in water	soluble
Melting point	625 °C
National Fire Protection Association	

2.4.3 Sodium tripolyphosphate (STPP)

Sodium tripolyphosphate is a solid, inorganic compound. The stable form of STPP is the hexahydrated salt. The chemical structure of STPP is shown in Fig. 2.6. STPP is manufactured by combining comparatively pure chemicals, caustic soda (NaOH), or soda ash (Na_2CO_3) with phosphoric acid (H_3PO_4). STPP is used in household cleaning products such as detergents, laundry detergents and dishwasher. It hydrolyses grease and oils which facilitated the washing process. Moreover, STPP is also uses in industrial cleaning product, food additive, animal feeds and ceramics production [27].

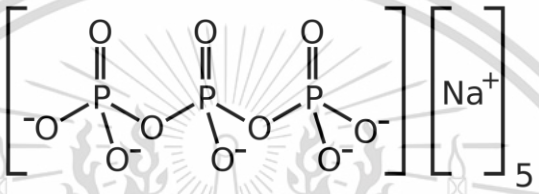

Figure 2.6 Chemical structure of Sodium tripolyphosphate (STPP) [27]

Table 2.7 Physical and chemical properties of STPP [27]

Information	Identification
Name	Sodium tripolyphosphate
Molecular Weight	367.86 g/mole
pH	9.0-10 in 1% aqueous solution
Physical State	solid
Color	white
Solubility in water	soluble
Melting point	620 °C
National Fire Protection Association	

2.5 Composites

Composites are the combinations of two materials in which one of the material is called the reinforcing phase, is in the form of particles, fibers or sheets (Figure 2.7). It is embedded in the other phase called the matrix phase. Typically, the reinforcing materials are strong with low densities while the matrix phase is usually a ductile or tough material [28]. The advantages of composite materials are their high strength and stiffness, combined with low density, when compared with bulk materials [29]. If the composite is designed and fabricated correctly, it combines the strength of the reinforcement with the toughness of the matrix to achieve a combination of desirable properties which not available in any single material.

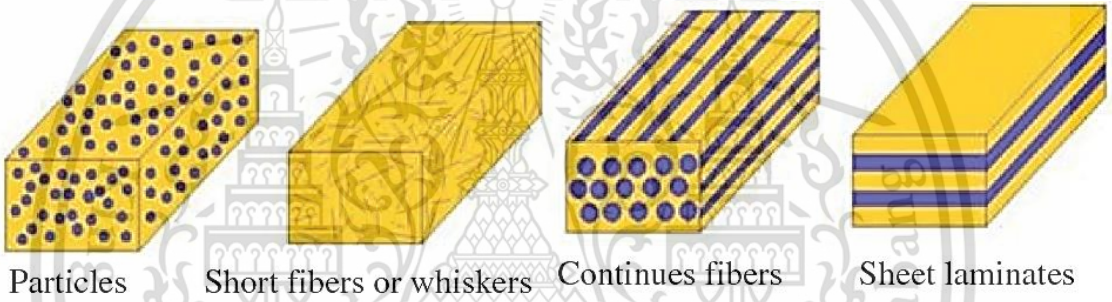

Figure 2.7 Types of reinforcing phase of the composites [29]

The reinforcing phase normally improves the strength and stiffness. Generally, the reinforcing material is harder, stiffer and stronger than the matrix phase. Particulate composites may be spherical, platelets, or any other regular or irregular shape. Particulate composite has approximately equal in all directions dimensions. Compared to fiber composites, the particulate composites are weaker and less stiff than fiber composites. A fiber composites have a length much greater than its diameter. The length-to-diameter (l/d) ratio is called aspect ratio. Continuous fibers have high aspect ratios, while discontinuous fibers have low aspect ratios. Continuous fiber composites generally have a preferred orientation, while discontinuous fibers normally have a random orientation [29].

The continuous phase or matrix phase could be a polymer, metal, or ceramic. The matrix phase performs several critical functions, for example, maintaining the fibers in the proper orientation and spacing and protecting them from the environment. In the case of

polymer matrix composites, polymer and reinforcing agent form a bond each other, the matrix transmits loads to the fibers through shear loading at the interface [29].

2.5.1 Polymer-based nanocomposites

Polymer–nanoparticle composite materials have also attracted the interest of a number of researchers, due to their synergistic and hybrid properties. Ease of processability of organic polymers combined with the better mechanical and optical properties of nanoparticles has led to the fabrication of many devices. There are the nanocomposites based on polymer filler in any matrix, described as nano filled polymer composites can be prepared. The important step in fabrication of polymer-based nanocomposites is the dispersion of filler in the matrix. Various techniques approache, including sonication by ultrasound, can be used for this purpose. However, the scope of such approaches for dispersing the nanoparticles is limited by reaggregation of the individual nanoparticles and establishment of an equilibrium state under certain conditions, which determines the size distribution of the agglomerate of the dispersed nanoparticles [29].

In some cases, the process of polymer-based nanocomposite formation and nanoparticle preparation can be combined into one (the in situ approach). In the in situ methods, nanocomposites are generated inside a polymer matrix by precursors, which are transformed into the desired nanoparticles by appropriate reactions. In situ approaches are currently getting much attention because of their obvious technological advantages. One-step synthesis leads to improved compatibility of the filler and the polymer matrix and enhanced dispersion of the filler [29].

2.5.2 Advantages and disadvantages of composite materials

The important advantages of composites materials is the ability to tailor the optimum properties of composite material such as strength and fatigue life. Moreover, composite materials are lightweight, can reduce assembly costs due to fewer detail parts and fasteners.

The disadvantages of composites include: properties of material are highly anisotropic due to the orientation of reinforcing agent, strength perpendicular to the direction of alignment is considerably less and loss electrical/optical/chemical (barrier) properties [29].

2.5.3 Applications of composite materials

The numbers of applications of composites have been growing at a rapid rate. The worldwide production is estimated to exceed 600,000 tonnes and is set to cover the following key areas in the next five to ten years [30]:

- Superior strength fibers and films
- Fire retardant materials
- UV Protection gels
- Anti-corrosion barrier coatings
- Drug delivery systems
- Scratch/abrasion resist materials

An improvements of mechanical property have results in major interest in nanocomposite in various applications. These include potential for utilization as mirror housing on various vehicles types, door handles, engine covers and intake manifolds and timing belt covers. More general applications is currently being considered include usage as impellers and blades for vacuum cleaners, power tool housings, mower hood and covers for portable electronic equipment such as mobile phones [30].

2.5.4 Zinc oxide nanoparticles (ZnONP)

Zinc oxide (ZnO) is a semiconductor material (n-type semiconductor) with a characteristic direct and band gap energy of 3.37 eV. It has been found highly attractive because of its remarkable application potential, for example, antibacterial materials, in solar cells, sensors, displays, gas sensors, piezoelectric devices, electroacoustic transducers, photodiodes and UV light emitting devices, gas sensors, UV absorbers, and antireflection coatings [31].

In polymer science, composites are materials comprising a polymeric matrix (continuous phase) and a filler (discontinuous phase). Recent advances have allowed the application of nanotechnology in the development of novel materials with improved properties. The addition of ZnO nanoparticles can offer several advantages. This is due to the wide use of ZnO as Zn supplements in the food industry. The main applications of ZnO nanoparticles for food packaging materials include providing antimicrobial activity, since the presence of ZnO nanoparticles in the polymeric matrix allows the packaging to interact with the food and have a dynamic role in its preservation. In addition, ZnO nanoparticles allow for the improvement of packaging properties, such as mechanical strength, barrier properties, and stability [11]. In recent years nanostructures of ZnO, including particles and rods, have received increasing attention due to lower cost, white appearance and UV blocking property, compared to other metallic nanoparticles. Zinc oxide nanoparticles (ZnO-NP) are used to reinforce polymeric nanocomposites because of their very large surface area, crystalline structure and excellent mechanical properties [31].

Table 2.8 Physical and chemical properties of ZnONP [31]

Information	Identification
Name	Zinc Oxide nano powder
Molecular Weight	81.38 g/mole
pH	7
Physical State	powder
Color	white
Solubility in water	insoluble
Melting point	1975 °C
National Fire Protection Association	

2.5.4.1 Antibacterial activity of ZnONP

ZnO nanoparticles have been incorporated into different materials including glass, low-density polyethylene (LDPE), polypropylene (PP), polyurethane (PU), poly(vinyl chloride) (PVC), paper, and chitosan, using different incorporation methods. The most common methods for antibacterial activity testing of ZnO-containing nanocomposite materials are agar diffusion and direct contact tests [31]. ZnO have a fundamental characteristic, which is their strong antimicrobial activity allowing them to use as antibacterial agent. Nanosized particles of ZnO have more pronounced antibacterial activities than large particles, since the small size and high surface to volume ratio of nanoparticles allow for better interaction with bacteria.

One cause of the antibacterial function could be the induction of intercellular reactive oxygen species, a strong oxidizing agent harmful to bacterial cell. ZnONP has been known to generate hydrogen peroxide (H_2O_2), which damage the cell membrane of bacteria. In addition, these nanoparticles may release Zn^{2+} ions, which could penetrate through the cell wall of bacteria and react with interior components that finally affects on viability of the cells [32]. The antibacterial activity of ZnONP is dependent on the cell wall structure of the bacteria. The thin peptidoglycan layer of Gram negative cell wall is

sandwiched between an inner cytoplasmic cell membrane and a bacterial outer membrane, while Gram positive bacteria possess only one cytoplasmic membrane with a thick cell wall consisting of multilayers of peptidoglycan [32]. In addition, because of their excellent mechanical properties, ZnONP was used as reinforcement in various materials with polymer matrix. The incorporation of ZnO-NP in starch matrix composites can improve their mechanical properties and provide antibacterial properties, expanding the range of application in food packaging, medical and pharmaceutical uses [32].

2.6 Freeze drying technique

Freeze drying or Lyophilization is a process whereby a product is dried under low temperature and vacuum. The fundamental principle in freeze drying is sublimation. The water in the sample is first frozen to a solid and then removed directly by turning the ice into vapor. This is done under vacuum and without having to pass through the liquid phase. The unique advantage of Freeze drying is that the samples are kept at low temperatures and remain frozen during the entire drying process, thereby preserving thermo labile components (proteins, flavors, colors), all while maintaining the original shape and size. The dried product can then be stored for long periods without the risk of changing composition (i.e. enzymatic, genetic) or being infected by microorganisms, which is all made possible due to the lack of water. Freeze Drying is a dehydration technique. The freeze drying process is difference from other dehydration techniques, the dehydration takes place while the product is in a frozen state and under a vacuum. These conditions stabilize the product, minimizing the effects of oxidation and other degradation processes. Freeze Drying has become an accepted method of processing heat sensitive products that require long term storage at temperatures above freezing. Freeze Drying is widely used in the pharmaceutical as well as other industries. Disadvantages of this technique is expensive unit operations due to the high energy consumption. Moreover, freeze Drying cycles need long processing times, which increase the cost of production [33].

2.6.1 Freeze Drying Process

There are three stages in the complete freeze-drying process [34].

(1) Freezing:

Freezing, or Pre-freezing, is when the sample is frozen to a temperature below its "eutectic point" or safe freezing point, the lowest temperature at which the solid and liquid phases of the material can coexist. This ensures that sublimation rather than melting will occur in the following steps. During pre-freezing, the freeze dryer works as a freezer in that no vacuum is applied. Pre-freezing could also be done separately from the dryer. The freezing step is of paramount importance, as it determines the ice morphology and pore size distribution. Larger crystals are easier to freeze-dry. To produce larger crystals, the product should be frozen slowly or can be cycled up and down in temperature. This cycling process is called annealing. However, in the case of food, or objects with formerly-living cells, large ice crystals will break the cell walls.

(2) Primary drying:

Primary drying phase is where the ice sublimates (turns directly into vapor) under ultra-low pressure, typically down to 0.01 hPa (mBar) or lower, depending on the pre-freezing temperature of the sample. The driving force of sublimation is the pressure difference related to the corresponding temperature difference between the product ice surface and the condenser ice surface. Larger temperature differences mean larger pressure differences, which allow for a faster process. The vacuum speeds up the process by removing air molecules to allow sample vapor molecules to move easier from the sample, through the chamber and into the condenser.

(3) Secondary drying:

The secondary drying phase aims to remove unfrozen water molecules, since the ice was removed in the primary drying phase. This part of the freeze-drying process is governed by the material's adsorption isotherms. In this phase, the temperature is raised higher than in the primary drying phase, and can even be above 0 °C, to break any physico-chemical interactions that have formed between the water molecules and the frozen material.

2.6.1 Application of Freeze Drying [34]

(1) Preserve biological samples for long periods of time. Freeze drying remove up to 95% of water, so food and pharmaceuticals could be stored for a longer period of time.

(2) Freeze-drying significantly reduces the total weight of the food.

(3) Pharmaceutical freeze dryers are used to preserve biological products such as vaccines, proteins, enzymes, and hormones. The shelf-life of a live virus vaccine can be extended.

(4) Dietary nutritional supplements such as aloe vera and echinacea are stored using commercial freeze dry machines.

(5) Meat, vegetables and fish can be freeze-dried, while their taste and nutritional value are retained.

2.7 Plasticizer

Plasticizers or dispersants are additives that increase the plasticity or decrease the viscosity of a material. These are the substances which are added in order to alter their physical properties. These are either liquids with low volatility or solids. They decrease the attraction between polymer chains to make them more flexible. Over the last 60 years, more than 30,000 different substances have been evaluated for their plasticizing properties. The dominant applications are for plastics, especially poly(vinyl chloride; PVC). The properties of other materials may also be modified when blended with plasticizers including concrete, clays, and related products. The majority is used in films and cables [35]. It was commonly thought that plasticizers work by embedding themselves between the chains of polymers, spacing them apart (increasing the "free volume") and thus significantly lowering the glass transition temperature for the plastic and making it softer; however it was later shown that the free volume explanation could not account for all of the effects of plasticization. For plastics such as PVC, the more plasticizer added, the lower their cold flex temperature will be. Plastic items containing plasticizers can exhibit improved flexibility and durability [35].

2.7.1 Glycerol

Glycerol (1, 2, 3-propanetriol) is an odorless, colorless, viscous liquid and a sweet taste, derived from both petrochemical and natural feedstocks [36]. The chemical structure of glycerol is shown in Figure 2.9.

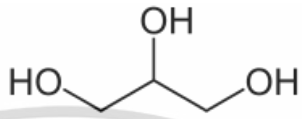

Figure 2.8 Structure of glycerol [37]

Glycerol (also known as glycerin) is a polyol (1,2,3-propanetriol), naturally present in the structure of triglycerides, which are fatty acid esters of this alcohol. Glycerol is one of the most valuable and versatile and chemical substances. It is absolutely soluble in alcohols and water, is slightly soluble in many collective solvents such as dioxane and ether, but is insoluble in hydrocarbons. There are currently a high number of applications found for this substance (more than 2000) in different fields such as the cosmetic, pharmaceutical or food industry, where it is mainly employed as humectant, thickener, lubricant, sweetener or anti-freezer, among others uses. Its production from soap manufacture or fatty acid production was quantitatively [36]. Physical and chemical properties of glycerol are shown in Table 2.10. Glycerol includes three hydrophilic hydroxyl groups, which are sensible for water and its hygroscopic nature. Glycerol has a highly flexible molecule forming both intra- and inter-molecular hydrogen bonds [37].

Table 2.9 Physical and chemical properties of glycerol [37]

Information	Identification
Chemical formula	$C_3H_5(OH)_3$
Molecular Weight	92.09 g/mole
Physical State	liquid
Color	clear
Solubility in water	soluble
Melting point	18.2 °C
Boiling point	290 °C
National Fire Protection Association	

2.8 Literature reviews

H. Wang *et al.* (2019) examined the effect of crosslinking on the preparation of chitosan/methylcellulose composite films. In this study, chitosan/methylcellulose composite films were prepared by casting technique using STMP crosslinking agent (0-0.5 wt%). It was observed that physicochemical properties of the composite film were improved by crosslinking with STMP. The crosslinked films showed an increased tensile strength, higher elongation at break, lower swelling ratio and solubility, and lower enzymatic degradation than the non-crosslinked films. [38].

T. K. Mohammed *et al.* (2018) studied the preparation of heparinized PVA/chitosan (CS)/nano zinc oxide (nZnO) hydrogel. The combination of heparinized PVA, chitosan, and nZnO was used to produce hydrogels using the freeze drying technique. SEM image presented the decrease in average density of pores of hydrogel after adding nZnO. In addition, by increasing the amount of nZnO for 0.5% weight, the gel content and swelling of the sample were decreased which indicated an increase in the interaction between the nanoparticle and the polymer chains. The prepared hydrogel presented good mechanical properties in both dry and wet states and the addition of nZnO also improved their water vapor permeability. For antibacterial activity, inhibition zone increased as nZnO was increased. The highest inhibition zone was observed in *S. aureus* (gram positive) samples [39].

A. I. Raafat *et al.* (2018) fabricated a nanocomposite dressing hydrogel based on xanthan gum and PVA reinforced with ZnO nanoparticles. The hydrogel was prepared by casting technique. The presence of ZnO nanoparticles reconstructed the internal structure of (Xan-PVA) network which aid in a homogenous porous structure. Moreover, the increased amount of ZnO favored a more dense structure with smaller pore size. Such adequate porosity along with the presence of ZnO nanoparticles improved the fluid uptake ability, water retention and water vapor transmission property of the (Xan-PVA) dressing. Also, the inhibitory effect increased by the increase of ZnO nanoparticles embedded within (Xan-PVA) dressings as indicated by higher inhibition zone. The results showed higher antibacterial activity against *S. aureus* than that observed against *E. coli* [14].

S. K. Bajpai *et al.* (2017) synthesized and characterized zinc oxide nanoparticles/gum acacia/poly(acrylate) nanocomposites using hydrothermal approach. [40]. From SEM image, it is noteworthy that most of the particles occupied a diameter range of 40–60 nm. In addition, an increase in ZnONP content resulted in a decreased in degree of swelling of the sample. Finally, the antimicrobial action of nanocomposites was

studied using *E. coli* as model bacteria. It was found zone of inhibition' with the radius of 3.2±0.07 cm [40].

Z**.** Lu *et al.* (2017) synthesized a sponge-like nanoAg/ZnO-loaded chitosan composite dressing via preparing a chitosan sponge by lyophilization process, followed by the incorporation of Ag/ZnO nanocomposites into chitosan sponge. The presence of Ag/ZnO nanorods slightly reduced the porosity of the sample (88–81%). The composite dressings showed 21–24 of swelling ratio. The cell viability test indicated low cytotoxicity of chitosan-Ag/ZnO composite [41].

J**.** Tavakoli (2017) designed and fabricated a wound dressing gelatin–starch foam using borax as a crosslinking agent (0-40 wt%). The gelatin–starch foam was prepared with vacuum oven at 60 ℃ and -80 kPa for 24h. SEM image revealed denser sample with the increase of borax content. Moreover, an increase in borax content decreased the swelling ratio and improved dimensional stability and mechanical properties of the foam [8].

N. Thombare *et al***.** (2017) studied the preparation of borax cross-linked guar gum hydrogels as potential adsorbents. The result indicated that with increase in borax proportion from 5 to 20%, the swelling was decreased and the cross-linked networking of the product was improved. From TGA thermograms, an additional step was found at 330–508 °C after crosslinking, which attributed to degradation of the borax cross-linked guar gum [18].

H. S. Rathore *et al***.** (2016) fabricated a sponge by blending natural polymer gum kondagogu with gelatin by freeze drying technique. The SEM micrographs depicted the porous structure with its cross sectional view and showed many pores with good interconnectivity to each other. The sponge exhibited high swelling ratio (~47) and porosity (~40-70). Moreover, the sponge was impregnated with ciprofloxacin (CP) drug. CP loaded sponge was evaluated against *S. aureus* and *E. coli* and it exhibited good antimicrobial activities [7].

N**.** Khazaei *et al***.** (2014) studied the using of basil seed gum (BSG) as a new film-forming material under the influence of addition of glycerol as plasticizer (25-50 wt%). The film was prepared by casting technique. The films obtained from this research was transparent films with good mechanical properties and excellent barrier properties. It was observed that, glycerol affected physical and mechanical properties of BSG films. Tensile strength decreased and elongation at break of the films increased with increasing concentrations of glycerol [42].

P.R. Sarika *et al.* (2014) studied the preparation of gum arabic cross-linked gelatin scaffold for biomedical applications by freeze drying technique. The scaffold was improved the properties by crosslinking with borax. SEM micrograph presented interconnected porous scaffold. The scaffold indicated high porosity and swelling ratio (68-81). The scaffold was confirmed non-cytotoxic and non-adherent nature by cytocompatibility evaluation using L-929 and HepG2 cells [43]

M. Shi *et al.* (2013) studied the effect of cross-linking on physicochemical properties of pea starch. Pea starch was crosslinked using different levels of sodium trimetaphosphate and sodium tripolyphosphate (99:1, w/w). Compared to the native pea starch, solubility and swelling power of cross-linking starch were decreased. From XRD diffractogram, there was no pronounced difference between the native and modified starches, both the native and modified pea starch showed C-type XRD pattern. [44]

Chapter 3
Research methodology

3.1 Chemicals

1. Basil seeds (Food grade, Raithip Co., Ltd.)

Table 3.1 Chemical composition of BSM [1]

Composition of BSM	Percentage by weight
Moisture	5.9±0.54
Ash	5.3±0.23
Protein	2.3±0.08
Glucomannan	43
Xylan	24
Other polysaccharides	13
Uronic acid	6.51±0.54

2. Borax (BO) (Food grade, Chemipan Co., Ltd.)

Table 3.2 Information of borax

Analysis	Results	Specifications
H_3BO_3	100.01%	99.9-100.9%
Cl	0.00052%	0-0.001%
Fe	0.0008%	0-0.004%
SO_4	0.018%	0-0.025%
20 mesh	1.0%	0-2%

3. Sodium Trimetaphosphate (STMP) (Food grade, Chemipan Co., Ltd.)

Table 3.3 Information of STMP

Analysis	Results	Specifications
Appearance	White crystal	
Assay	98.2%	98% (min)
pH (1wt% solution)	9.7	9.5-10
Moisture	4.5%	5 % (max)
Fluoride	<0.003%	0.003 % (max)
Arsenic	<0.0003%	0.0003 % (max)
Particle size -through #32 mesh - through #80 mesh	 20% 99%	 22% (max) 80% (min)

4. Sodium Tripolyphosphate (STPP) (Food grade, nanomaterials technology Co., Ltd.)

Table 3.4 Information of STPP

Analysis	Results	Specifications
Appearance	White crystal	
Assay	98.5%	98% (min)
pH (1wt% solution)	9.8	9.5-10
Moisture	4.0%	5 % (max)
Fluoride	<0.003%	0.003 % (max)
Arsenic	<0.0003%	0.0003 % (max)
Particle size -through #32 mesh - through #80 mesh	 20% 99%	 22% (max) 80% (min)

5. Zinc oxide nanoparticle (ZnONP) 40-80 nanometer (Food grade, Union Chemical Co., Ltd.)

Table 3.5 Information of ZnONP [47]

Information	Identification
Appearance	White, powder
%ZnO	99.76
%Pb	0.0053
%Cd	0.0006
%Al	Not detected
%Moisture	0.020
Particle size	40-80 nm

6. Glycerol (Lab system, Co., Ltd.)

7. Distilled water (AR grade, Lab system, Co., Ltd.)

3.2 Equipment

1. Stirring rod
2. Magnetic bar
3. Beakers
4. Petri dish (100 mm×15mm)
5. Thermometer
6. Hot air oven (MEMMERT, ULM 600/l, Germany)
7. Hotplate stirrer (IKA, C-MAG HS7, Germany)
8. Digital balance 4 digits (ITS, Thailand)
9. Digital balance 2 digits (ITS, Thailand)
10. Freezer (DW-40L92, Haier, China)
11. Freeze dryer (Coolsafe 110-4, Scan Vac, Denmark)
12. Scanning Electron Microscopy (SEM) [LEO 1450 VP] [FEI, Quanta 250, USA]
13. Universal testing Machine [LLYOD Instrument, LR5k, USA]
14. Thermogravimetric analyzer (TGA) [Perkin Elmer, Pyris 1, Massachusetts, USA]

3.3 Procedures

3.3.1 BSM extraction

1. The basil seeds were soaked in distilled water at the weight ratio of seed:water at 1:30 for 1 h at room temperature.

2. The swollen seed was stirred with a blender for 1 min to scrape the mucilage off the seed surface.

3. The mucilage was filtered from the swollen seeds with cheese cloth and centrifuged at 5000 rpm for 5 min to remove seed residue.

4. The mucilage was refrigerated at -40 ℃ for 24 h in a freezer followed by lyophilization at -100 ℃ for 24 h using a freeze dryer to obtain dried BSM

3.3.2. Preparation of BSM hydrogel sponge incorporated with ZnONP

Flowchart of the preparation and characterization of BSM hydrogel sponge incorporated with ZnONP is shown in Figure 3.1.

1. The dried BSM (1 wt% of distilled water) was dissolved in 100 ml of distilled water.

2. Glycerol was added to BSM solution as a plasticizer (15 wt% of dried BSM).

3. The various contents of ZnONP, from 0-50 wt% (0-0.5 g), were added to the solution (Table 3.6). Then, the solution was mechanically stirred using a magnetic stirrer at 40 °C for 45 min.

4. 30 ml of the solution was poured into a petri dish (100 mm × 15 mm) to control the thickness of the sample.

5. The sample was refrigerated at -40°C for 24 h in a freezer and lyophilized at -100 °C for 24 h using a freeze dryer.

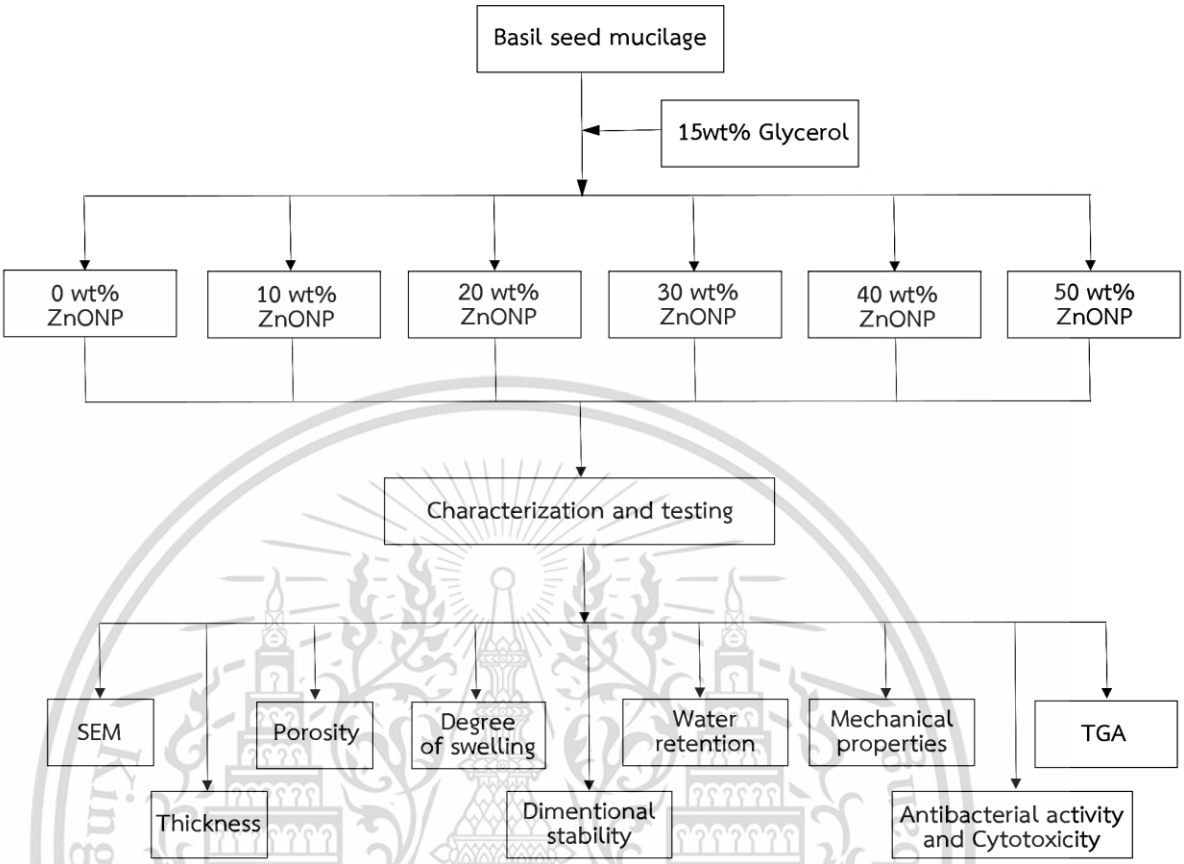

Figure 3.1 Flowchart of the preparation and characterization of different BSM hydrogel sponges incorporated with ZnONP

Table 3.6 Different ZnONP contents of BSM hydrogel sponges

Sample	Contents				Note*	
	Dried BSM (g)	DI water (ml)	Glycerol (g)	ZnONP* (g)	ZnONP (wt%)	ZnONP (vol%)
BSM	1	100	0.15	0	0	0
10ZnONP	1	100	0.15	0.1	10	0.01
20ZnONP	1	100	0.15	0.2	20	0.02
30ZnONP	1	100	0.15	0.3	30	0.03
40ZnONP	1	100	0.15	0.4	40	0.05
50ZnONP	1	100	0.15	0.5	50	0.08

3.3.3 Preparation of BSM hydrogel sponge crosslinked with borax or STMP/STPP and incorporated with ZnONP

Flowchart of the preparation and characterization of BSM hydrogel sponge crosslinked with borax or STMP/STPP and incorporated with ZnONP is shown in Figure 3.2.

1. Dried BSM (1 wt %) and glycerol (15 wt% of BSM) were dissolved in 100 ml of distilled water.

2. Different amounts of crosslinkers (0, 5, 10, 20 wt% of dried BSM) were separately dissolved in 20 ml distilled water and added to the BSM solution (Table 3.7), then pH was adjusted to 9.

3. ZnONP was added at 30 and 50 wt% based on the weight of dried BSM (the most suitable amount from part 3.3.2).

4. The solution was magnetically stirred for 2 h at 40°C.

5. 30 ml of the solution was placed in a petri dish (100 mm × 15 mm) to control the sample thickness

6. The sample was refrigerated for 24 h at -40 °C in a freezer and lyophilized at -100 °C for 24 h using a freeze dryer.

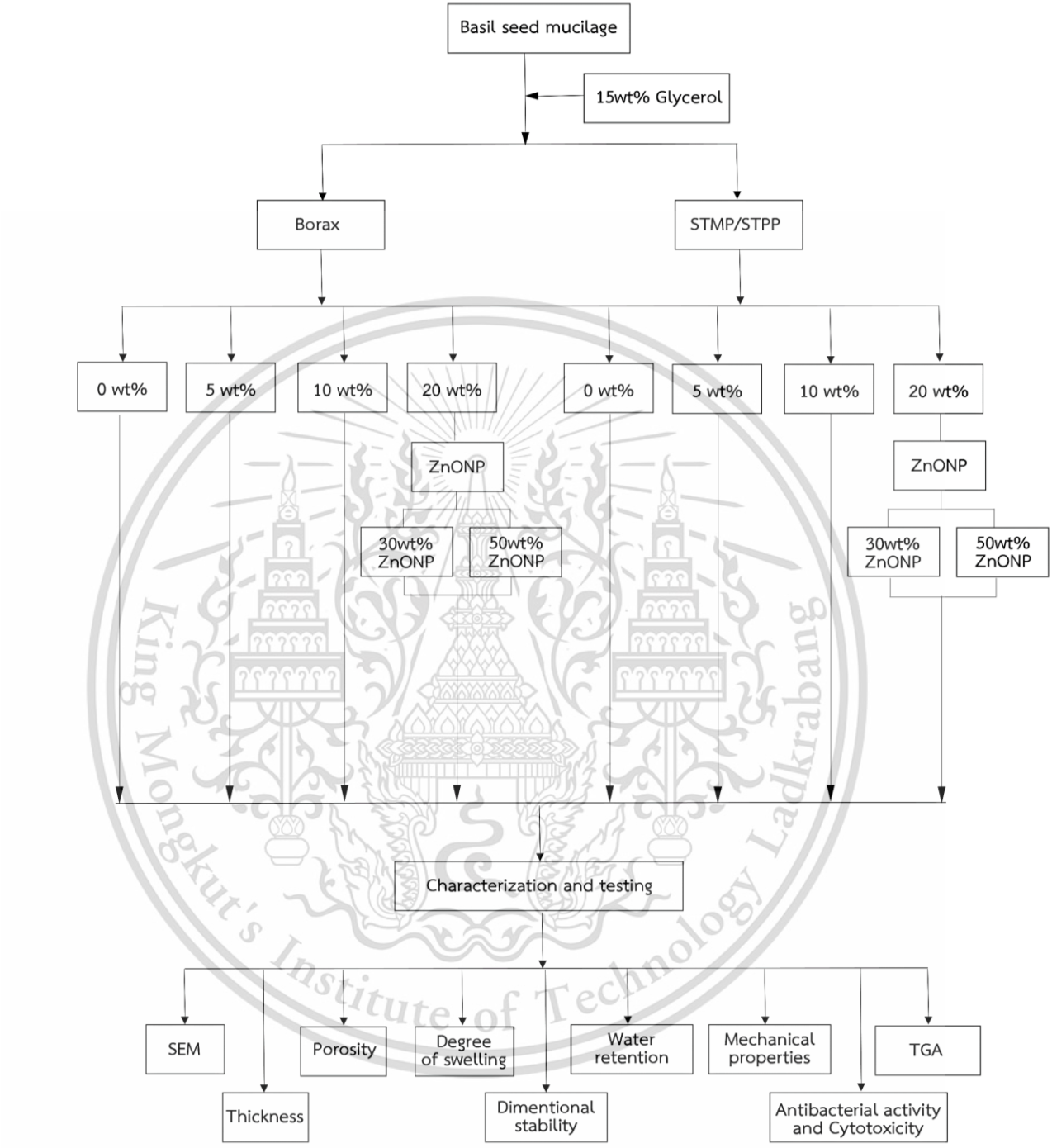

Figure 3.2 Flowchart of the preparation and characterization of various BSM hydrogel sponges crosslinked with borax or STMP/STPP and incorporated with ZnONP

Table 3.6 Different crosslinkers and ZnONP contents of BSM hydrogel sponges

Sample	Contents					
	Dried BSM (g)	DI water (ml)	Glycerol (g)	ZnONP (g)	Borax (g)	STMP/STPP (g)
BSM	1	100	0.15	0	0	0
5BO	1	100	0.15	0	0.05	0
10BO	1	100	0.15	0	0.1	0
20BO	1	100	0.15	0	0.15	0
20BO30ZnONP	1	100	0.15	0.3	0.2	0
20BO50ZnONP	1	100	0.15	0.5	0.2	0
5ST	1	100	0.15	0	0	0.05
10ST	1	100	0.15	0	0	0.1
20ST	1	100	0.15	0	0	0.15
20ST30ZnONP	1	100	0.15	0.3	0	0.2
20ST50ZnONP	1	100	0.15	0.5	0	0.2

3.4 Characterization of BSM hydrogel sponge

3.4.1 Morphology

A sample morphology was examined by a scanning electron microscope (SEM), (LEO 1455VP, ZEISS, Germany). The sample was immersed and fractured in liquid nitrogen before the examination. Prior to the examination, the sample was covered with a thin layer of gold for electrical conduction.

3.4.2 Thickness

A thickness of sample was determined with a micrometer (Model G, Peacock, Japan). The micrometer was applied to a 20×20 mm^2 piece of the sample. The thickness was reported as an average of 8 measurements.

3.4.3 Porosity

For measuring a porosity of sample, the porosity was measured by a displacement liquid method using ethanol, assuming all pores are open pores. The sample was immersed in a known volume (V_1) of ethanol in a graduated cylinder for 10 min. The total volume of ethanol after sample immersion was recoded as V_2. Then, the sample was removed from the cylinder, and the volume of the remaining ethanol was recorded as V_3. The porosity percentage was calculated by equation (1) below,

$$\text{Porosity (\%)} = \frac{V_1 - V_3}{V_2 - V_3} \times 100 \qquad (1)$$

3.4.4 Degree of swelling

Degree of swelling of a sample was carried out according to ASTM D-570 standard method. A dried sample (20×20 mm^2) was weighed and immersed in deionized water at room temperature. The degree of swelling of the sample was measured after 48 h. The swollen sample was taken out of the water, removed off the water that adhered on its surface by gentle blotting with filter paper and immediately weighed. The degree of swelling was calculated by equation (2) below,

$$\text{Degree of swelling} = \frac{M_w - M_0}{M_0} \quad , \qquad (2)$$

where M_0 and M_w were the weights of the sample before and after immersion, respectively.

3.4.5 Dimensional stability

A sample was cut into rectangular piece of 20×20 mm^2. The sample was soaked in distilled water for 48 h. Variation of length in each direction (width, length and thickness) was measured using a vernier caliper (Super caliper, Mitutoyo, Japan) at 24 and 48 h. Data was reported as an average from 8 measurements.

3.4.6 Water retention capacity

Water retention capacity of a sample was determined by using a modified version of ASTM D-570 standard method. A sample (20×20 mm^2) was allowed to swell in deionized water until it reached an equilibrium. After the sample was wiped off excess water with a filter paper, it was left at ambient temperature for 24 h then weighed. The water retention capacity was calculated by equation (3),

$$\text{Water retention capacity (\%)} = \frac{W_T}{W_0} \times 100 \ , \qquad (3)$$

where W_0 and W_T were the initial weight and the weight after 24 h, respectively.

3.4.7 Mechanical properties

The mechanical properties of a sample were measured with a universal testing machine (Lloyd Instrument, LR 5K, West Sussex, UK) using a 100 N load cell at a crosshead speed of 50 mm/min, following the ASTM D-638 standard. The sample was cut into 15 mm × 100 mm rectangular pieces and kept under controlled conditions of the ambient temperature and a relative humidity (RH) of 58±2% for 24 h before testing.

3.4.8 Thermal properties

The thermogravimetric (TGA) and derivative thermal gravimetric (DTG) properties of a sample were determined using thermogravimetric analyzer (Pyris I TGA HT, Perkin Elmer, USA) in the temperature range of 30 to 900 °C at a heating rate of 10 °C /min under nitrogen atmosphere.

3.4.9 Antibacterial activity

The antibacterial activity against *Escherichia coli* (Gram-negative) and *Staphylococcus aureas* (Gram-positive) of a samples was assessed from the size of the inhibition zone in the agar discs. A sample was cut into 8 mm circular discs with a sharp metal cutter. The disc was placed on an agar plate containing a bacterial lawn and incubated at 37 °C for 24 h. After that, the diameter of the zone of inhibition was measured to examine the antibacterial activity.

3.4.10 Cytotoxicity

Cytotoxicity of a sample was assessed by an MTT assay with human keratinocytes (HaCat) cells. A sample was soaked in phosphate buffered saline at 37 ℃ for 24 h. The soaked sample was filtered, and the filtrate was added with DMEM (Dulbecco's Modified Eagle Medium). The mixture was then incubated in a medium of DMEM supplemented with 10% FBS (Fetal Bovine Serum). Next, 100 µl of 1x105 cells/ml HaCat cells were seeded and incubated at 37 ℃ for 24 h in a well of a 96-well plate. After that, 100 ml of the incubated filtrate mixture were added into the well. Next, 10 µL of MTT solution (5 mg/mL) was added into the well and further incubated at 37 ℃ for another 4 h. Then, formazan crystals were dissolved in 100 µl of 100% DMSO:10% SDS solution and 100 µl of the resulting solution was added into the well. The qualitative analysis was observed with optical microscope.

3.4.11 Statistical analysis

Statistical analysis was performed using the analysis of variance (ANOVA) procedure with IBM SPSS statistics 25 software. Tukey's test was used to determine differences among the means ($p < 0.05$).

Chapter 4
Results and Discussion

This research focused on the property improvement of BSM hydrogel sponge by crosslinking with borax and STMP/STPP and incorporation of ZnONP. In this chapter, results and discussion were divided into 2 sections; effect of ZnONP and effect of crosslinking agents (Borax and STMP/STPP) and their contents on various properties of BSM hydrogel sponge, i.e., morphology, thickness, porosity, water retention capacity, degree of swelling, dimensional stability, mechanical and thermal properties. Moreover, antibacterial activity and also cytotoxicity were also studied. Abbreviations of the terms used in this research were shown in Table 4.1.

Table 4.1 Abbreviations and means

No.	Abbreviations	Means
1	BSM	Unmodified BSM hydrogel sponge
2	10ZnONP	BSM hydrogel sponge incorporated with 10 wt% ZnO nanoparticles
3	20ZnONP	BSM hydrogel sponge incorporated with 20 wt% ZnO nanoparticles
4	30ZnONP	BSM hydrogel sponge incorporated with 30 wt% ZnO nanoparticles
5	40ZnONP	BSM hydrogel sponge incorporated with 40 wt% ZnO nanoparticles
6	50ZnONP	BSM hydrogel sponge incorporated with 50 wt% ZnO nanoparticles
7	5BO	BSM hydrogel sponge crosslinked with 5 wt% borax
8	10BO	BSM hydrogel sponge crosslinked with 10 wt% borax
9	20BO	BSM hydrogel sponge crosslinked with 20 wt% borax
10	20BO30ZnONP	BSM hydrogel sponge crosslinked with 20 wt% borax and incorporated with 30 wt% ZnO nanoparticles
11	20BO50ZnONP	BSM hydrogel sponge crosslinked with 20 wt% borax and incorporated with 50 wt% ZnO nanoparticles
12	5ST	BSM hydrogel sponge crosslinked with 5 wt% STMP/STPP

Table 4.1 Abbreviations and symbols **(**continued**)**

No.	Abbreviations	Means
13	10ST	BSM hydrogel sponge crosslinked with 10 wt% STMP/STPP
14	20ST	BSM hydrogel sponge crosslinked with 20 wt% STMP/STPP
15	20ST30ZnONP	BSM hydrogel sponge crosslinked with 20 wt% STMP/STPP and incorporated with 30 wt% ZnO nanoparticles
16	20ST50ZnONP	BSM hydrogel sponge crosslinked with 20 wt% STMP/STPP and incorporated with 50 wt% ZnO nanoparticles

4.1 Effect of ZnONP and its contents on various properties of BSM hydrogel sponge

This section reported on the effect of the incorporation of ZnONP on properties of BSM hydrogel sponge. The effect of different contents of ZnONP (0-50 wt%) were investigated on morphology, thickness, porosity, water retention capacity, degree of swelling, mechanical properties, thermal properties, antibacterial activity and also cyctotoxicity of BSM hydrogel sponge.

The possible chemical structure of BSM hydrogel sponge incorporated with ZnONP is presented in Figure 4.1. ZnONP may attach with BSM matrix via physical adhesion and hydrogen bonding (Figure 4.1 (a) and (b)). Also, A. Nafchi and co-workers reported that ZnONP could form electrostatic interaction with sago starch since ZnONP has a point of zero charge at 9.3, it means that at pH below 9.3, the net surface charge of ZnONP is positive charge [53, 54]. So the electrostatic interaction could form between the positive charge of ZnONP surface and negative dipole of BSM (Figure 4.1(c)) [45]. This phenomenon was also reported by Lu, Z. et al. that ZnONP could form electrostatic interaction with hydroxyl group of gum acacia [40]. Furthemore, ZnONP is generally N-type semiconductor; the number of electrons is more than the holes, so electrons are the majority charge carriers. Therefore, free electrons of ZnONP could form electrostatic interaction with BSM matrix (Figure 4(d)) [55].

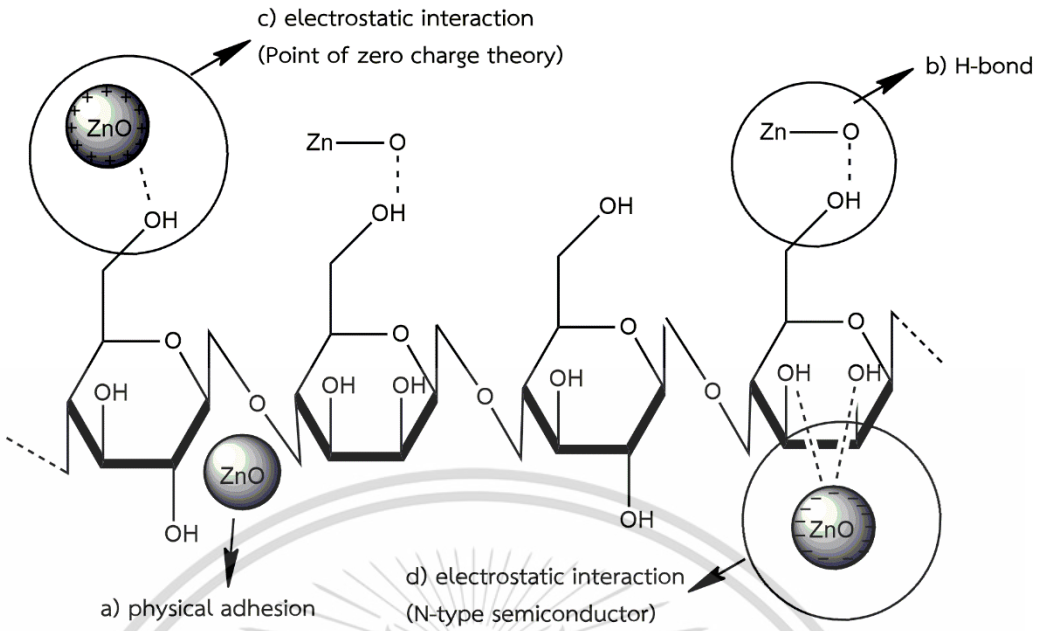

Figure 4.1 The possible chemical structure of BSM hydrogel sponge incorporated with ZnONP

4.1.1 Effect of ZnONP on morphology of BSM hydrogel sponge

The effect of ZnONP on morphology of BSM hydrogel sponge was observed by scanning electron microscope (SEM). The microstucture of the cross-section of BSM hydrogel sponge with different contents of ZnONP is presented in Figure 4.2

From Figure 4.2, after pre-freezing and freeze-drying, water molecules in BSM solution formed ice and sublimed, then left empty pores. Interconnected open-cell structure of the pores was observed. After the incorporation of ZnONP, BSM hydrogel sponges with various ZnONP contents showed a change in the morphology. The round open-pored structure became tighter network structure as ZnONP content was increased. This may be due to various interaction between the hydroxyl groups of BSM and ZnONP. These interaction between two components led to reduced numbers of BSM hydroxyl groups available to interact with water and cause a poor distribution of water in BSM matrix [45]. As a result of poor distribution of water, the pores were collapsed during freeze drying process under vacuum condition. So the rounded pore turned to stacked-like structure as seen in Figure 4.2. A similar change in morphology has also been reported for ZnONP loaded gum acacia/polyacrylate [40]. These observations showed that ZnONP content played an important role in changing the pore shape of samples obtained by freeze drying.

In addition, Figure 4.3 shows high magnification images of BSM hydrogel sponge incorporated with various ZnONP contents cross-section. It is evident that small ZnONPs were uniformly distributed over the BSM matrix and strongly attached to the sponge surface (see Appendix A for EDS mapping image).

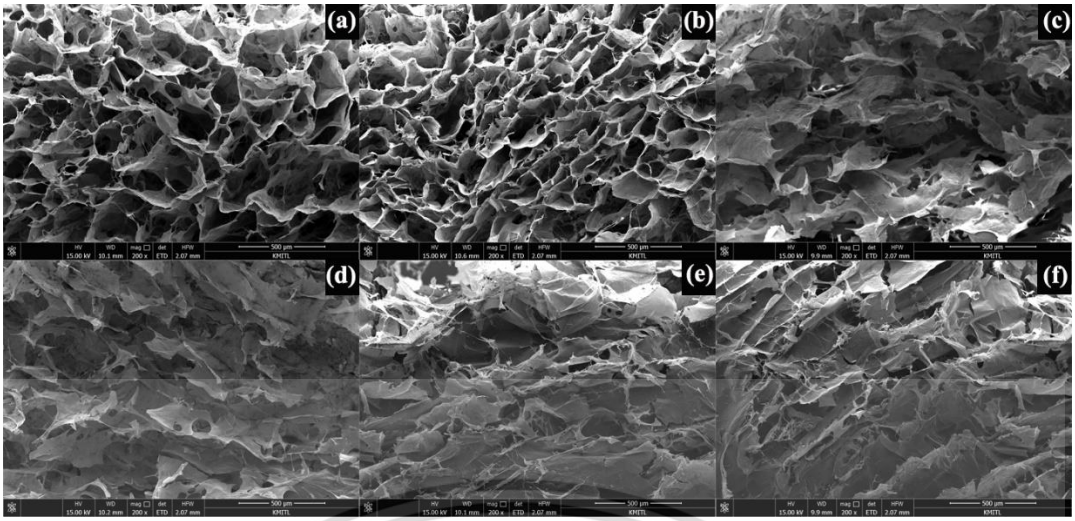

Figure 4.2 Cross-sectional SEM images of BSM hydrogel sponges prepared with various ZnONP contents; 200×magnification: (a) BSM, (b) 10ZnONP, (c) 20ZnONP, (d) 30ZnONP, (e) 40 ZnONP and (f) 50ZnONP

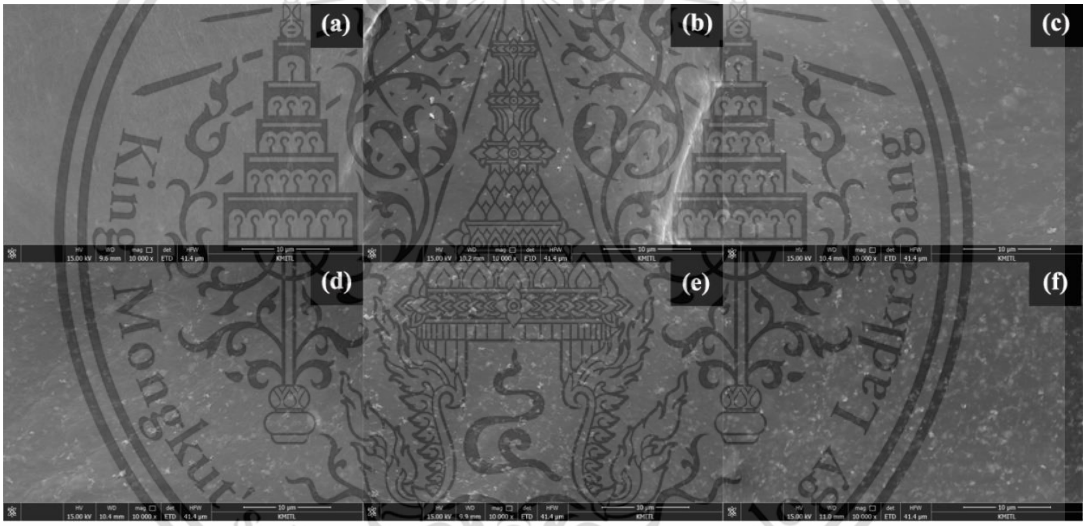

Figure 4.3 Cross-sectional SEM images of BSM hydrogel sponges prepared with various ZnONP contents; 10,000×magnification: (a) BSM, (b) 10ZnONP, (c) 20ZnONP, (d) 30ZnONP, (e) 40 ZnONP and (f) 50ZnONP

4.1.2 Effect of ZnONP on thickness and porosity of BSM hydrogel sponge

A hydrogel sponge with high porosity can absorb a large volume of exudate from a wound surface. The thickness and porosity of BSM hydrogel sponge incorporated with various contents of ZnONP were shown in Table 4.2.

Table 4.2 Thickness and porosity of BSM hydrogel sponge incorporated with various ZnONP contents

Sample	Thickness (mm)	Porosity (%)
BSM	1.53 ± 0.11[a]	92.1 [a]
10ZnONP	1.31 ± 0.06 [b]	89.3 [b]
20ZnONP	1.18 ± 0.04 [c]	86.4 [c]
30ZnONP	1.06 ± 0.05 [d]	82.7 [d]
40ZnONP	0.93 ± 0.05 [e]	79.2 [e]
50ZnONP	0.82 ± 0.04 [f]	76.1 [f]

Different superscript letters in the same column are significantly different ($p<0.05$), based on Tukey's test.

From Table 4.2, BSM hydrogel sponge without the incorporation of ZnONP presented a thickness of 1.53 mm and a high porosity of 92.1%. However, increasing ZnONP content led to the decrease of thickness (1.53 to 0.82 mm) and porosity (92.1 to 76.1%) of hydrogel sponge. This was related to the consequences of the change in morphology when ZnONP content was increased as seen in Figure 4.2.

4.1.3 Effect of ZnONP on degree of swelling and water retention capacity of BSM hydrogel sponge

The Effect of ZnONP on degree of swelling and water retention capacity of BSM hydrogel sponge prepared with different ZnONP contents were shown in Table. 4.3. It was found that all of BSM hydrogel sponges showed a considerable degree of swelling (80.5-109). This was due to the hydrophilic nature of BSM molecules that contain a high number of hydroxyl groups which strongly interacting with water. Also, the high porosity of the sponge (Table 4.2) serve to facilitate water diffusion into BSM porous structure. However, the increase in ZnONP content resulted in the decrease in degree of swelling. As expected, the highest degree of swelling was found in BSM hydrogel sponge prepared without ZnONP. This was related to the decrease in porosity of BSM hydrogel sponge when ZnONP was added. Moreover, electrostatic interaction and hydrogen bonding between ZnONP and the BSM matrix led to fewer hydroxyl groups of the hydrogel available to interact with water. Additionally, ZnONP may occupy some

vacancies in the hydrogel network, restricting its expansion and hindering water penetration.

Table 4.3 Degree of swelling and water retention capacity of BSM hydrogel sponge incorporated with various ZnONP contents

Sample	Degree of swelling	Water retention capacity (%)
BSM	109.0 ± 2.2 [a]	31.2 [a]
10ZnONP	98.7 ± 1.7 [b]	35.3 [b]
20ZnONP	92.1 ± 2.8 [c]	36.7 [b]
30ZnONP	88.8 ± 2.4 [c,d]	40.1 [c]
40ZnONP	84.4 ± 1.3 [d]	42.0 [c]
50ZnONP	80.5 ± 2.1 [e]	44.8 [d]

Different superscript letters in the same column are significantly different ($p<0.05$), based on Tukey's test.

Another important property of wound dressing, water retention capacity is the ability of a dressing material to hold moisture within its structure. The water retention capacity of sponges prepared with various ZnONP contents, after exposure to air at room temperature for 24 h is shown in Table 4.3. BSM hydrogel sponge without the incorporation of ZnONP showed the lowest water retention capacity (31.2%). After increasing of ZnONP content from 0-50 wt%, the water retention capacity of BSM sponge slightly increased from 31.2 to 44.8%. Because the tighter pore structure of BSM sponges, when ZnONP content was increased (as seen in Figure 4.2), cause the difficulty to release water from its structure, leading to the higher water retention capacity. This results also agree with Z. Lu and co-workers who studied microporous chitosan-Ag/ZnO composite dressing [41].

4.1.4 Effect of ZnONP on mechanical properties of BSM hydrogel sponge

The effect of ZnONP on stress at maximum load, Young' s modulus and percentage strain at maximum load of BSM hydrogel sponge were shown in Figure 4.4 (see Appendix C for raw data).

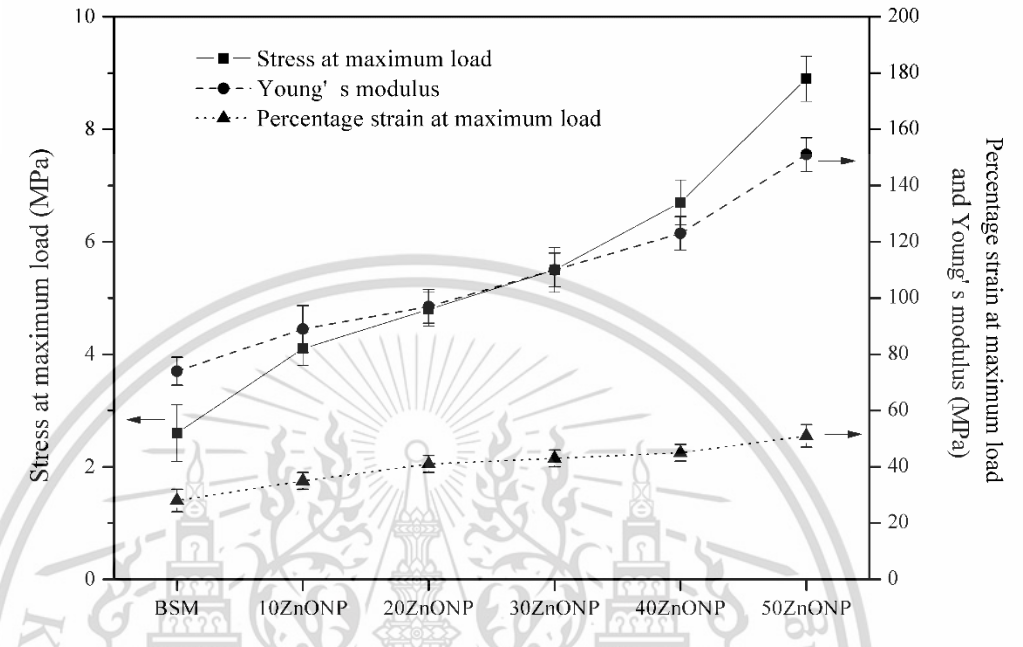

Figure 4.4 Stress at maximum load, Young's modulus and percentage strain at maximum load of BSM hydrogel sponges incorporated with various ZnONP contents

From Figure 4.4, stress at maximum load, Young's modulus and percentage strain of BSM hydrogel sponge were 2.6 MPa, 74 MPa and 28%, respectively. Moreover, the mechanical properties of BSM hydrogel sponges were greatly improved by increasing ZnONP content. BSM hydrogel sponge incorporated with 50wt% ZnONP showed the highest stress at maximum load (8.9 MPa), Young's modulus (151 MPa) and strain at maximum load (51%). This may be caused by the shorter distance between BSM layers and the tighter network structure as seen in SEM image (Figure. 4.2), resulting in a stronger interaction between layers. Futhermore, the stacked-like structure after the incorporation of ZnONP caused high percentage strain at maximum load in the same direction with the stacked-like structure of BSM hydrogel sponge. In addition, the hydrogen bonding and electrostatic interaction between ZnONP and BSM matrix resulted in a greater stress transfer of the nanoparticles' mechanical properties to the matrix. Furthermore, ZnONP also acted as a good reinforcing agent because of its high strength and high surface area, as well as its uniform distribution in the BSM matrix (Figure 4.3).

4.1.5 Effect of ZnONP on thermal properties of BSM hydrogel sponge

Thermal properties of BSM hydrogel sponge incorporated with various ZnONP contents were characterized by thermogravimetric (TGA) and derivative thermogravimetric (DTG) analysis (see Appendix D for raw data). Figure 4.5 and Table 4.4 show TGA and DTG thermograms of BSM hydrogel sponges incorporated with various ZnONP contents. Four thermal degradation steps were observed. The first step, between 35-100°C, was related to moisture vaporization. The second step, at 120-210°C, was associated with thermal degradation of glycerol in BSM hydrogel sponge. The main (third) step, approximately at 255-340 °C, was arisen from thermal degradation of glucomannan, xylan and other polysaccharides in the hemicellulose in BSM molecules [42, 46]. The forth step, at 410-460°C, was caused by the thermal decomposition of cellulose and lignin in BSM [42, 46].

Moreover, the decomposition temperature of BSM hydrogel sponge significantly shifted to higher temperature (3rd step), after ZnONP was added into the sponge. Also, percentages of weight loss at 3rd step were decreased with the increase of ZnONP. These are attributed to hydrogen bonding and electrostatic interaction between hydroxy groups of BSM with polar segments of ZnONP. This is clearly that the incorporation of ZnONP improved the thermal stability of the BSM hydrogel sponges. Similar observations were found in agar/carrageenan/carboxymethylcellulose films incorporated with ZnONP [47]. However, there was no significant difference in thermal decomposition temperature when ZnONP content was increased.

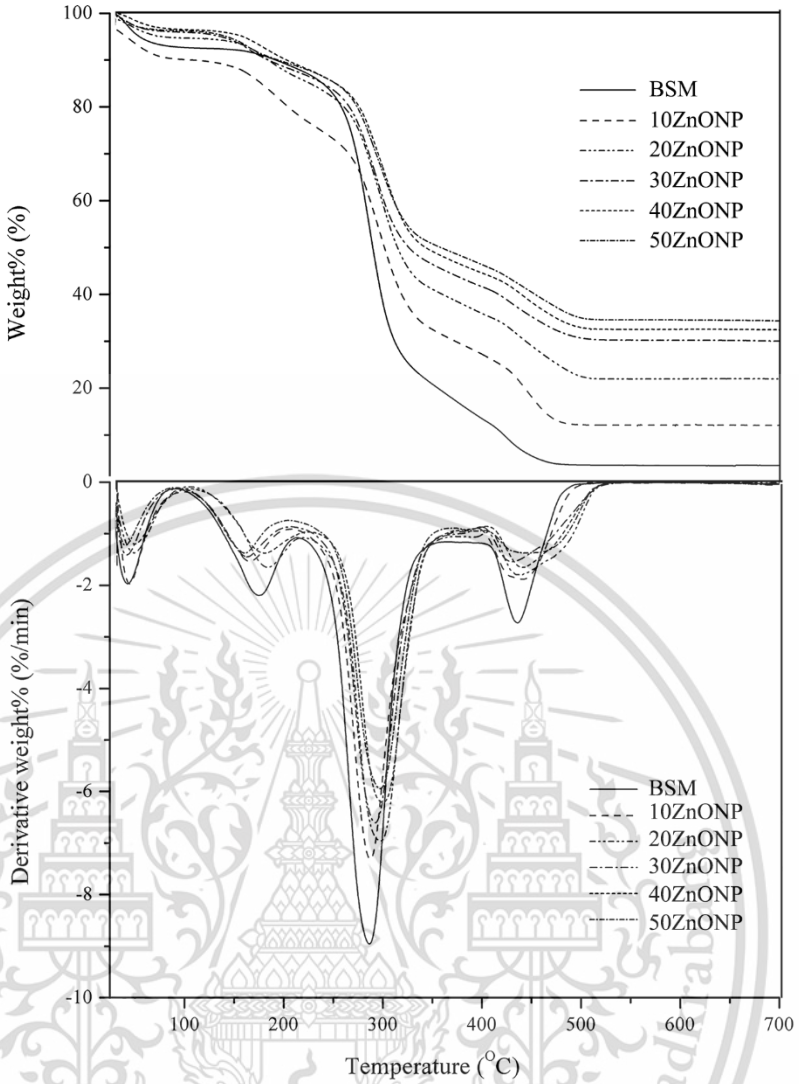

Figure 4.5 TGA and DTG curves of BSM hydrogel sponges incorporated with various ZnONP contents

Table 4.4 Decomposition temperatures and residual weight percentage of BSM hydrogel sponge incorporated with various ZnONP contents obtained from TGA and DTG thermograms

Sample	Decomposition temperature (°C)				Residues
	1st step	2nd step	3rd step	4th step	(%)
BSM	43.3	180.4	287.2	425.1	3.1
10ZnONP	50.3	195.2	295.1	445.1	13.4
20ZnONP	49.5	184.2	297.7	441.7	23.3
30ZnONP	41.1	162.8	295.2	445.2	30.1
40ZnONP	49.5	179.1	299.4	441.7	32.6
50ZnONP	40.2	161.5	299.7	445.7	34.8

4.1.6 Effect of ZnONP on antibacterial activity of BSM hydrogel sponge

The ability of BSM hydrogel sponge as an effective wound dressing was evaluated against two representatives of bacteria commonly found in a wound; *S. aureus* (Gram-positive) and *E.coli* (Gram-negative).

Table 4.5 Zone of inhibition of BSM hydrogel sponges incorporated with various ZnONP content for *E. coli* and *S. aureus*

Sample	Zone of inhibition (mm)	
	E. coli	*S. aureus*
0	Inactive	Inactive
10	Inactive	14.4± 0.07
20	Inactive	15.7± 0.05
30	15.3± 0.04	15.9± 0.08
40	15.5± 0.03	16.2± 0.04
50	15.9± 0.03	16.7± 0.06

Table 4.5 and Figure 4.6 show antibacterial activity of BSM hydrogel sponge incorporated with various ZnONP contents. It was found that BSM hydrogel sponge without the incorporation of ZnONP exhibited no antibacterial activity. Moreover, after the incorporation of ZnONP, BSM hydrogel sponges tended to show effective antibacterial activity against both *S. aureus* and *E.coli*. The proposed mechanism of ZnONP antibacterial activity, involves the production of reactive oxygen species, which elevates membrane lipid peroxidation that causes membrane leakage and reduces DNA, proteins and cell viability. Another proposed mechanism for ZnONP antibacterial activity explains that ZnONP can also bind on bacterial surface via the electrostatic forces [45]. Moreover, the diameter of the inhibition zone for *S. aureus* was 14.4 mm. for 10ZnONP BSM hydrogel sponge and increased to 16.7 mm for 50ZnONP BSM hydrogel sponge. For *E.coli*, the inhibition zone was initially measured at 15.5 mm for 30ZnONP BSM hydrogel sponge and slightly increased to 15.9 mm with 50ZnONP BSM hydrogel sponge. The higher antibacterial activity against *S. aureus* vs *E. coli* were also observed in xanthan-based hydrogel embedded ZnONP and agar, carrageenan and CMC films with ZnONP [14, 47]. This observation was due to the difference in Gram-positive and Gram-negative bacteria cell wall structures. Generally, Gram-positive bacteria cell wall is composed of thick layers of peptidoglycan, while Gram-negative bacteria cell wall is a complex multilayered structure that serves to protect these organism from unpredictable environment [11].

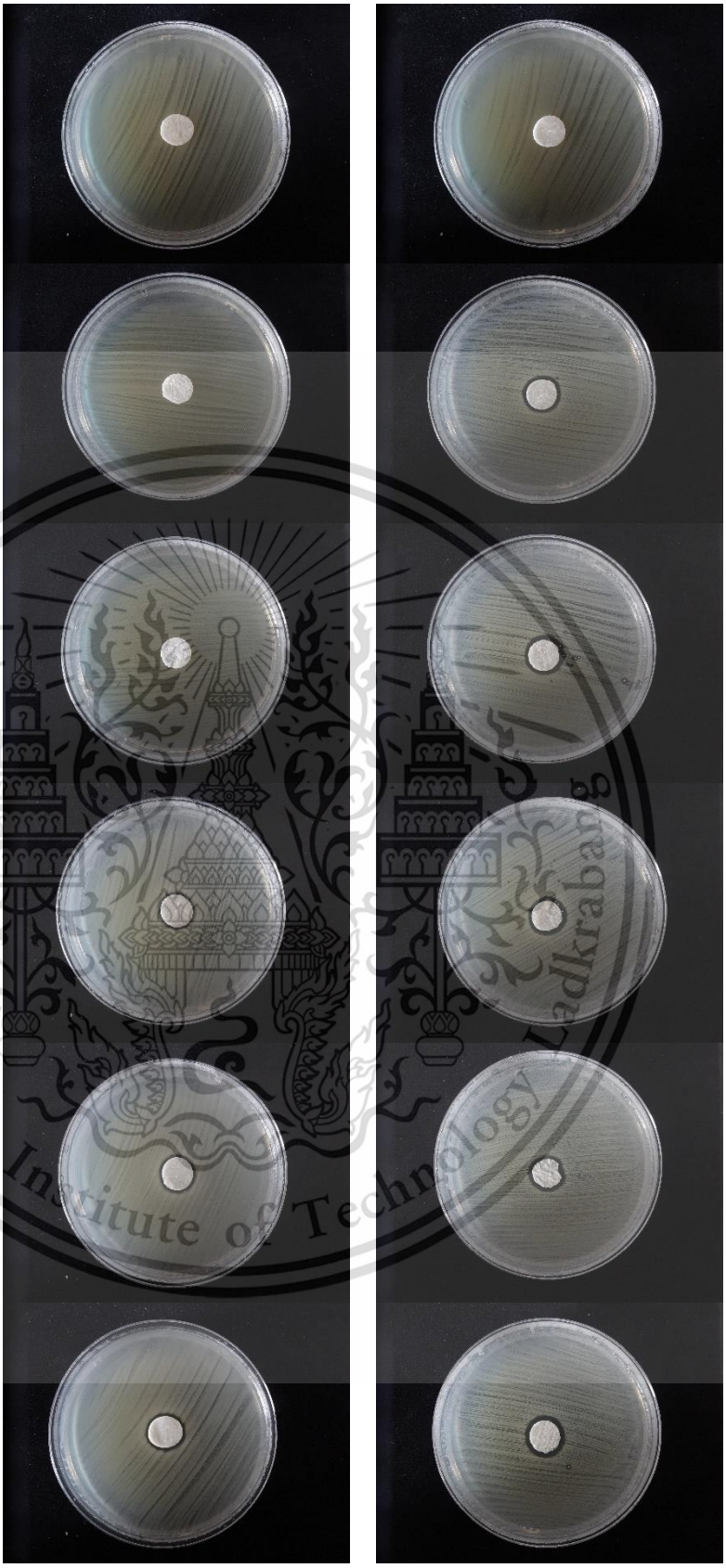

Figure 4.6 Inhibition zone of BSM hydrogel sponges incorporated with various ZnONP contents; *E.coli* (left) and *S. aureus* (right)

4.1.7 Effect of ZnONP on cytotoxicity of BSM hydrogel sponge

Since the incorporation of ZnONP into BSM hydrogel sponge may cause a toxic effect with human skin, the cytotoxicity of BSM hydrogel sponge incorporated with various ZnONP contents was assessed and compared to a negative control by MTT assay with human keratinocytes (HaCat) cells.

The *in vitro* cytotoxicity study of BSM hydrogel sponge with different ZnONP contents was shown in Figure 4.7.

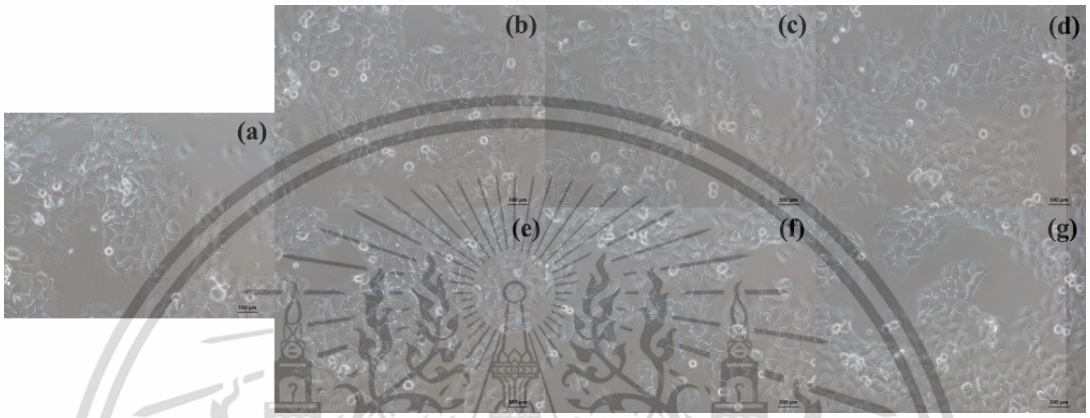

Figure 4.7 Optical microscopy images (200× magnification) of the control and BSM hydrogel sponges incorporated with various ZnONP contents: (a) negative control (b) BSM, (c) 10ZnONP, (d) 20ZnONP, (e) 30ZnONP, (f) 40 ZnONP and (g) 50ZnONP

It was observed in Figure 4.7 that there were no significant differences between the control cells (Figure 4.7 (a)) and all of BSM hydrogel sponge (Figure 4.7 (b)- (g)). There was no morphological hallmark, for example, nuclear fragmentation, chromatin condensation or chromatin fragmentation. Thus, it can be concluded that BSM sponges incorporated with ZnONP were not toxic to human keratinocytes cells.

4.2 Effect of crosslinking agents and their contents on various properties of BSM hydrogel sponge

This section reported on the effect of crosslinking reaction by borax and STMP/STPP and their contents (0-20 wt%) on various properties of BSM hydrogel sponge. The effect of different crosslinking agents (borax and STMP/STPP) and their contents (0-20 wt%) were investigated on morphology, thickness, porosity, water retention capacity, degree of swelling, dimensional stability, mechanical properties, thermal properties, antibacterial activity and also cyctotoxicity of BSM hydrogel sponge. Additionally, the crosslinked BSM hydrogel sponges by borax or STMP/STPP incorporated with different ZnONP contents (30 and 50 wt%) were prepared and also studied.

For the proposed mechanism of BSM crosslinking, the hydroxyl groups in BSM molecules at the C-2, C-3 or C-6 positions could react with crosslinking agents (borax or STMP/STPP) to form three-dimensional crosslinked network structure.

In case of borax crosslinking, borax dissociates to boric acid and borate ions in aqueous medium as suggested by Sarika et al. (Figure 4.8) [43].

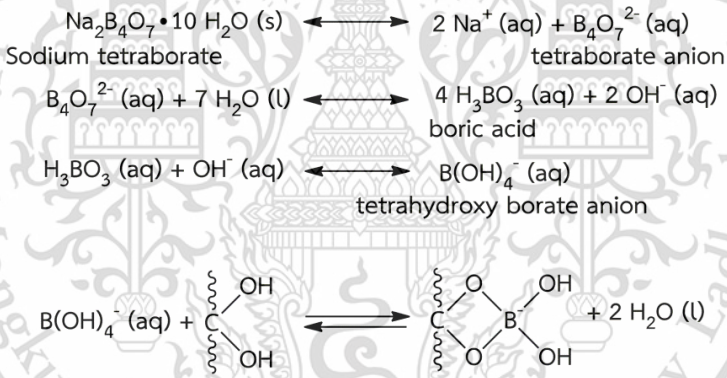

Figure 4.8 The schematic representation for synthesis of BSM hydrogel sponge

Borate can crosslink with the hydroxyl groups at C-2, C-3 and C-6 of polysaccharides in BSM, i.e. glucomannan, the major component in BSM and form coordinate covalent bond between boron and oxygen atoms (Figure 4.8). This mechanism was also reported for other polysaccharides crosslinked with borax, i.e. guar gum and starch [18, 43]. Figure 4.9 (a) shows the possible chemical structure of BSM hydrogel sponge crosslinked with borax. Figure 4.9 (b) shows BSM hydrogel sponge crosslinked with borax and incorporated with ZnONP. It can be seen that both three-dimensional crosslinked network structure after crosslinking and the interaction between BSM and ZnONP (section 4.1) cause the improvement of BSM structure which affect various properties.

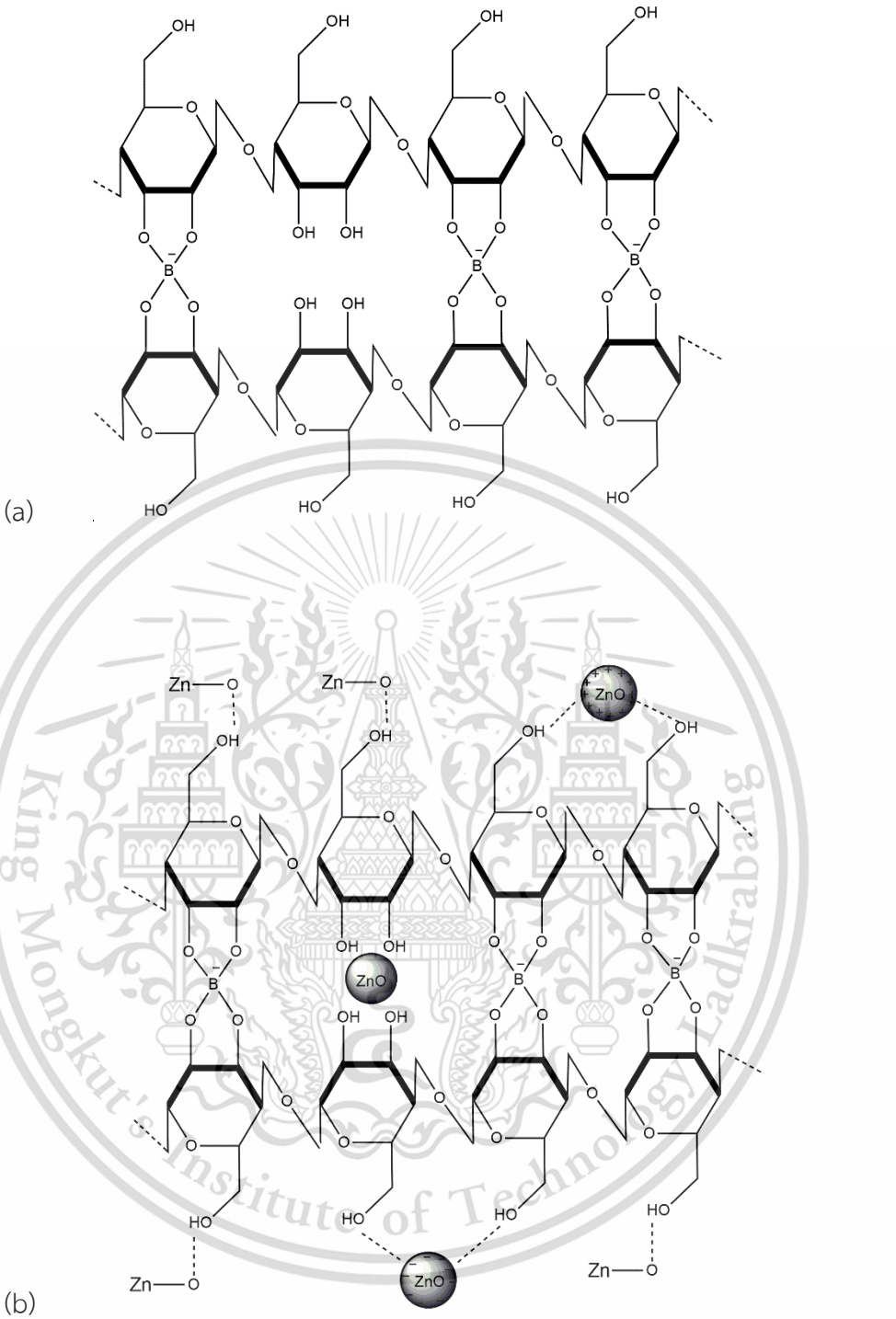

Figure 4.9 The possible schematic representation for synthesis of BSM hydrogel sponge: (a) crosslinked with borax and (b) crosslinked with borax and incorporated with ZnONP

On the other hand, for STMP/STPP crosslinking, phosphate can generally crosslink with two hydroxyl groups of BSM molecule as seen in Figure 4.10. Moreover, possible crosslinked BSM and ZnONP interaction was shown in Figure 4.10 (b). Electrostatic interaction and also hydrogen bonding between two components can be occurred.

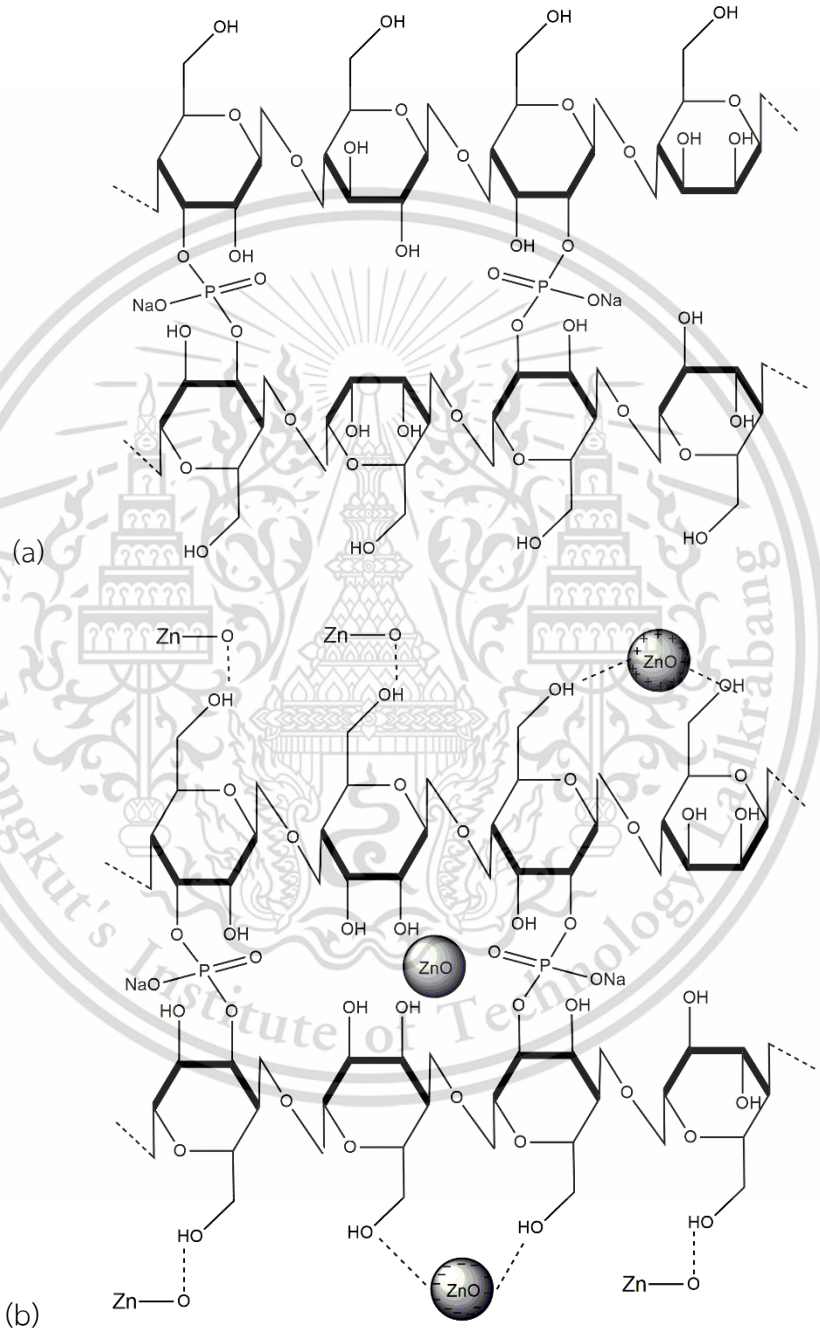

Figure 4.10 The possible schematic representation for synthesis of BSM hydrogel sponge: (a) crosslinked with STMP/STPP and (b) crosslinked with STMP/STPP and incorporated with ZnONP

4.2.1 Effect of different crosslinking agents and their contents on morphology of BSM hydrogel sponge

Effect of different crosslinking agents and their contents on morphology of BSM hydrogel sponge was shown in Figures 4.11 - 4.14. It is clear that all BSM hydrogel sponges showed a uniform interconnected opened-cell structure. For borax crosslinking, it was observed from Figures 4.11 and 4.12 that the increase in borax crosslinking agent content created smaller cells and a more compact pore structure. This may attributed to the effect of crosslinking between hydroxyl groups of BSM and borax (Figure 4.9 (a)), resulting in a decrease in free volume and mobility of polysaccharide chains in the BSM. A similar change in morphology after crosslinking has also been reported for crosslinked starch-borax sponge [8]. Furthermore, it was seen that, the pore structure became a slightly tighter network after the addition of ZnONP (Figure 4.11). This was caused by electrostatic interaction and hydrogen bonding, between polar segments of BSM and ZnONP (Figure 4.9 (b)), resulted in the decrease of free hydroxyl groups able to interact with water. Moreover, Figure 4.12 shows 10,000× SEM cross section images of BSM hydrogel sponges crosslinked with borax and incorporated with ZnONP. A rougher surface is evident for sponges crosslinked with higher borax loading (Figure 4.12 (a-d)). This is a consequnce of a decrease in chain mobility of BSM after crosslinking. Additionally, ZnONP was seen to distribute evenly over BSM matrix for the 20BO30ZnONP and also the 20BO50ZnONP (Figure 4.12 (e) and 4.12 (f)).

Figures 4.13 and 4.14. present the effect of STMP/STPP crosslinking and its content on morphology of BSM hydrogel sponge. STMP/STPP crosslinking and its content were shown in the same way with borax crosslinking. The increase in STMP/STPP content as well as ZnONP resulted in the decrease in pore size and tighter network (Figure 4.13). This was due to the effect of crosslinking between hydroxyl groups of BSM and STMP/STPP and also electrostatic interaction and hydrogen bonding, between polar segments of BSM and ZnONP (Figure 4.10). In addition, high magnification of SEM images (10,000×) in Figure 4.14 show a good distribution of ZnONP over BSM matrix (see EDS mapping images in Appendix A).

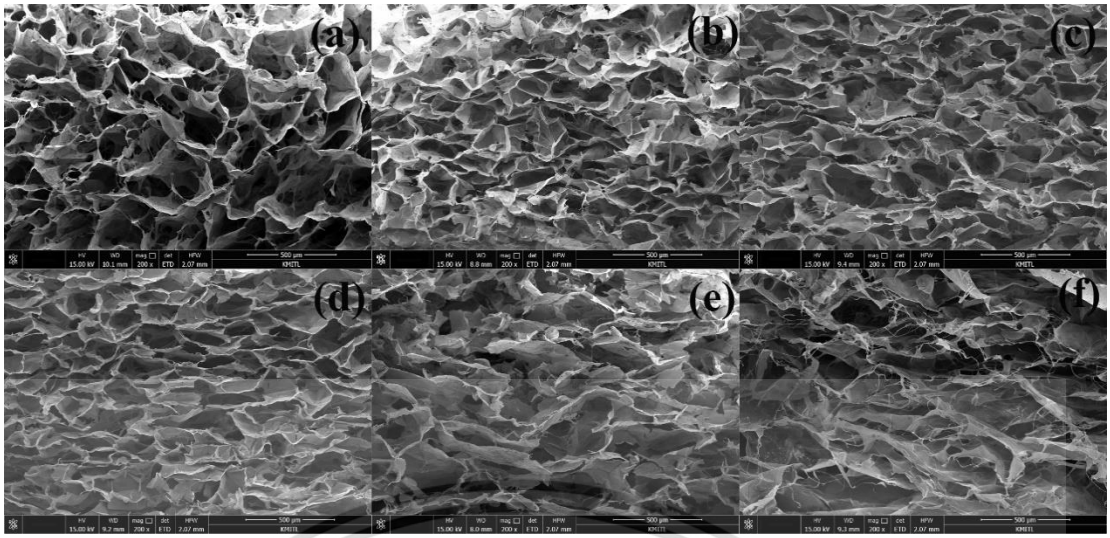

Figure 4.11 SEM cross section images (200×magnification) of BSM hydrogel sponges with various borax and ZnONP contents: (a) BSM (b) 5BO, (c) 10BO, (d) 20BO, (e) 20BO30ZnONP and (f) 20BO50ZnONP

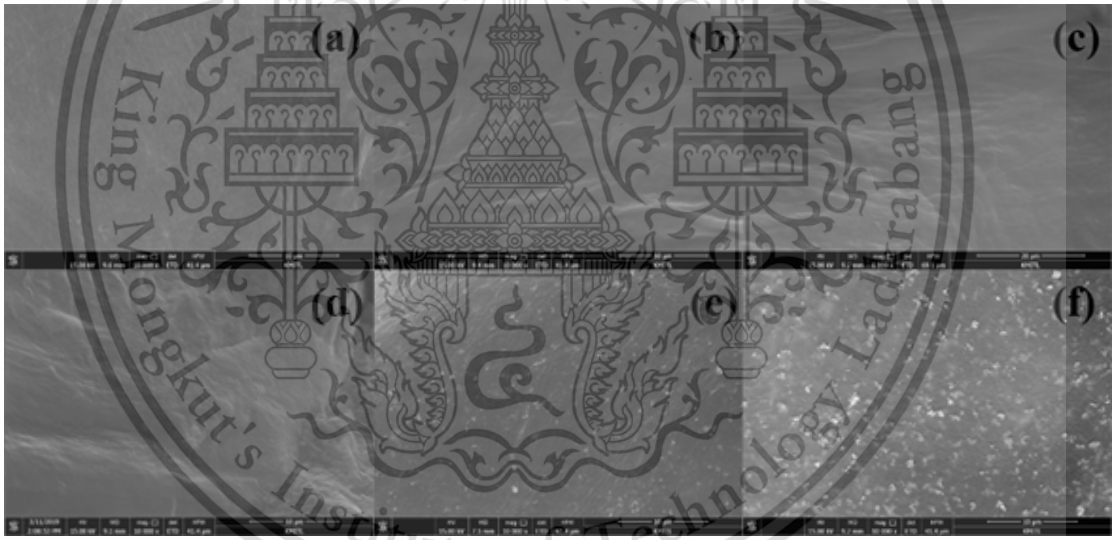

Figure 4.12 SEM cross section images (10,000×magnification) of BSM hydrogel sponges with various borax and ZnONP contents: (a) BSM (b) 5BO, (c) 10BO, (d) 20BO, (e) 20BO30ZnONP and (f) 20BO50ZnONP

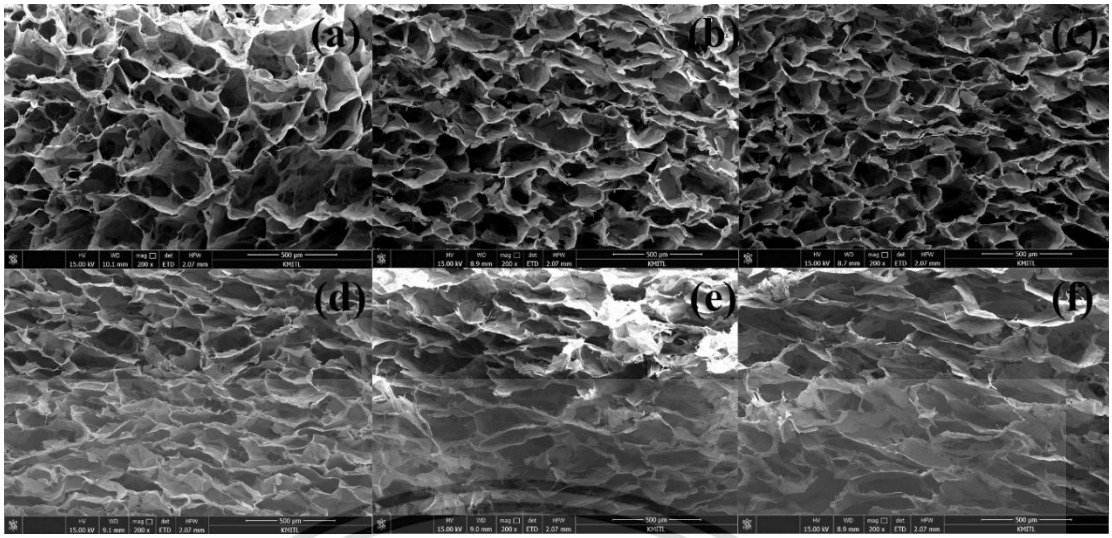

Figure 4.13 SEM cross section images (200×magnification) of BSM hydrogel sponges with various STMP/STPP and ZnONP contents: (a) BSM (b) 5ST, (c) 10ST, (d) 20ST, (e) 20ST30ZnONP and (f) 20ST50ZnONP

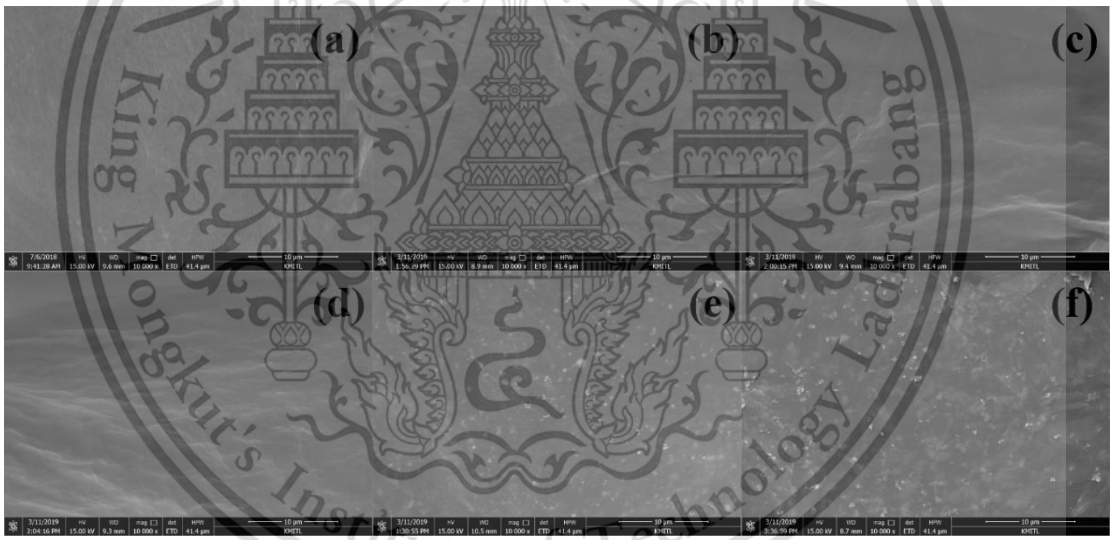

Figure 4.14 SEM cross section images (10,000×magnification) of BSM hydrogel sponges with various STMP/STPP and ZnONP contents: (a) BSM (b) 5ST, (c) 10ST, (d) 20ST, (e) 20ST30ZnONP and (f) 20ST50ZnONP

4.2.2 Effect of different crosslinking agents and their contents on thickness, porosity and water retention capacity of BSM hydrogel sponge

The effect of borax or STMP/STPP crosslinking agents and their contents as well as ZnONP on thickness and porosity of BSM hydrogel sponge was shown in Table 4.6. It was found that the tighter structure of the pores after crosslinking and the addition of ZnONP affected the thickness and porosity of BSM hydrogel sponge (Figures 4.10 and 4.12). Unmodified BSM hydrogel sponge prepared without any crosslinking agent and ZnONP was shown the thickest and the highest porosity. The addition of borax and ZnONP decreased the thickness (1.53 mm to 1.34 mm) and porosity (92% to 73%). Also, the addition of STMP/STPP and ZnONP decreased the thickness (1.53 mm to 1.36 mm) and porosity (92% to 73.6%). Furthermore, there was no significant difference between the effect of borax and STMP/STPP crosslinking agents on thickness and porosity of BSM hydrogel sponge.

Table 4.6 Thickness, porosity and water retention capacity of BSM hydrogel sponge crosslinked with different crosslinking agents and incorporated with ZnONP

Sample	Thickness (mm)	Porosity (%)	Water retention capacity (%)
BSM	1.53 ± 0.23^{a}	92.1^{a}	31.2^{a}
5BO	1.44 ± 0.11^{b}	89.1^{b}	38.7^{b}
10BO	1.41 ± 0.03^{c}	85.8^{c}	$39.2^{b,c}$
20BO	1.42 ± 0.06^{c}	82.3^{d}	39.9^{c}
20BO30ZnONP	1.39 ± 0.07^{c}	76.5^{e}	$40.7^{c,d}$
20BO50ZnONP	1.34 ± 0.05^{d}	73.3^{f}	41.3^{d}
5ST	1.46 ± 0.08^{b}	88.8^{b}	38.4^{b}
10ST	1.42 ± 0.05^{c}	86.1^{c}	$40.3^{b,c}$
20ST	1.41 ± 0.08^{c}	82.5^{d}	40.9^{c}
20ST30ZnONP	1.40 ± 0.04^{c}	77.1^{e}	$41.2^{c,d}$
20ST50ZnONP	1.36 ± 0.06^{d}	73.6^{f}	41.4^{d}

Different superscript letters in the same column are significantly different ($p<0.05$), based on Tukey's test.

The effect of different crosslinking agents and their contents on water retention capacity of BSM hydrogel sponge were also shown in Table 4.6. It was observed that unmodified sponge showed 31% water retention. Moreover, water retention of BSM hydrogel sponges increased slightly from 31 to ~40% after crosslinking with both borax and STMP/STPP and also adding of ZnONP. This was attributed to the tighter pore structure of the sponges after crosslinking and addition of ZnONP, which made it difficult to lose water from the sponge structure, as shown in SEM images (Figures 4.11

and 4.13). It is another key property for a wound dressing, which should keep the environment at the wound surface moist [48].

4.2.3 Effect of different crosslinking agents and their contents on degree of swelling and dimensional stability of BSM hydrogel sponge

Degree of swelling and dimensional stability of hydrogel sponge are important parameters for wound dressing application. Also, these results can confirm the efficiency of crosslinking reactions. The degree of swelling of BSM hydrogel sponge was investigated by immersing a sample in distilled water at the period of 48 h. The degree of swelling of each BSM hydrogel sponge was presented in Table 4.7. The unmodified BSM hydrogel sponge showed the highest degree of swelling (109). This was due to the hydrophilic nature of BSM molecules which contains the main composition of glucomamnan. Glucomannan is composed of many hydroxyl groups, which can interact strongly with water. However, degree of swelling was clearly decreased after crosslinked with borax or STMP/STPP (from 109 to ~60). This result was because the hydrophilic hydroxyl groups in BSM molecules were depleted by crosslinking process. Some hydroxyl groups of BSM reacted with crosslinking agents (borax and STMP/STPP) leading to a decrease in hydroxyl groups available to interact with water. When considering the influence of crosslinking agents on degree of swelling, it was observed that BSM hydrogel sponges crosslinked with borax showed lower degree of swelling than BSM hydrogel sponges crosslinked with STMP/STPP at the same content. This could be because of lower crosslinking efficiency of STMP/STPP compared with borax: STMP/STPP could react with two hydroxyl groups of BSM molecules, while borax could react with up to four hydroxyl groups of BSM molecules as seen in Figures 4.9 and 4.10. It could be stated that BSM hydrogel sponges crosslinked with borax showed higher crosslink density than BSM hydrogel sponges crosslinked with STMP/STPP at the same content. This result was also related to the work of Y. Tanetrungroj *et.al.* (2019) who studied crosslinking reaction between starch and borax or STMP/STPP [49].

Table 4.7 Degree of swelling and dimensional stability of BSM hydrogel sponge crosslinked with different crosslinking agent and incorporated with ZnONP

Sample	Degree of swelling	Swelling time (h)	Dimension variation (mm)		
			Width	Length	Thickness
BSM	109 ± 2	24	2.4±0.61^{a}	2.6±0.43^{a}	N/A*
		48	N/A*	N/A*	N/A*
5BO	82 ± 3	24	1.2±0.1^{b,A}	1.1±0.15^{b,A}	0.7±0.13^{b,A}
		48	1.6±0.41^{A}	1.4±0.21^{A}	0.8±0.22^{A}
10BO	74 ± 2	24	0.9±0.19^{b,A}	0.8±0.22^{b,A}	0.6±0.14^{b,A}
		48	1.2±0.34^{A}	1.1±0.43^{A}	0.7±0.18^{A}
20BO	65 ± 4	24	0.3±0.06^{c,A}	0.3±0.12^{c,A}	0.2±0.04^{c,A}
		48	0.4±0.09^{A}	0.3±0.07^{A}	0.3±0.11^{A}
20BO30ZnONP	60 ± 1	24	0.4±0.11^{c,A}	0.3±0.13^{c,A}	0.2±0.11^{c,A}
		48	0.4±0.05^{A}	0.4±0.07^{A}	0.3±0.05^{A}
20BO50ZnONP	56 ± 2	24	0.3±0.12^{c,A}	0.3±0.15^{c,A}	0.2±0.11^{c,A}
		48	0.3±0.06^{A}	0.4±0.05^{A}	0.3±0.02^{A}
5ST	87 ± 3	24	1.5±0.2^{b,A}	1.5±0.2^{b,A}	0.7±0.15^{b,A}
		48	1.8±0.31^{A}	1.8±0.13^{A}	0.7±0.12^{A}
10ST	80 ± 2	24	1.2±0.24^{b,A}	0.9±0.32^{b,A}	0.6±0.21^{b,A}
		48	1.4±0.43^{A}	1.3±0.36^{A}	0.7±0.15^{A}
20ST	72 ± 3	24	0.6±0.07^{c,A}	0.6±0.14^{c,A}	0.3±0.03^{c,A}
		48	0.5±0.07^{A}	0.5±0.05^{A}	0.3±0.14^{A}
20ST30ZnONP	65 ± 2	24	0.6±0.10^{c,A}	0.6±0.24^{c,A}	0.3±0.08^{c,A}
		48	0.4±0.05^{A}	0.3±0.12^{A}	0.3±0.07^{A}
20ST50ZnONP	60 ± 2	24	0.4±0.22^{c,A}	0.4±0.07^{c,A}	0.2±0.06^{c,A}
		48	0.3±0.25^{A}	0.3±0.02^{A}	0.3±0.05^{A}

Reported values are mean±standard deviation. Different superscript letters (a-d) in the same column are significantly different ($p<0.05$) between each sample, different letters (A-B) are significantly different ($p<0.05$) between the same sample at different swelling times, based on Tukey's test

*N/A: not available

In spite of the highest degree of swelling of unmodified BSM hydrogel sponge, it showed the lowest dimensional stability which is not appropriate property for wound dressing (Table 4.7). The dimensions of unmodified BSM hydrogel sponge could not be measured accurately after 24 h, because some edges and outer surfaces of the sponge were partially dissolved by water. As expected, after crosslinking, the increased borax and STMP/STPP content resulted in an improvement of dimensional stability (see Appendix B for raw data of dimensional stability). This was caused by crosslinking

between hydroxyl groups of polysaccharide molecules in BSM and both crosslinking agents leading to a decrease in hydroxyl groups available to interact with water. Moreover, the crosslinking reaction also enhanced the stabilization of BSM molecules. Further, the decrease in porosity, after crosslinking, contributed to lower degree of swelling. From the decrease in degree of swelling and better dimensional stability, this can confirm crosslinking reaction between borax or STMP/STPP and BSM molecules. Additionally, there was no significant difference between the effect of borax and STMP/STPP crosslinking agents on dimensional stability of BSM hydrogel sponge.

The effect of ZnONP on degree of swelling and dimensional stability of BSM hydrogel sponge is also shown in Table 4.7. It was observed that an increase of ZnONP content resulted in slightly decreased degree of swelling of the sponge. This was attributed to the hydrogen bonding and electrostatic interaction between BSM molecules and ZnONP (Figures 4.9 and 4.10). Additionally, voids in BSM network could be filled with high content of ZnONP; therefore, network expansion and water penetration could be restricted. Similar observation was founded in xanthan gum-ZnONP sponge [14]. Although, lower swelling was found by the incorporation of crosslinking agents (borax or /STMP/STPP) and ZnONP, the dimensional stability of BSM hydrogel sponges could be improved.

4.2.4 Effect of different crosslinking agents and their contents on mechanical properties of BSM hydrogel sponge

The effect of different crosslinking agents and their contents on stress at maximum load, Young's modulus, and strain at the maximum load of BSM hydrogel sponge were illustrated in Figures 4.15 and 4.16.

It was found that an increasing in crosslinking agent contents resulted in the increased in all mechanical properties, i.e., stress at maximum load, Young's modulus and also percentage strain at maximum load (see Appendix C for raw data). These mechanical properties were improved by the increase of crosslinking density between both of crosslinking agent and hydroxyl group of polysaccharide molecules in BSM as shown in Figures 4.9 and 4.10. In addition, the tighter network structure and the decreased distance between the BSM sponge layers after crosslinking is clear in the SEM images (Figures 4.11 and 4.13), resulted in stronger layer to layer interactions. The improvement of mechanical properties by borax crosslinking was also found by Tavakoli (2017) [8].

Furthermore, the increase of stress at maximum load, Young's modulus and percentage strain of BSM hydrogel sponge by the incorporation of ZnONP was observed. ZnONP acted as a good reinforcement due to its high strength and large surface area as well as the good distribution of ZnONP in BSM hydrogel sponge (as seen in Figures 4.12 and 4.14). Additionally, the electrostatic interaction and hydrogen bond between ZnONP and BSM matrix resulted in the greater transfer of the nanoparticle mechanical properties to the matrix.

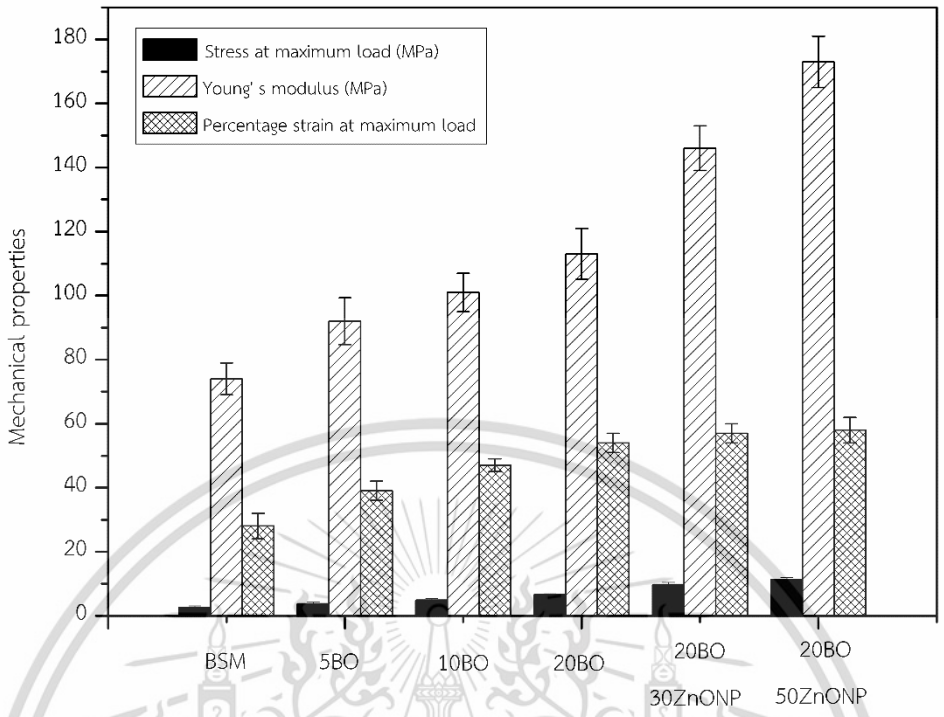

Figure 4.15 Mechanical properties of BSM hydrogel sponges with various borax and ZnONP contents

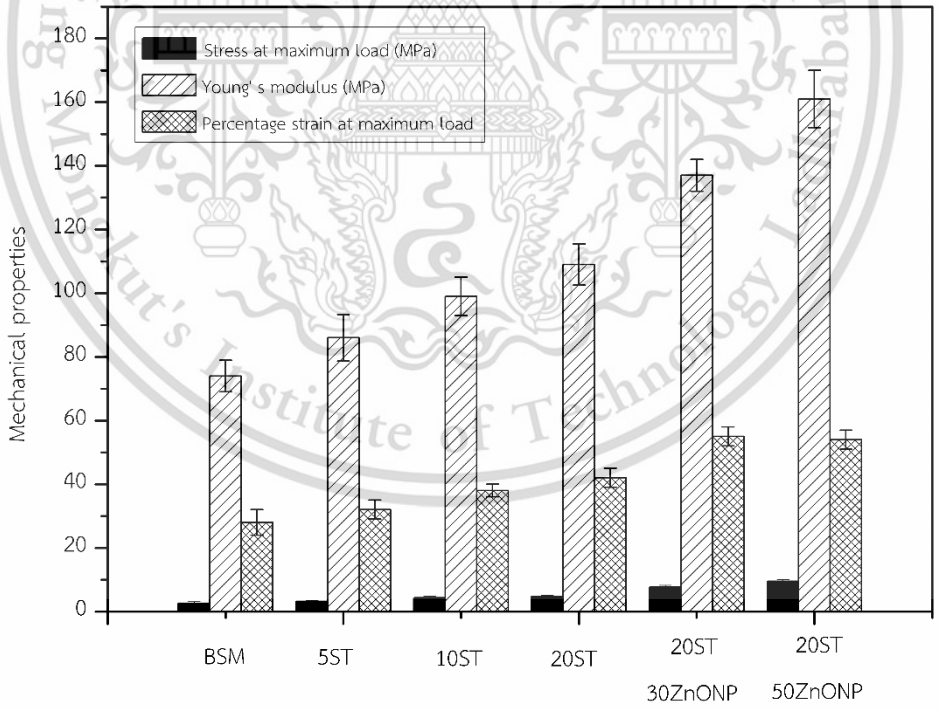

Figure 4.16 Mechanical properties of BSM hydrogel sponges with various STMP/STPP and ZnONP contents

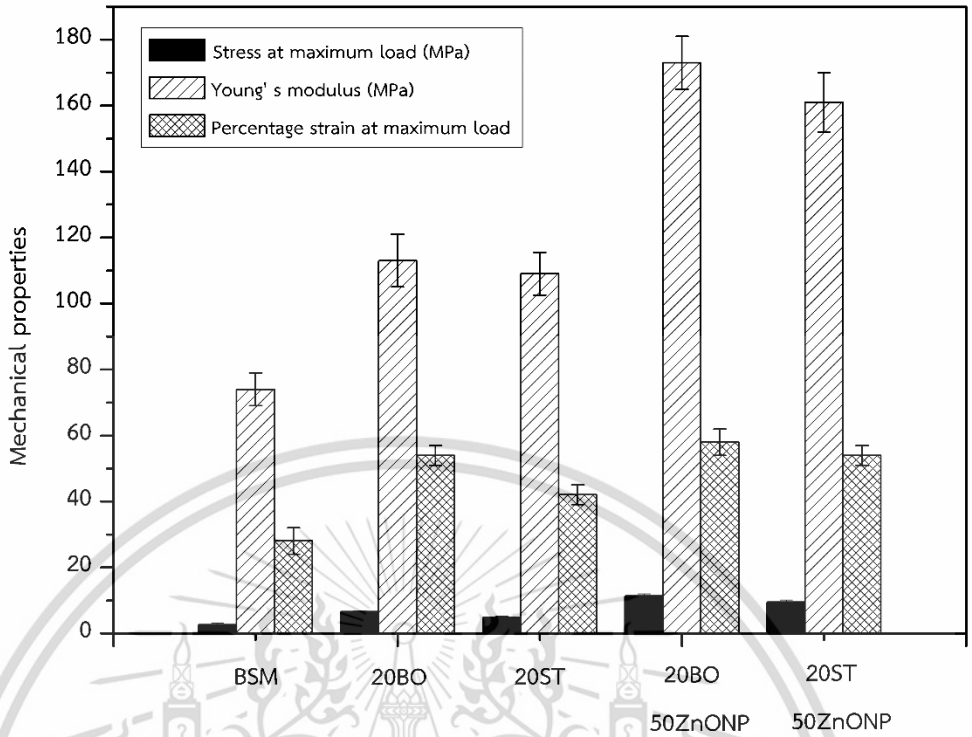

Figure 4.17 Mechanical properties of BSM hydrogel sponges with various crosslinking agents incorporated with ZnONP

Figure 4.17 presents a comparison of mechanical properties between different types of cross-linking agents. BSM hydrogel sponge crosslinked with borax showed slightly higher mechanical properties than those of crosslinked with STMP/STPP. This result was related to the lower crosslinking density of STMP/STPP than borax as shown in Figures 4.9 and 4.10. Borax could react with up to four hydroxyl groups of BSM molecules. While STMP/STPP could react with two hydroxyl groups of BSM molecules because of its steric hindrance. These results were consistent with water retention capacity, degree of swelling and dimensional stability of BSM hydrogel sponges (Tables 4.6 and 4.7). As a result, it can be stated that borax or STMP/STPP crosslinking and the incorporation of ZnONP could promote better mechanical properties of BSM hydrogel sponge.

4.2.5 Effect of different crosslinking agents and their contents on thermal properties of BSM hydrogel sponge

The effect of different crosslinking agents and their contents on thermal properties of BSM hydrogel sponge were investigated by the TGA technique in the temperature range of 50-600˚C under a nitrogen atmosphere at the heating rate of 10˚C/min in order to determine the maximum degradation temperature. TGA and DTG curves of BSM hydrogel sponges crosslinked with different crosslinking agents were shown in Figures 4.18 and 4.19. Moreover, decomposition temperatures and residual weight percentage of BSM hydrogel sponge were presented in Table 4.8 (see Appendix D for raw data).

It was illustrated that, for the unmodified sponge, four thermal degradation stages were found. The initial step in the ranges of 35 and 100 °C was due to the loss of moisture from the sponge. The second stage at 120 to 210 °C was caused by the decomposition of glycerol plasticizer. The main (third) degradation stage at 255-287 °C was due to the decomposition of the polysaccharides (glucomannan, xylan, etc) of hemicellulose in BSM [46, 50-51]. The fourth stage decomposition at 400 – 460 °C was attributed to cellulose and lignin in BSM composition [46, 50]. In addition, it was observed that decomposition temperature significantly shifted to higher temperature and the residual weight percentage increased when crosslinking agents (borax or STMP/STPP) contents were increased. This was because of the crosslinking reaction between crosslinking agents and numerous hydroxyl groups of the polysaccharides in BSM (Figures 4.9 and 4.10), leading to the strong linkages and stronger BSM backbone chains.

By comparison, borax crosslinked BSM hydrogel sponges showed higher shifted of degradation temperature than STMP/STPP crosslinked BSM hydrogel sponges, at the same content. This can be explained by the lower crosslinking density of STMP/STPP as seen in Figure 4.11, providing lower thermal stability of STMP/STPP crosslinked sponges. Moreover, this was attributed to base hydrolysis from pH adjustment in STMP/STPP crosslinked BSM hydrogel sponge preparation. Especially, at high content of STMP/STPP, it showed that there were two main degradation steps of STMP/STPP crosslinked BSM hydrogel sponge, at ~280 °C (hydrolyzed BSM from pH adjustment) and 300-320 °C (crosslinked BSM) as seen in Table 4.8. This behavior was also related to the work of Y. Tanetrungroj *et al.* (2019) who studied crosslinking reaction between starch and borax and STMP/STPP [49]. Besides, these results clearly correspond to the water retention capacity, degree of swelling, dimensional stability and mechanical properties of BSM hydrogel sponges.

Conversely, the incorporation of ZnONP in crosslinked BSM hydrogel sponges resulted in the shift to slightly lower degradation temperatures than the crosslinked BSM hydrogel sponge without the addition of ZnONP. This may be caused by the interaction between ZnONP and BSM leading to lower free hydroxyl groups available to interact with crosslinking agents. Moreover, ZnONP is a good thermal conductor. Therefore, ZnONP transfers heat to BSM matrix, leading to the the lower degradation temperature of BSM. This phenomena was related with K. Sornsumdang' s work who studied crosslink stach filled with metal oxide particles [52]. However, all crosslinked BSM hydrogel sponges incorporated with ZnONP showed higher degradation temperature than that of unmodified BSM hydrogel sponge. This was attributed to electrostatic interaction and hydrogen bond between polar segment of BSM and ZnONP.

Accordingly, the significantly shifted of degradation temperature and the increased of residual weight loss indicated that the crosslinking with borax or STMP/STPP and the ZnONP incorporation could improve thermal stability of BSM hydrogel sponges.

Table 4.8 Decomposition temperatures and residual weight percentage of BSM hydrogel sponge crosslinked with different crosslinking agents and incorporated with ZnONP obtained from TGA and DTG thermograms

Sample	Decomposition temperature (°C)				Residues (%)
	1st step	2nd step	3rd step	4th step	
BSM	43.3	180.4	287.2	425.1	3.1
5BO	46.9	178.6	315.4	461.6	5.5
10BO	45.3	218.6	315.5	502.4	9.5
20BO	48.6	-	320.1	506.8	11.2
20BO30ZnONP	44.1	165.1	305.3	484.9	29.7
20BO50ZnONP	48.1	165.6	303.2	470.8	39.5
5ST	41.9	159.6	294.3	458.6	8.7
10ST	43.2	163.4	286.3 307.5	478.2	14.5
20ST	44.7	164.9	286.2 321.3	506.3	20.4
20ST30ZnONP	43.4	155.6	300.1	485.3	29.2
20ST50ZnONP	48.43	162.9	300.5	480.6	38.9

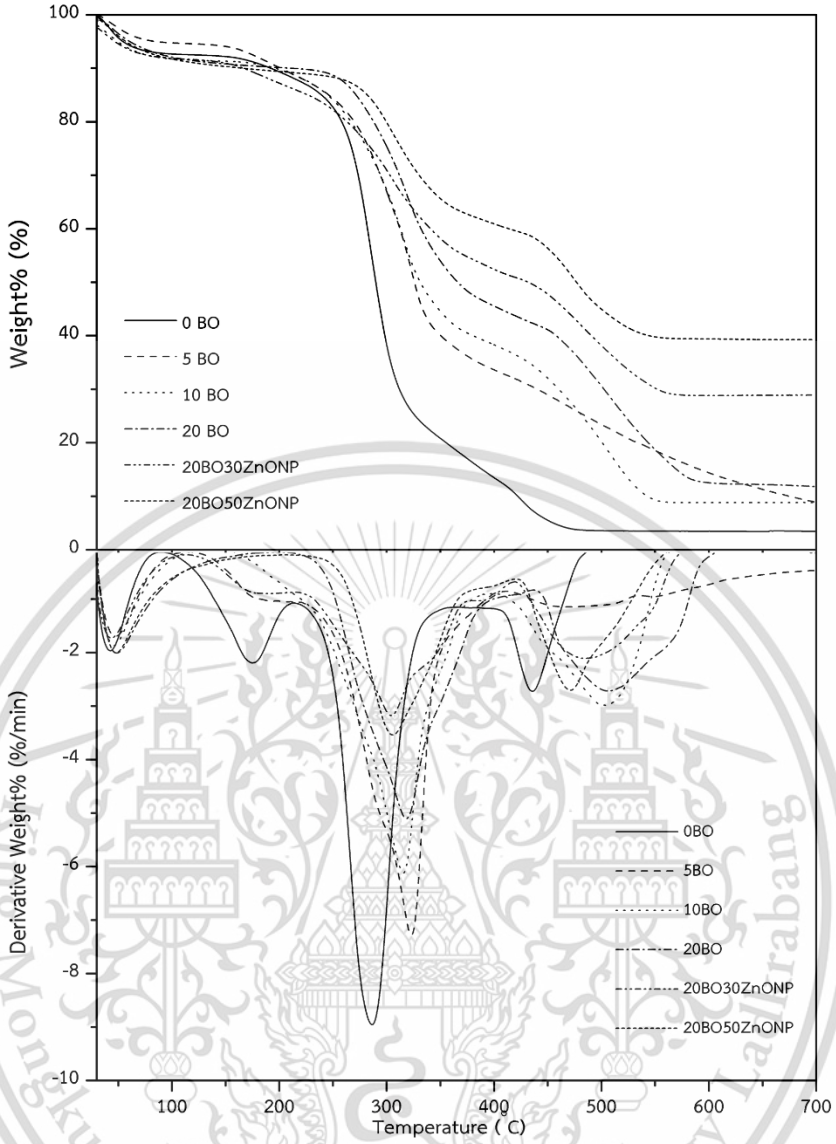

Figure 4.18 TGA and DTG curves of BSM hydrogel sponges crosslinked with various borax contents and incorporated with ZnONP

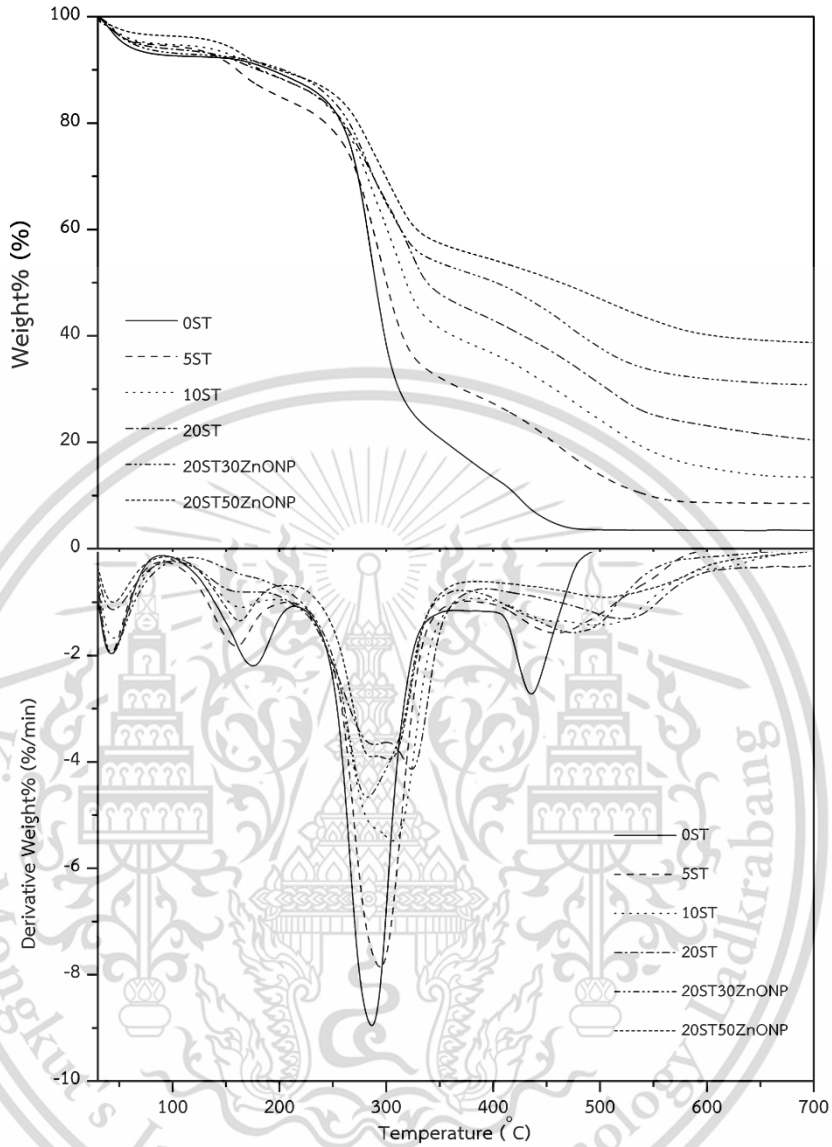

Figure 4.19 TGA and DTG curves of BSM hydrogel sponges crosslinked with various STMP/STPP contents and incorporated with ZnONP

4.2.6 Effect of different crosslinking agents and their contents on antibacterial activities of BSM hydrogel sponge

The effectiveness of BSM hydrogel sponges as wound dressings was assessed by measuring antibacterial activity against two bacteria commonly found in wounds - *S. aureus* (Gram-positive) and *E.coli* (Gram-negative). The antibacterial activities of different crosslinked BSM hydrogel sponges were shown in Table 4.9 and Figure 4.20-4.21. It was found that the incorporation of different crosslinking agents (borax and STMP/STPP) did not show any antibacterial activity of BSM hydrogel sponge. Nevertheless, the incorporation of ZnONP resulted in an improvement of antibacterial activity against both of *S. aureus* and *E.coli*. It was observed a slightly increased of antibacterial activities after ZnONP content was increased. Furthermore, greater antibacterial activities were observed against *S. aureus* than *E.coli.* This is likely due to differences in cell wall structures of both bacteria: Gram-positive bacteria possess thick cell walls of peptidoglycan; whereas, Gram-negative cell wall structures are more complex, and, thus, more resistant to attack by any antibacterial agent [11]. Several biomaterial incorporated with ZnONP, have shown similar behavior, for example, xanthan gum-based hydrogels and agar/carrageenan/CMC films [14, 47]. It can be mentioned that the crosslinking agents did not affect to any antibacterial property of BSM hydrogel sponge.

Table 4.9 *E. coli* and *S. aureus* inhibition zones for BSM hydrogel sponges crosslinked with borax and STMP/STPP and incorporated with ZnONP

Sample	Zone of inhibition (mm)	
	S. aureus	*E. coli*
BSM	Inactive	Inactive
5BO	Inactive	Inactive
10BO	Inactive	Inactive
20BO	Inactive	Inactive
20BO30ZnONP	15.2	14.2
20BO50ZnONP	16.7	14.8
5ST	Inactive	Inactive
10ST	Inactive	Inactive
20ST	Inactive	Inactive
20ST30ZnONP	15.5	14.1
20ST50ZnONP	16.5	14.4

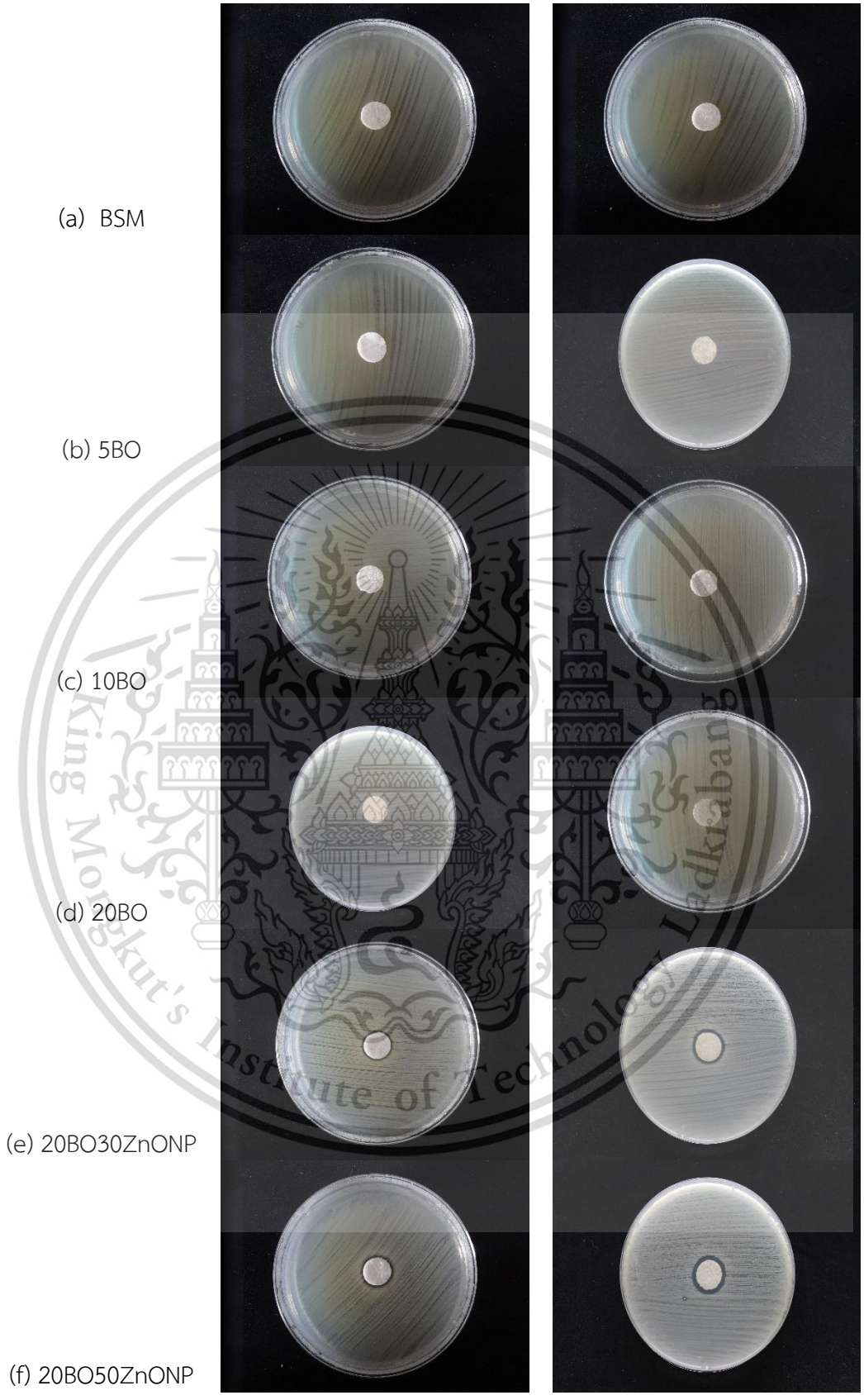

Figure 4.20 Inhibition zone of BSM hydrogel sponges crosslinked with borax and incorporated with various ZnONP contents; *E.coli* (left) and *S. aureus* (right)

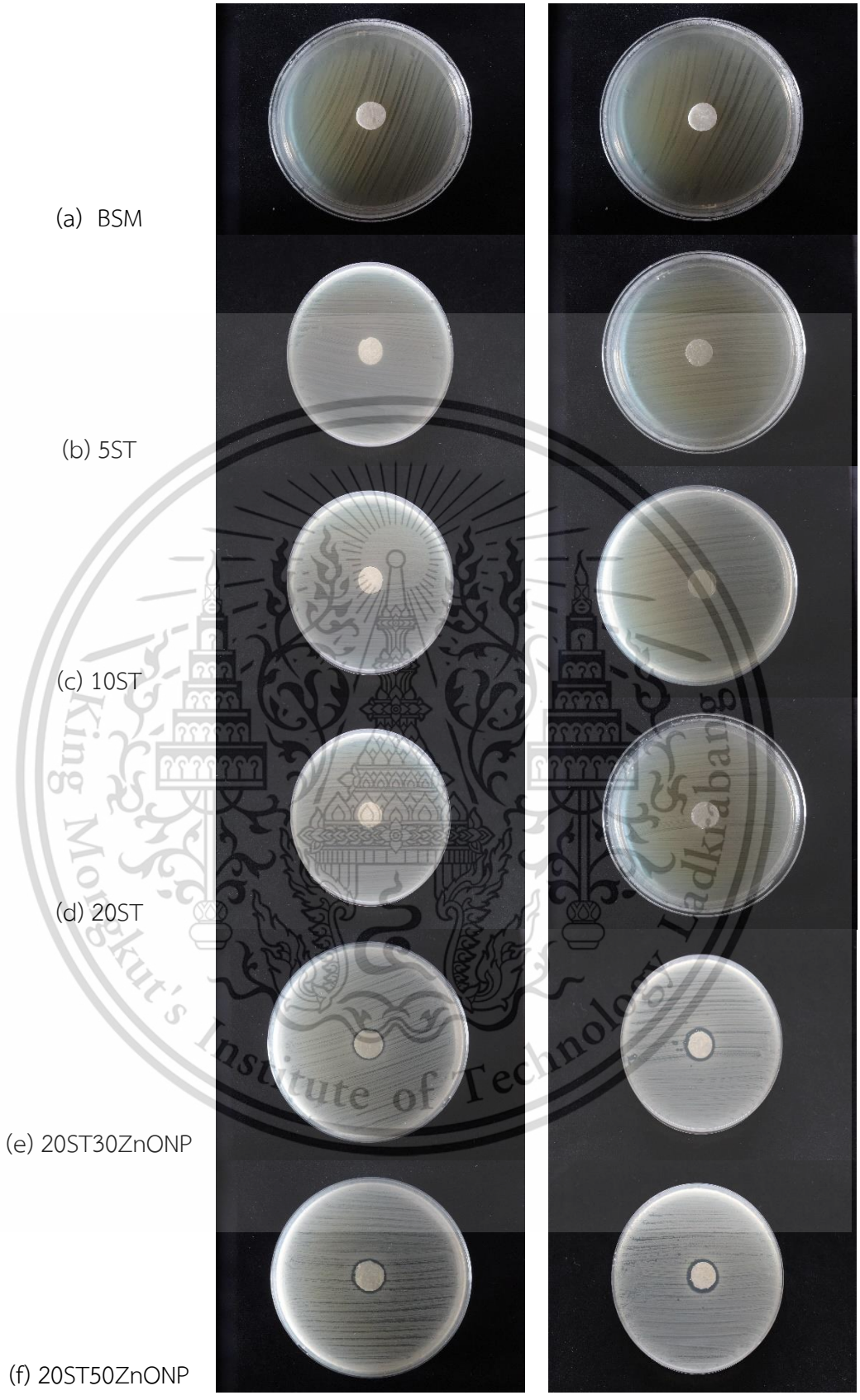

Figure 4.21 Inhibition zone of BSM hydrogel sponges crosslinked with STMP/STPP and incorporated with various ZnONP contents; *E.coli* (left) and *S. aureus* (right)

4.2.7 Effect of different crosslinking agents and their contents on cytotoxicity of BSM hydrogel sponge

Since BSM hydrogel sponge crosslinked with borax showed the best overall properties, it was chosen to study its cytotoxicity. The amount of borax and ZnONP in the BSM hydrogel sponge may cause toxic to humans, cytotoxicity of the various BSM sponges was; therefore, assessed by comparing to that of a control, by MTT assay with human keratinocytes (HaCat) cells**.** The cytotoxicity of BSM hydrogel sponges with HaCat cells were observed in optical microscopy images (Figure 4.22). It was seen that there were no significant differences between the control cells and BSM hydrogel sponge crosslinked with various borax contents and incorporated with ZnONP. In particular, there was no morphological hallmark, for example, chromatin condensation, chromatin fragmentation or nuclear fragmentation. Hence, it could be summarized that borax and ZnONP did not affect to cytotoxicity of BSM hydrogel sponge.

Figure 4.22 Optical microscopy images (200× magnification) of the control and BSM hydrogel sponges crosslinked with various borax contents and incorporated with ZnONP (a) negative control (b) BSM, (c) 5BO, (d) 10BO, (e) 20BO, (f) 20BO30ZnONP and (g) 20BO50ZnONP

Chapter 5

Conclusion and Suggestions

5.1 Conclusion

In this research, the effect of ZnONP and crosslinking agents (Borax and STMP/STPP) and their contents on various properties of BSM hydrogel sponge were studied. It could be concluded as follows:

5.1.1 Effect of ZnONP and its content on various properties of BSM hydrogel sponges.

1. BSM hydrogel sponge presented interconnected open-cell structure of the pores. The round open-pored structures changed to a tighter network structure as the ZnONP content was increased. Moreover, ZnONP uniformly distributed over the BSM matrix and strongly attached to the sponge surface.

2. An increase of ZnONP content led to the decrease in thickness and porosity of BSM hydrogel sponge.

3. BSM hydrogel sponges showed a considerable degree of swelling. However, the increase in ZnONP content resulted in the slight decrease in degree of swelling.

4. BSM hydrogel sponge without the incorporation of ZnONP showed the lowest water retention capacity. After incorporation of ZnONP, the water retention capacity of BSM sponge was slightly increased.

5. For mechanical properties, stress at maximum load, Young's modulus and percentage strain of BSM hydrogel sponges were greatly improved by increasing ZnONP content.

6. The decomposition temperature of BSM hydrogel sponge significantly shifted to higher temperature, after ZnONP was added into the sponge. In addition, the residual weight percentages was increased with the increase of ZnONP content.

7. Unmodified BSM hydrogel sponge exhibited no antibacterial activity. After the incorporation of ZnONP, BSM hydrogel sponges indicated effective antibacterial activity against both *S. aureus* and *E.coli*. In particular, it was observed the higher antibacterial activity for *S. aureus* than *E. coli*.

8. From MTT assay, BSM hydrogel sponges incorporated with ZnONP were not toxic to human keratinocytes cells.

9. The best overall properties of BSM hydrogel sponge incorporated with ZnONP in this study was found in 50ZnONP, determined by the highest water retention capacity, mechanical and antibacterial properties and degree of swelling.

5.1.2 Effect of crosslinking agents and their content on various properties of BSM hydrogel sponges.

1. From SEM micrograph, the increase in both borax and STMP/STPP crosslinking agents content created smaller pores and a more compact pore structure of BSM hydrogel sponge. Besides, there was no significant difference in morphology between BSM hydrogel sponge crosslinked with borax and BSM hydrogel sponge crosslinked with STMP/STPP.

2. The addition of both crosslinking agents (borax and STMP/STPP) caused the decrease in thickness and porosity of BSM hydrogel sponge.

3. The degree of swelling of BSM hydrogel sponge decreased after crosslinked with borax or STMP/STPP. The increase in crosslinking agents content led to the decrease in degree of swelling. Moreover, BSM hydrogel sponge crosslinked with STMP/STPP showed higher degree of swelling than BSM hydrogel sponge crosslinked with borax.

4. After crosslinking, the increased borax or STMP/STPP content resulted in an improvement of dimensional stability of BSM hydrogel sponge in aqueous media. This can confirm successful crosslinking reaction between borax or STMP/STPP and BSM molecules.

5. All mechanical properties, i.e., stress at maximum load, Young's modulus and percentage strain at maximum load were improved by the increase of both crosslinking agents (borax and STMP/STPP). Furthermore, BSM hydrogel sponge crosslinked with borax showed slightly greater mechanical properties than those of BSM hydrogel sponge crosslinked with STMP/STPP.

6. The decomposition temperature of BSM hydrogel sponge significantly shifted to higher temperature and the residual weight percentage increased when crosslinking agents (borax or STMP/STPP) contents were increased. By comparison, BSM hydrogel sponge crosslinked with borax presented higher degradation temperature than BSM hydrogel sponge crosslinked with STMP/STPP, at the same content.

7. For antibacterial activity, the incorporation of both crosslinking agents (borax and STMP/STPP) did not affect antibacterial activity. However, the incorporation of ZnONP resulted in an improvement of antibacterial activity against both of *S. aureus* and *E.coli*.

8. The cytotoxicity of BSM hydrogel sponges crosslinked with borax and incorporated with ZnONP showed no significant differences with the control cells. Also, borax and ZnONP did not affect to cytotoxicity of BSM hydrogel sponge.

9. For a comparison between borax and STMP/STPP crosslinking efficiency, both of crosslinking agents showed nearly crosslinking efficiency. Nevertheless, BSM hydrogel sponge crosslinked with borax showed slightly higher mechanical properties but lower in degree of swelling.

10. The best overall properties of BSM hydrogel sponges in this research was found in 20BO50ZnONP, which exhibited the highest dimensional stability, mechanical properties, water retention capacity and thermal properties. In addition, it presented effective antibacterial activity and non-toxic to human keratinocytes (HaCat) cells.

5.2 Suggestions

The BSM hydrogel sponge could be further improved and developed by the following suggestions:

1. It is of interesting to develope a new process for improving dimensional stability of the BSM hydrogel sponge, for example, the addition of gelling agents or natural fibers.

2. It would be interesting to incorporate ZnONP in different method such as treating ZnONP surface and coating on the BSM hydrogel sponge surface.

3. It is of interesting to prepare wound dressing from BSM in other forms, for example, film or hydrogel and compare their properties.

4. It would be interesting to load some drug into BSM hydrogel sponge wound dressing and study drug release control and its relating effect.

References

[1] Tabashi, S. N. Razavi, S. M. 2017. "Functional properties and applications of basil seed gum: An overview." *Food Hydrocolloids*. 73 : 313-325.

[2] Xie, H. Chen, X. Shen, X. He, Y. Chen, W., Luo, Q. Ge, W. Yuan, W. Tang, X. Hou, D. Jiang, D. Wang, Q. Liu, Y. Liu, Q. and Li, K. 2018. "Preparation of chitosan-collagen-alginate composite dressing and its promoting effects on wound healing." *International Journal of Bioloical Macromolecules* 107 : 93-104.

[3] Raguvaran, R. Balvinder, K.M. Meenu, C. Rajesh, T. Taruna, A. Anu, K. Anju, M. 2017. "Sodium alginate and gum acacia hydrogels of ZnO nanoparticles show wound healing effect on fibroblast cells." *International Journal of Bioloical Macromolecules* 96 : 185-191.

[4] Autissier, A. Visage, C. L. Pouzet, C. Chaubet, F. Letourneur, D. 2010. "Fabrication of porous polysaccharide-based scaffolds using a combined freeze-drying/cross-linking process." *Acta Biomaterialia* 6 : 3640–3648.

[5] Kamoun, E. A. Kenawy, E. S. and Chen, X. 2017. "A review on polymeric hydrogel membranes for wound dressing applications: PVA-based hydrogel dressings." *Journal of Advanced Research* 8 : 217–233.

[6] Zeinab F. 2018. "Freeze-drying technologies for 3D scaffold engineering." 151-174 **Functional 3D Tissue Engineering Scaffolds.** Newyork : Elsevier.

[7] Rathore, H. S. Sarubala, M. Ramanathan, G. Singaravelu, S. Raja, M. D. Gupta, S. and Sivagnanam, U. T. 2016. "Fabrication of biomimetic porous novel sponge from gum kondagogu for wound dressing." *Materials Letters* 177 : 108-111.

[8] Tavakoli, J. 2017. "Physico-mechanical, morphological and biomedical properties of a novel natural wound dressing material." *Journal of the mechanical behavior of biomedical materials* 65 : 373-382.

[9] Simões, D. Sónia, P. M. Ribeiro, M. P. Coutinho, P. Mendonça, A. G. and Correia, I. J. 2017. "Recent advances on antimicrobial wound dressing: A review." *European Journal of Pharmaceutics and Biopharmaceutics* 127 : 131-140.

[10] Nosar, M. N. and Zyta, Z. M. 2018. "Wound dressings from naturally-occurring polymers: A review on homopolysaccharide-based composites." *Carbohydrate Polymers* 189 : 378-389.

[11] Gutierrez, T. J. Seligra, P. G. Jaramillo, C. M. Fama, L. and Goyanes, S. 2017. "Effect of Filler Properties on the Antioxidant Response of Thermoplastic Starch Composites." In K. M. Vijay, K. T. Manju, & R. K. Michael (Eds.), **Handbook of Composites from Renewable Materials** (pp. 337-370). Argentina: Scrivener Publishing LLC

[12] Mohandas, A. Deepthi, S. Biswas, R. and Jayakumar, R. 2018. "Chitosan based metallic nanocomposite scaffolds as antimicrobial wound dressings." *Bioactive Materials* 3 : 267-277

[13] Khalid, A. Khan, R. Ul-Islam, M. Khan, T. and Wahid, F. 2017. "Bacterial cellulose-zinc oxide nanocomposites as a novel dressing system for burn wounds." *Carbohydrate Polymers* 164 : 214-221.

[14] Raafat, A. I. El-Sawy, N. M. Badawy, N. A. Mousa, E. A. and Mohamed, A. M. 2018. "Radiation fabrication of Xanthan-based wound dressing hydrogels embedded ZnO nanoparticles: In vitro evaluation." *International Journal of Biological Macromolecules* 118 : 1892-1902.

[15] Reddy, N. and Yang, Y. 2010. "Citric acid cross-linking of starch films." *Food Chemistry* 118 : 702-711.

[16] Ghanbarzadeh, B. Almasi, H. and Entezami, A. A. 2011. "Improving the barrier and mechanical properties of corn starch-based edibble films: Effect of citric acid and carboxymethyl cellose." *Industrial Crops and Products* 33 : 229-235.

[17] Seligra, P. G. Jaramillo, C. M. Famá, L. and Goyanes, S. 2016. "Biodegradable and non-retrogradable eco-films based on starch-glycero with citric acid as crosslinkinh agent." *Carbohydrate Polymers* 138 : 66-74.

[18] Thombare, N. Jha, U. Mishra, S. and Siddiqui, M. Z. 2017. "Borax cross-linked guar gum hydrogels as potential adsorbents for water purification." *Carbohydrate Polymers* 188 : 274-281.

[19] Mogosanu, G. D. and Grumezescu, A. M. 2014. "Natural and synthetic polymers for wounds and burns dressing." *International Journal of Pharmaceutics* 463 : 127-136.

[20] Kamoun, E. A. Kenawy, E. S. and Chen, X. 2017. "A review on polymeric hydrogel membranes for wound dressing applications: PVA-based hydrogel dressings." *Journal of Advanced Research* 8 : 217–233.

[21] Bucktowar, K. Bucktowar, M. and Bholoa, L. D. 2016. "A Review on Sweet Basil Seeds: *Ocimum basilicum*." *World Journal of Pharmacy and Pharmaceutical Sciences* 5 : 554-567.

[22] Reddy, N. Reddy, R. and Jiang, Q. 2015. "Crosslinking biopolymers for biomedical applications." *Trends in Biotechnology* 7 : 1-8.

[23] Azeredo, H. M. and Waldron, K. W. 2016. "Crosslinking in polysaccharide and protein films and coatings for food contact: A review." *Trends in Food Science & Technology* 52 : 109-122.

[24] Larsen, P. B. Nielsen, B. S. Fotel, F. L. Kortegaard, P. Slothuus, T. and Hjelmar, O. 2015. "Survey of Boric acid and sodium borates (borax)." *Copenhagen* : The Danish Environmental Protection Agency

[25] Fisher Scientific. 2009. "Material Safety Data Sheet Sodium tetraborate decahydrate." New jersey : Fisher Scientific.

[26] Gardena, C. A. 2006. "MSDS: Sodium Trimetaphosphate." New jersey : Sonia Owen.

[27] Human & Environmental Risk Assessment on ingredients of European household cleaning products 2003. "Sodium Tripolyphosphate (STPP)." Brussels : Hera Secretariat.

[28] Zhao, S. 2017. "Introduction to nanocomposites." University of Nebraska-Lincoln, Nebraska.

[29] Campbell, F. C. 2017. "Introduction to Composite Materials." 1-29 **Structural composite materials.** Ohio : ASM International.

[30] Pandya, S. 2015. "Nanocomposites and its application." Parul university.

[31] Espitia, P. J. P. Otoni, C. G. and Soares, N. F. F. 2016. "Zinc Oxide Nanoparticles for Food Packaging Applications." 425-431 **Antimicrobial Food Packaging.** Brazil : Elsevier.

[32] U. S. Zinc. 2018. "Safety datashett : Zinc Oxide." Salzburg, Austria.

[33] Shukla, S. 2011. "Freeze drying process : A review." *International journal of pharmaceutical science and research* 2 : 3061-3068.

[34] Ellab validation solution. 2018. "The freeze drying theory and process things to consider." Denmark.

[35] Edmund, H. I. and Herman, F. M. 1965. "Principles of Plasticization." 1-26 **Plasticization and plasticizer processes** Washington : ACS publication.

[36] García, J. I. García-Marín, H and Pires, E. 2010. "Glycerol based solvents: synthesis, properties and applications." *Green chemistry* 12 : 426-434.

[37] Pagliaro, M. and Rossi, M. 2008. "Glycerol: properties and production." 1-18 **The future of glycerol: new uses of a versatile raw material** London : Springer.

[38] Wang, H. Liao, Y. Wu, A. Li, B. Qian, J. and Ding, F. 2019. "Effect of sodium trimetaphosphate on chitosan-methylcellulose composite films: physicochemical properties and food packaging application." *Polymers* 11 : 1-15.

[39] Mohammad, T. K. Alireza, J. Armaghan, M. Hamidreza, S. and Zohreh, M. 2018. "Incorporation of ZnO nanoparticles into heparinised polyvinyl alcohol/chitosan hydrogels for wound dressing application." *International Journal of Biological Macromolecules* 114 : 1203-1215.

[40] Bajpai, S. K. Jadaun, M. Armaghan, M. and Tiwari, S. 2016. "Synthesis, characterization and antimicrobial applications of zinc oxide nanoparticles loaded gum acacia/poly(SA) hydrogels." *Carbohydrate Polymers* 153 : 60-65.

[41] Lu, Z. Gao, J. He, Q. Wu, J. Liang, D. Yang, H. and Chen, R. 2017. "Enhanced antibacterial and wound healing activities of microporous chitosan-Ag/ZnO composite dressing." *Carbohydrate Polymers* 156 : 460-469.

[42] Khazaei, N. Esmaiili, M. Djomeh, Z. E. Ghasemlou, M. and Jouki, M. 2014. "Characterization of new biodegradable edible film made from basil seed (*Ocimum basilicum* L.) gum." *Carbohydrate Polymers* 102 : 199-206.

[43] Sarika, P. R. Kuriakose, C. Jayakrishnan, A. Anilkumar, P. R. and James, N. R. 2014. "Modified gum arabic cross-linked gelatin scaffold for biomedical applications." *Materials Science and Engineering C* 43 : 272-279.

[44] Shi, M. Gu, F. Wu, J. Yu, S. R. and Gao, Q. 2013. "Preparation, physicochemical properties, and in vitro digestibility of cross-linked resistant starch from pea starch." *Starch/Starke* 65 : 947-953.

[45] Nafchi, A. M. Alias, A. K. Mahmud, S. and Robal, M. 2012. "Antimicrobial, rheological, and physicochemical properties of sago starch films filled with nanorod-rich zinc oxide." *Journal of Food Engineering* 113 : 511-519.

[46] Azwa, Z. N. Yousif, B. F. Manalo, A. C. and Karunasena, W. 2013. "A review on the degradability of polymeric composites based on nateral fibres." *Material and Design* 47 : 424-442.

[47] Kanmani, P. and Rhim, J. 2014. "Properties and characterization of bionanocomposite films prepared with various biopolymers and ZnO nanoparticles." *Carbohydrate Polymers* 106 : 190-199.

[48] Zahedi, P. Rezaeian, I. Ranaei, S. Jafari, S. and Supaphol, P. 2010. "A review on wound dressings with an emphasis on electrospun nanofibrous polymeric bandages." *Polymers advanced technologies* 21 : 77-95.

[49] Tanetrungroj, Y. 2019. "Properties of biodegradable dually modified cassava starch films from cross-linking and oxidation." *Thesis of department of chemistry, King mongkut' s institute of technology ladkrabang*.

[50] Kurd, K. Fathi, M. and Shekarchizadeh, H. 2017. "Basil seed mucilage as a new source for electrospinning: Production and physicochemical characterization." *International Journal of Biological Macromolecules* 95 : 689-695.

[51] Pinpueng, A. and Hongsriphan, N. 2015. “Study of water adsorption and fertilizer release of poly (butylene succinate) blended with natural absorbent for using in agriculture application.” *Thesis of department of materials science and engineering, Silapakorn university*.

[52] Sornsumdang, K. 2019. “Properties of biodegradable rice starch films cross-linked by citric acid filled with metal oxide particles as antibacterial agents.” *Thesis of department of chemistry, King mongkut’ s institute of technology ladkrabang*.

[53] Andrej, D. and Marija, K. 2000. “Effect of pH and impurities on the surface charge of zinc oxide in aqueous solution.” *Journal of the European Ceramic Society* 20 : 667-673.

[54] Blok, L. and De bruyn, P. L. 1969. “The Ionic Double Layer at the ZnO/Solution Interface I. The Experimental Point of Zero Charge.” *Journal of colloid and interface science* 32 : 518-526.

[55] Denise, W. Panagiota, L. Catherine, B. A. Jianhui, Z. and P, Alex. 2016. “A role of ZnO nanoparticle electrostatic properties in cell cytotoxicity.” *Nanotechnology, Science and Applications* 9 : 29-45.

Appendix A

Appendix A

Scanning electrom microscope (EDS mapping image)

Figure A1. EDS mapping images of BSM hydrogel sponges with various ZnONP contents

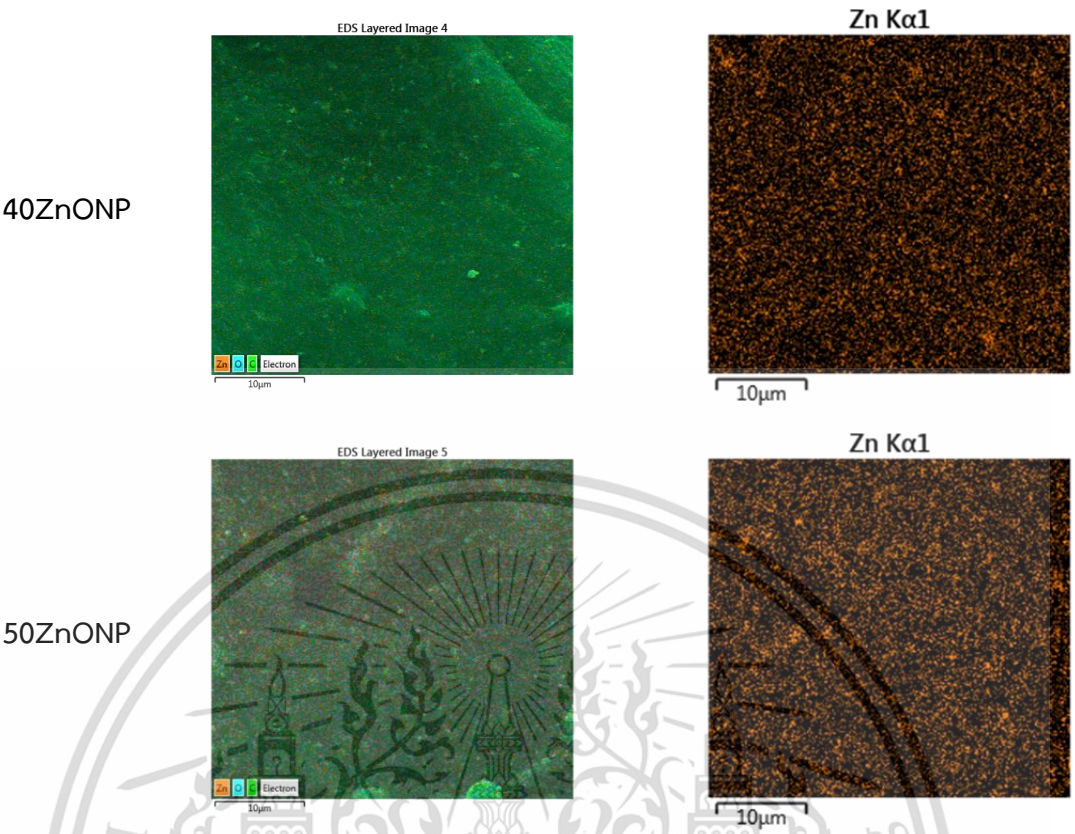

Figure A1. EDS mapping images of BSM hydrogel sponges with various ZnONP contents

Appendix B

Appendix B

Dimensional stability of samples after 48 hours of swelling

Figure B1. Dimensional stability of BSM hydrogel sponges crosslinked with borax or STMP/STPP and incorporated with ZnONP

Appendix C

Appendix C

Mechanical properties

Table C.1 Mechanical properties of BSM hydrogel sponge crosslinked with borax or STMP/STPP and incorporated with ZnONP

Sample	Mechanical properties		
	Stress at maximum load (MPa)	Young' s modulus (MPa)	Strain at maximum load (%)
BSM	2.6±0.5	74±5	28±4
10ZnONP	4.1±0.3	89±8	35±3
20ZnONP	4.8±0.5	97±6	41±3
30ZnONP	5.5±0.4	110±6	43±3
40ZnONP	6.7±0.4	123±8	45±2
50ZnONP	8.9±0.4	151±6	51±4
5BO	3.8±0.4	92±9	39±3
10BO	4.9±0.5	101±6	47±2
20BO	6.6±0.3	113±8	54±3
20BO30ZnONP	9.8±0.7	146±7	57±3
20BO50ZnONP	11.4±0.6	173±8	58±4
5ST	3.2±0.3	87±5	34±5
10ST	4.1±0.5	96±4	41±7
20ST	6.3±0.4	111±5	52±4
20ST30ZnONP	9.9±0.7	135±7	54±5
20ST50ZnONP	10.8±0.4	164±9	56±4

Appendix E

Appendix E

Volume fraction of ZnONP and BSM

Table E.1 Volume fraction of ZnONP and BSM

Sample	Weight fraction (wt%)	Volume fraction (vol%)
10ZnONP	10	0.007
20ZnONP	20	0.014
30ZnONP	30	0.021
40ZnONP	40	0.028
50ZnONP	50	0.035

Note: Density of ZnONP is 5.61 g/cm^3

Density of dry BSM is 0.004 g/cm^3

Appendix D

Appendix D

Thermogravimetric analysis

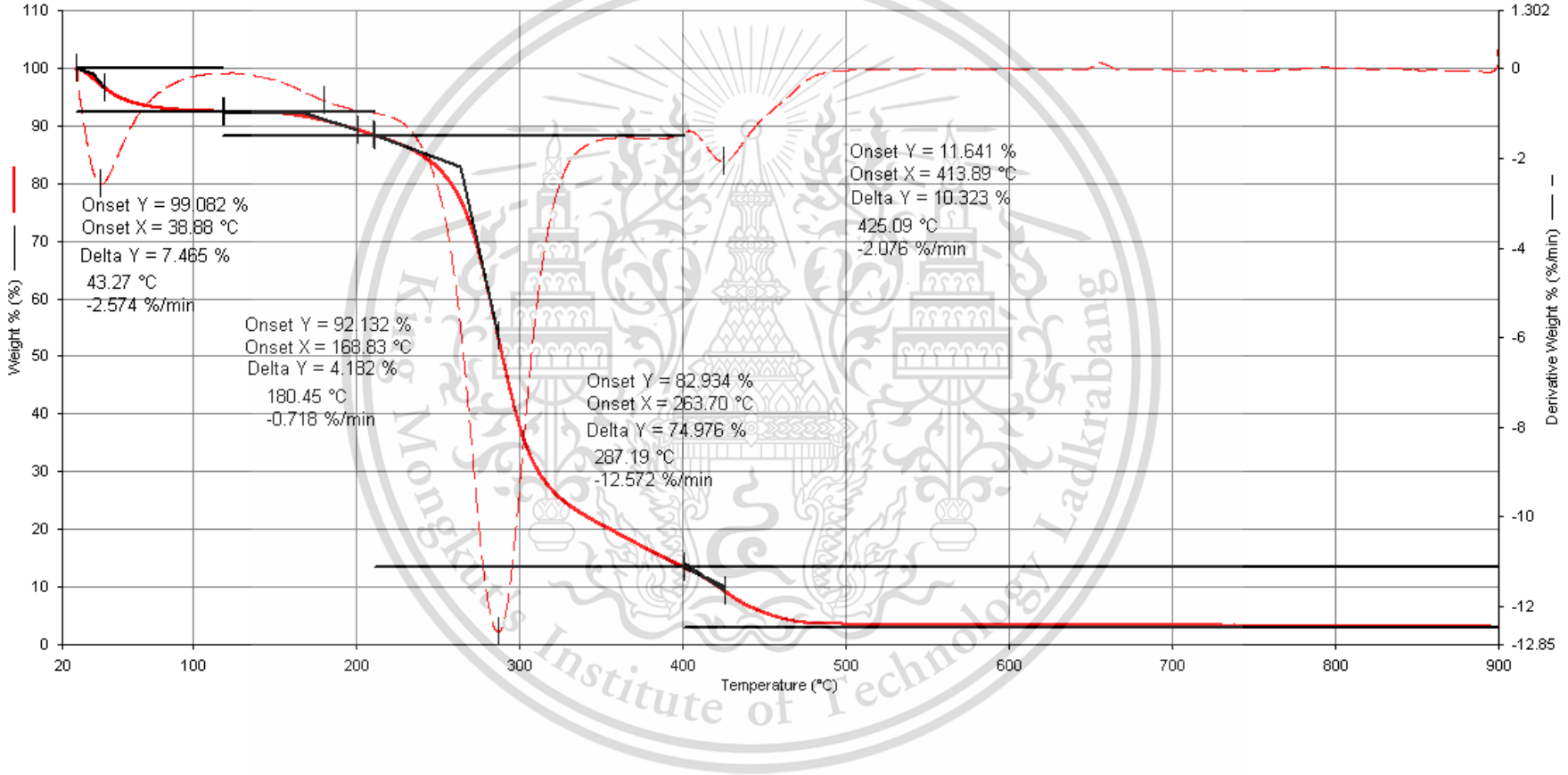

Figure D1. TGA and DTG thermograms of unmodified BSM hydrogel sponge

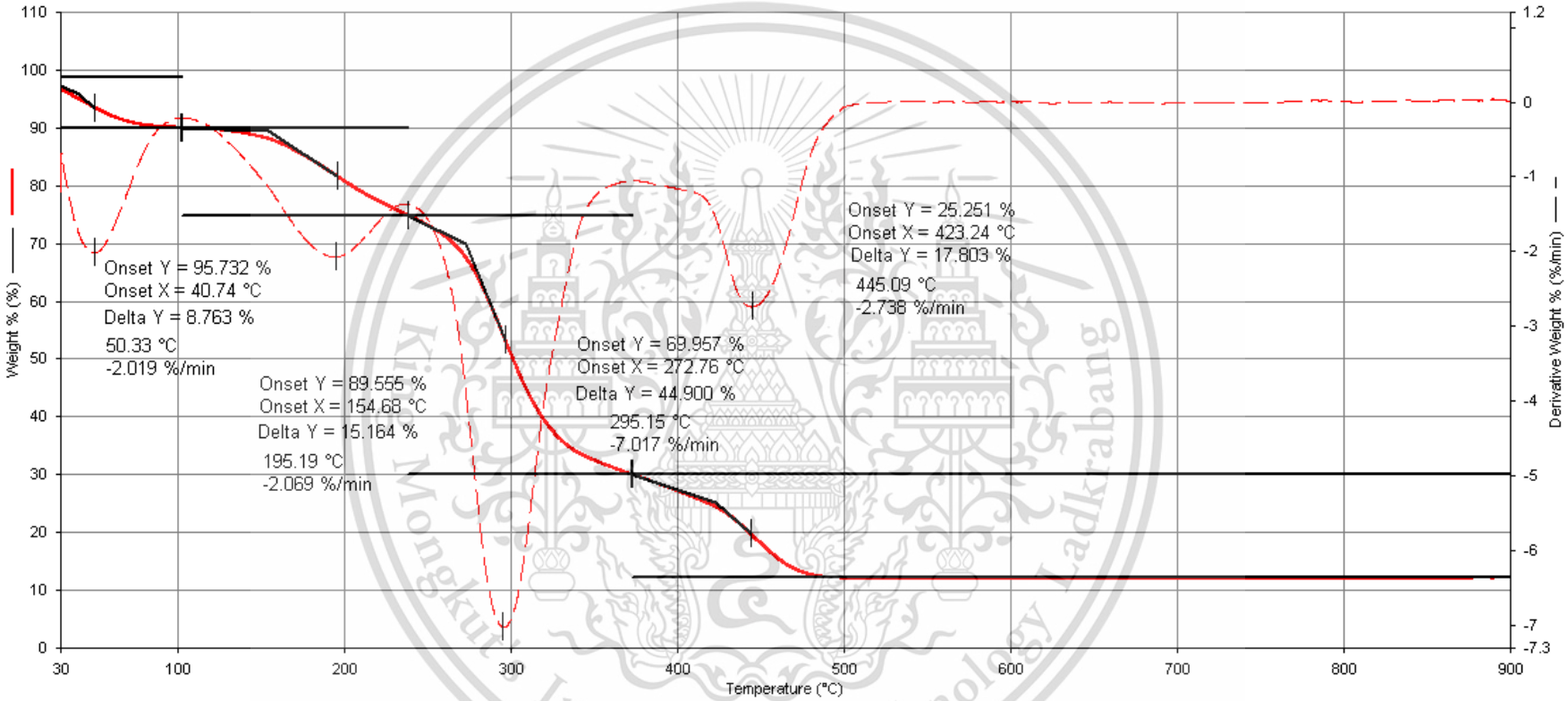

Figure D2. TGA and DTG thermograms of BSM hydrogel sponge incorporated with 10%wt of ZnONP

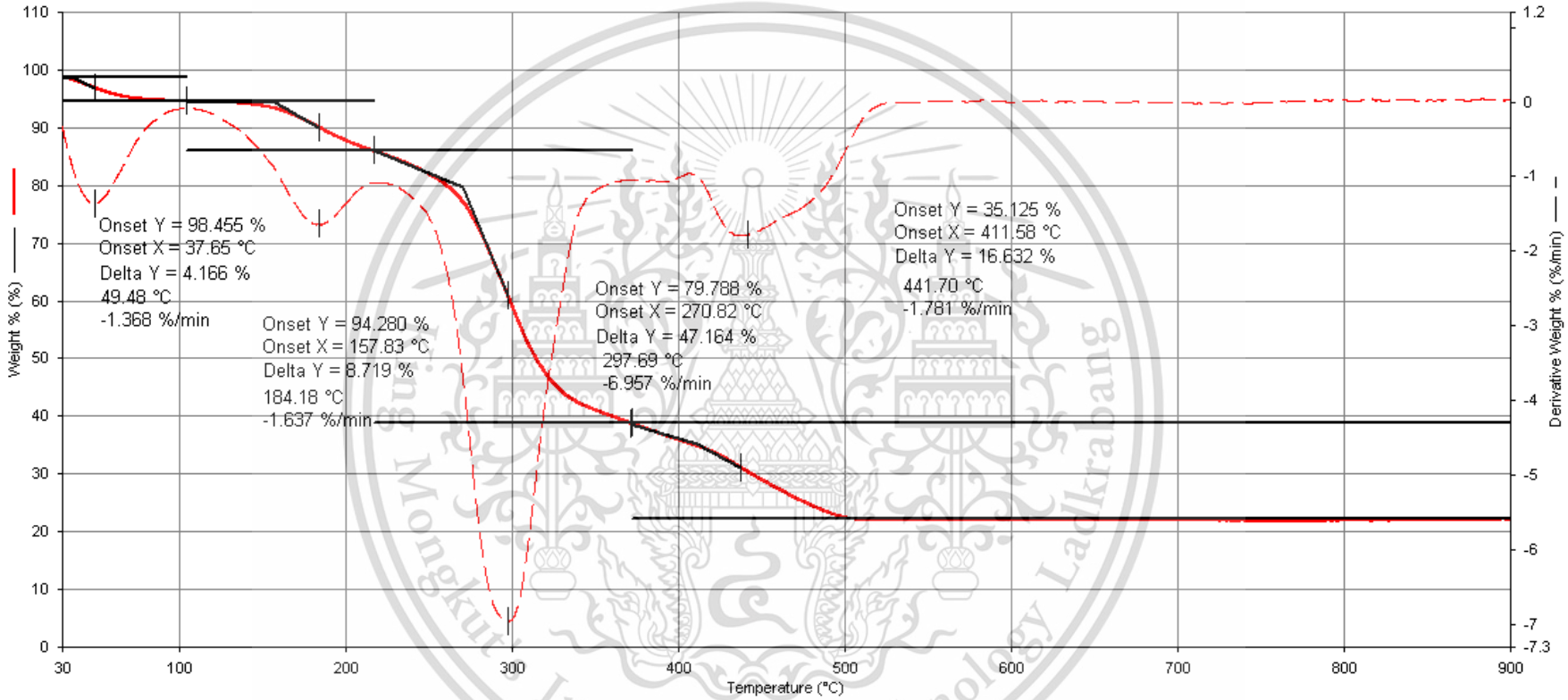

Figure D3. TGA and DTG thermograms of BSM hydrogel sponge incorporated with 20%wt of ZnONP

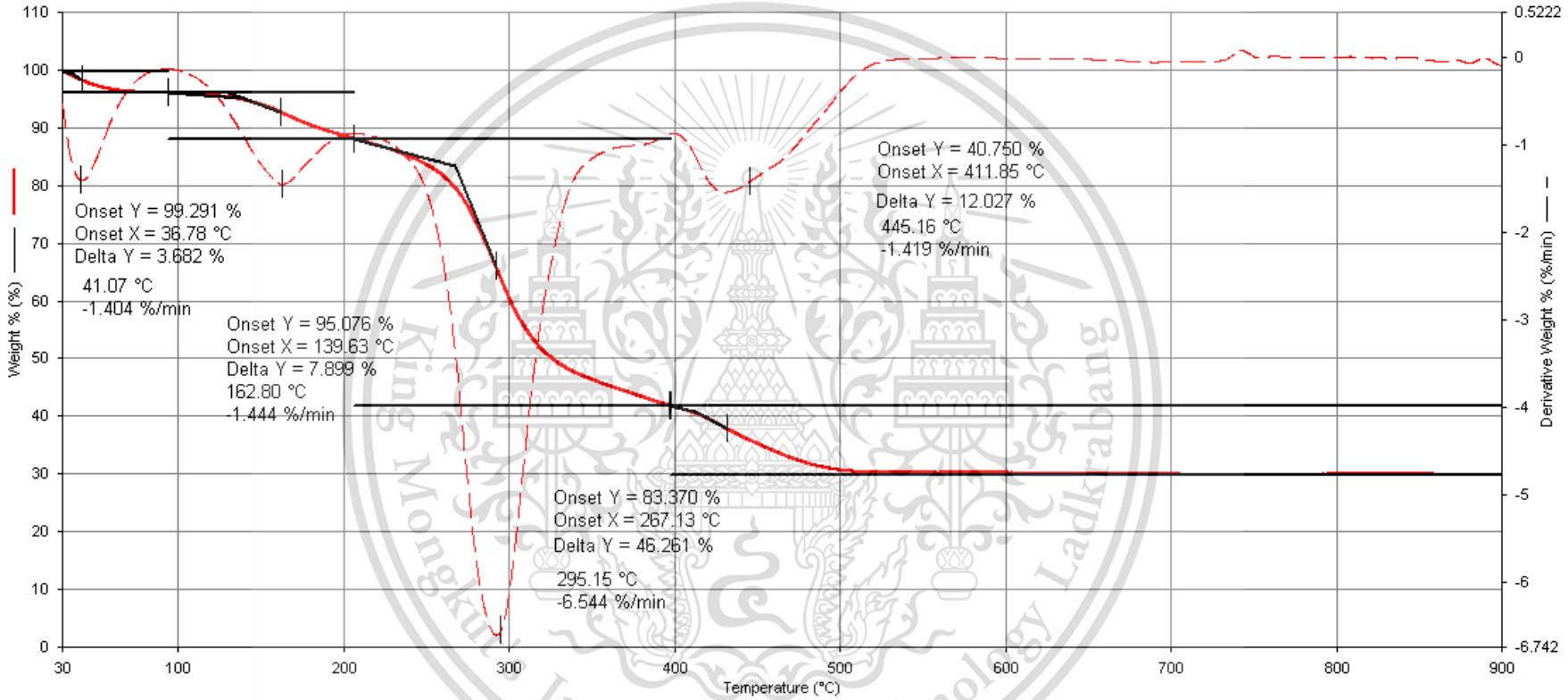

Figure D3. TGA and DTG thermograms of BSM hydrogel sponge incorporated with 30%wt of ZnONP

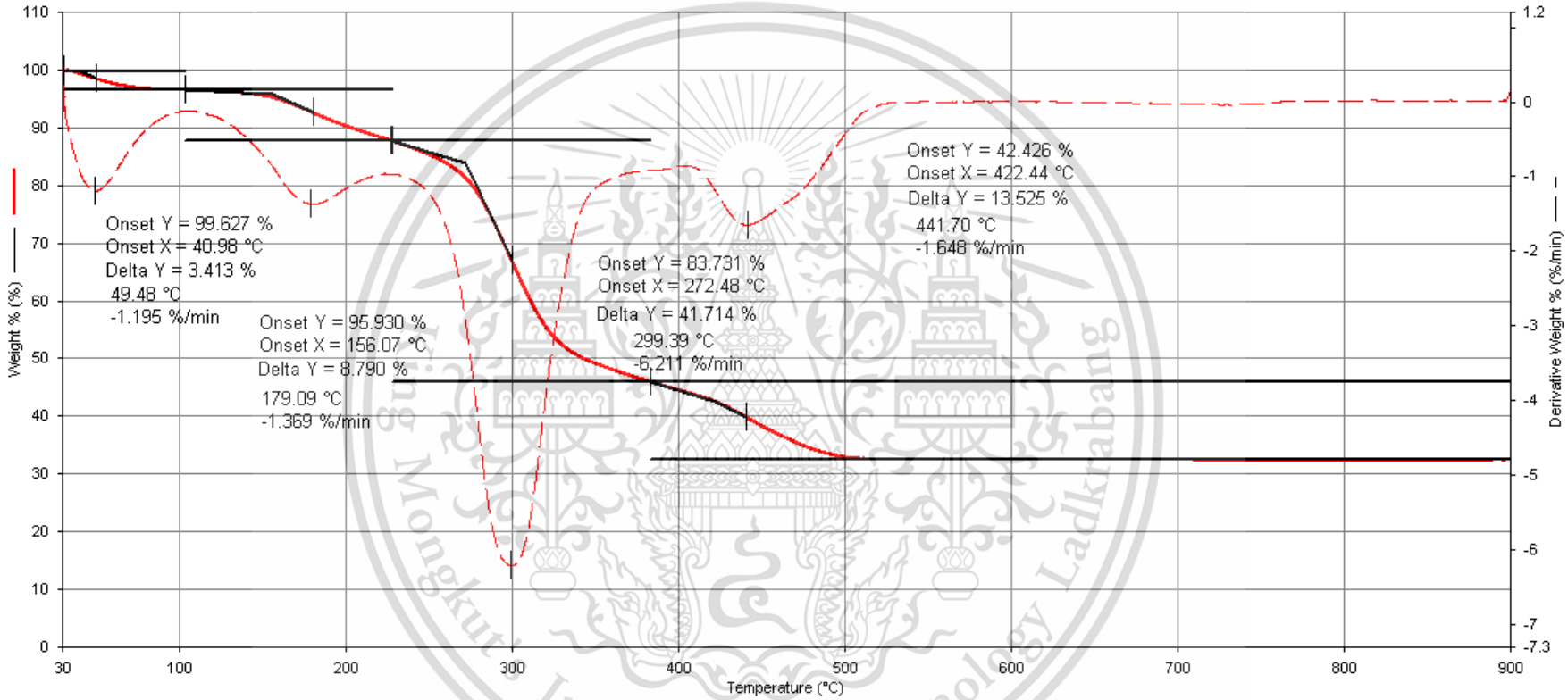

Figure D4. TGA and DTG thermograms of BSM hydrogel sponge incorporated with 40%wt of ZnONP

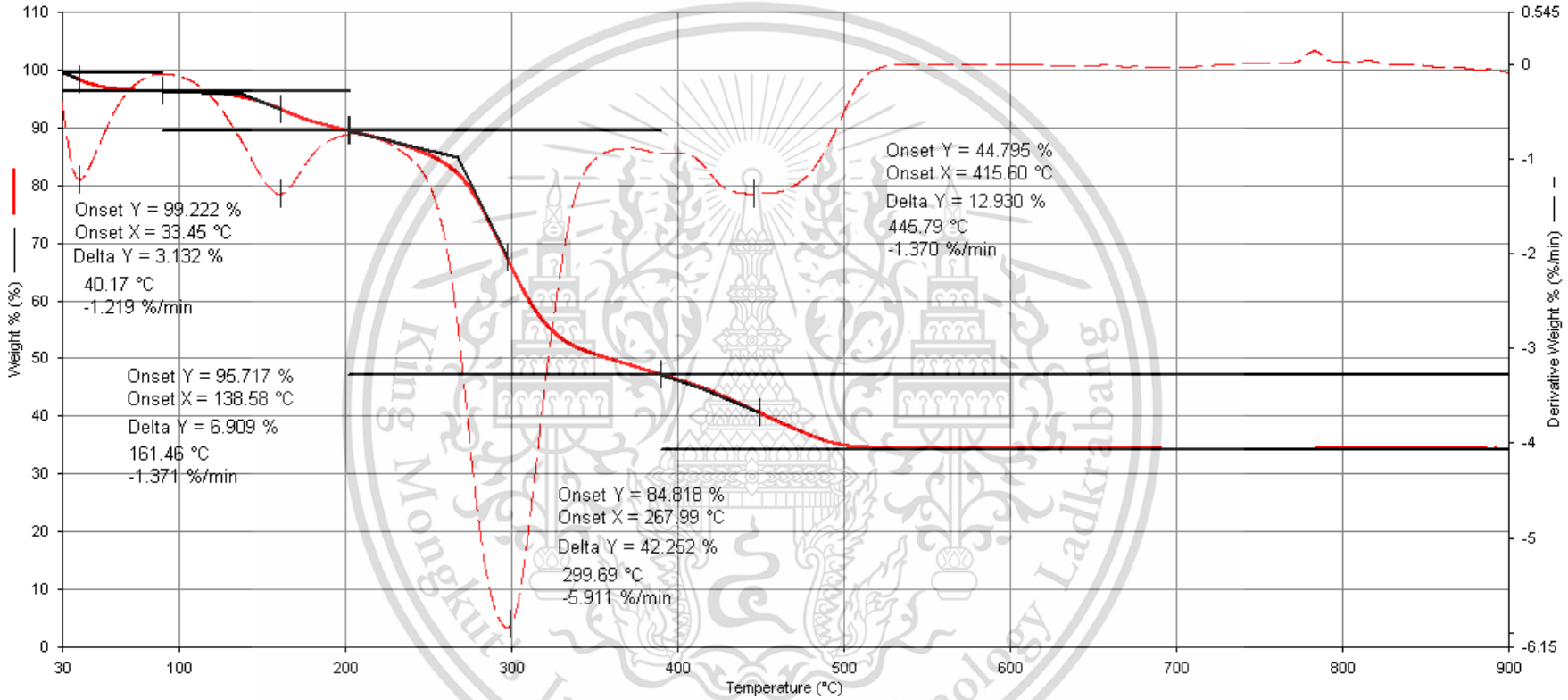

Figure D5. TGA and DTG thermograms of BSM hydrogel sponge incorporated with 50%wt of ZnONP

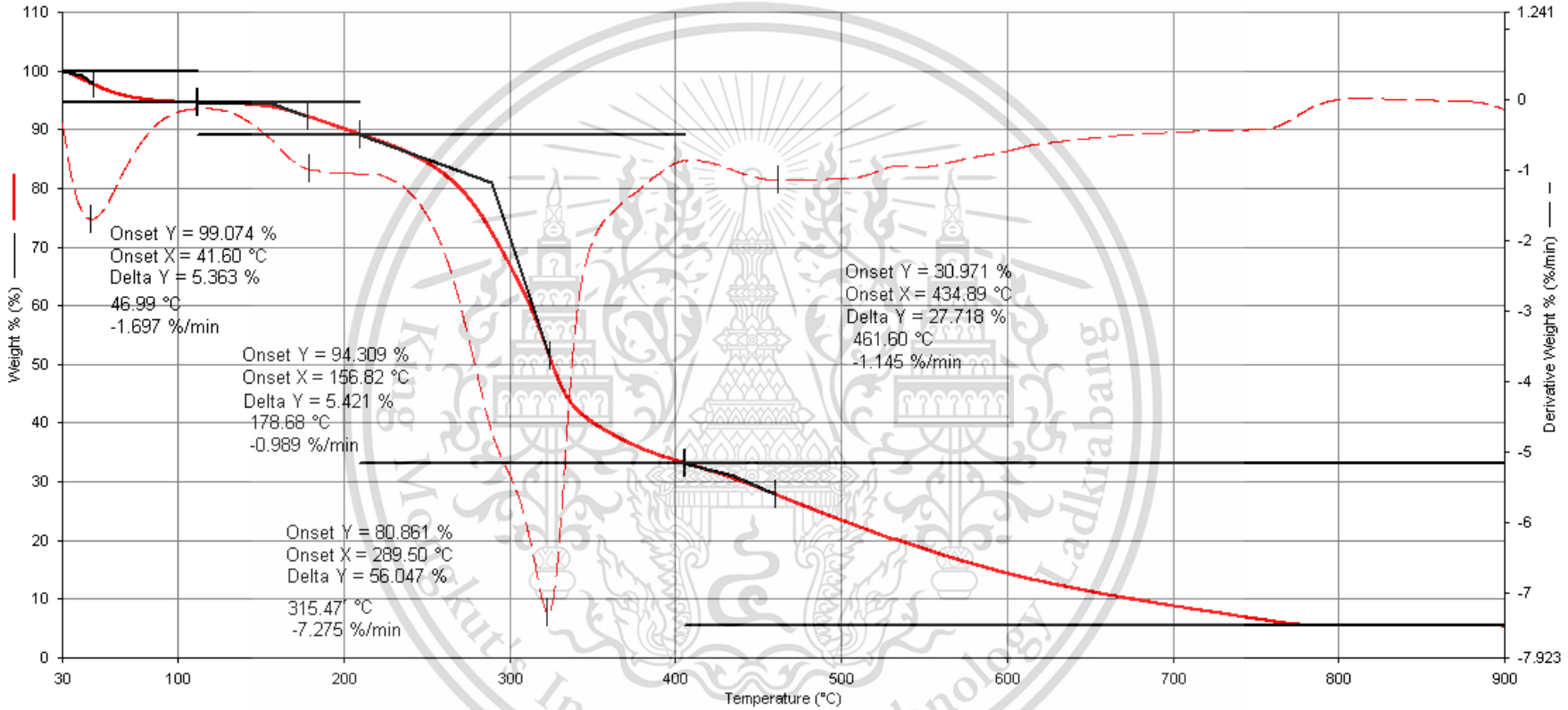

Figure D5. TGA and DTG thermograms of BSM hydrogel sponge crosslinked with 5%wt of borax

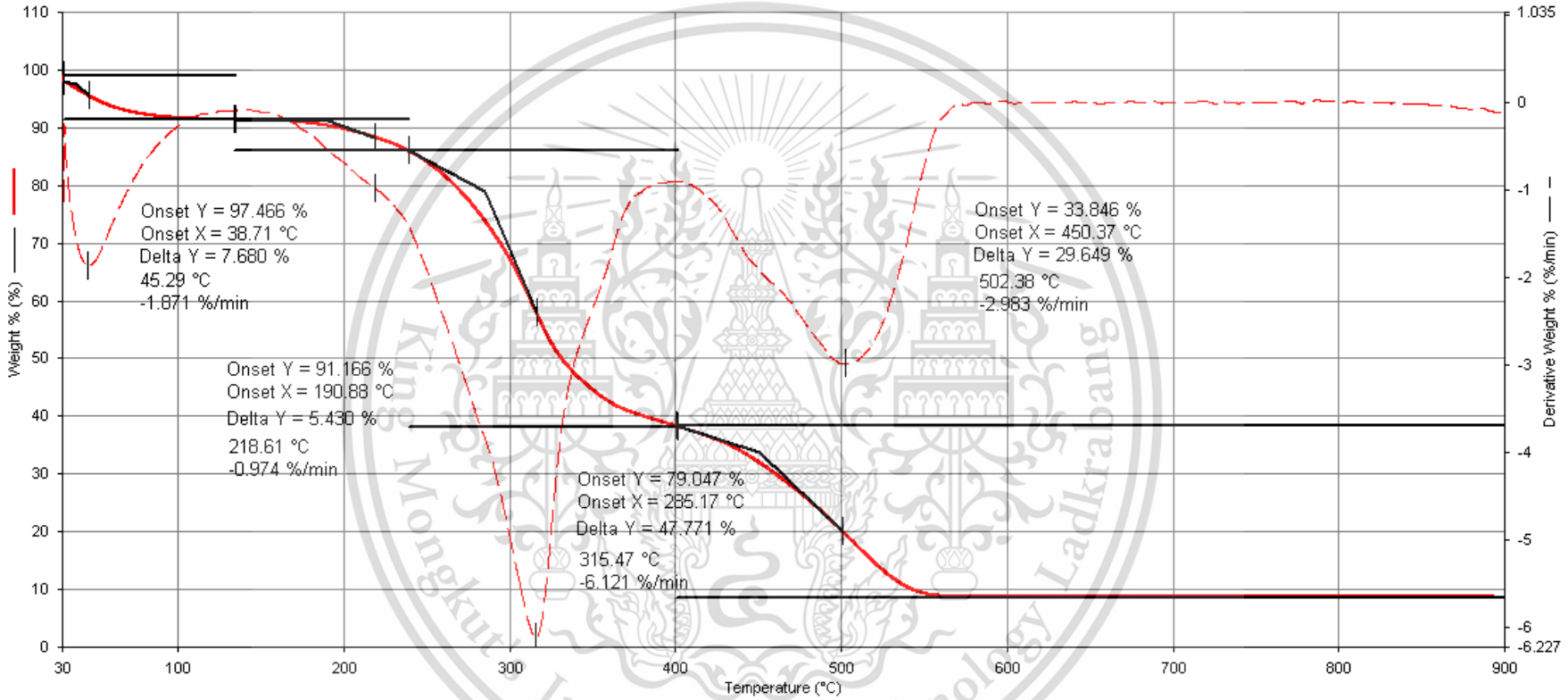

Figure D6. TGA and DTG thermograms of BSM hydrogel sponge crosslinked with 10%wt of borax

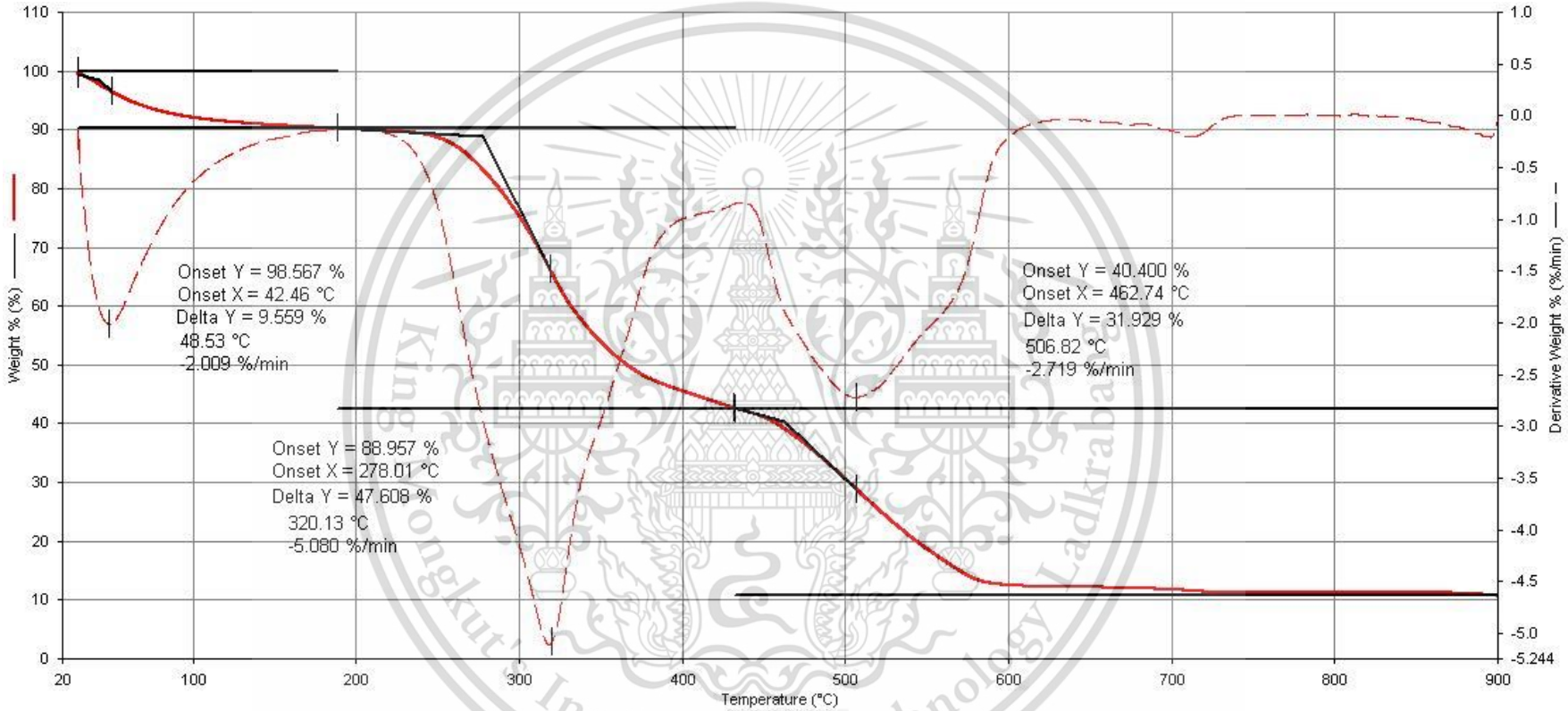

Figure D7. TGA and DTG thermograms of BSM hydrogel sponge crosslinked with 20%wt of borax

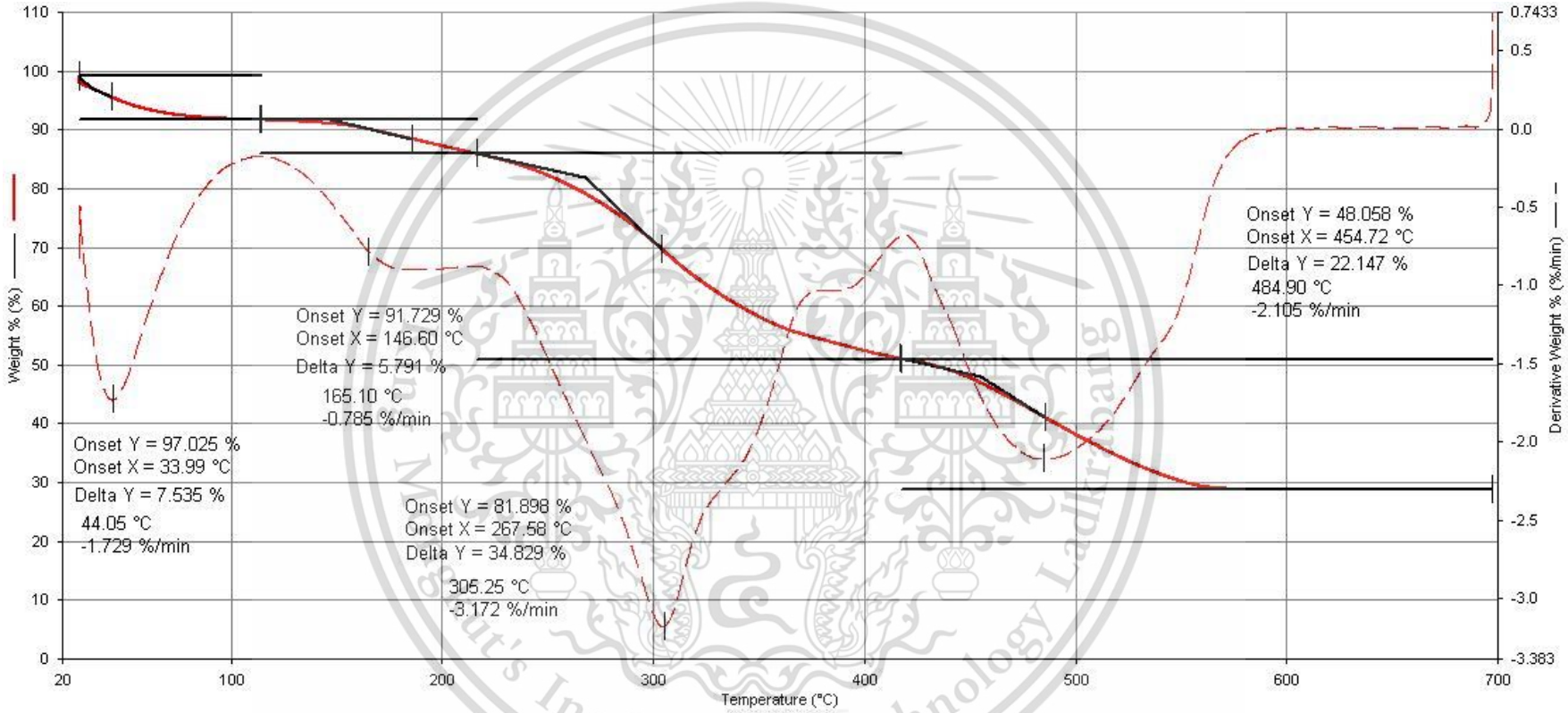

Figure D8. TGA and DTG thermograms of BSM hydrogel sponge crosslinked with 20%wt of borax with 30 wt% of ZnONP

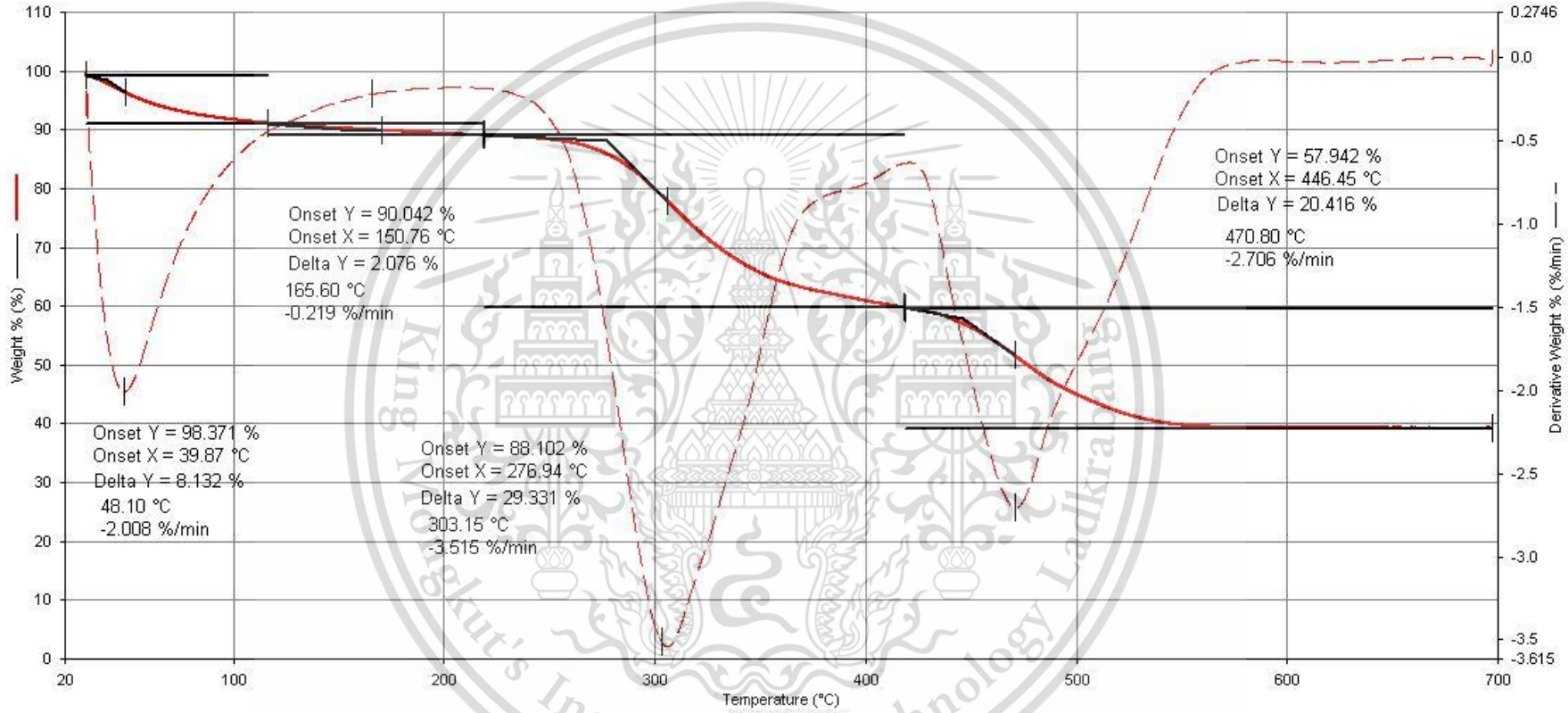

Figure D9. TGA and DTG thermograms of BSM hydrogel sponge crosslinked with 20%wt of borax and incorporated with 50 wt% of ZnONP

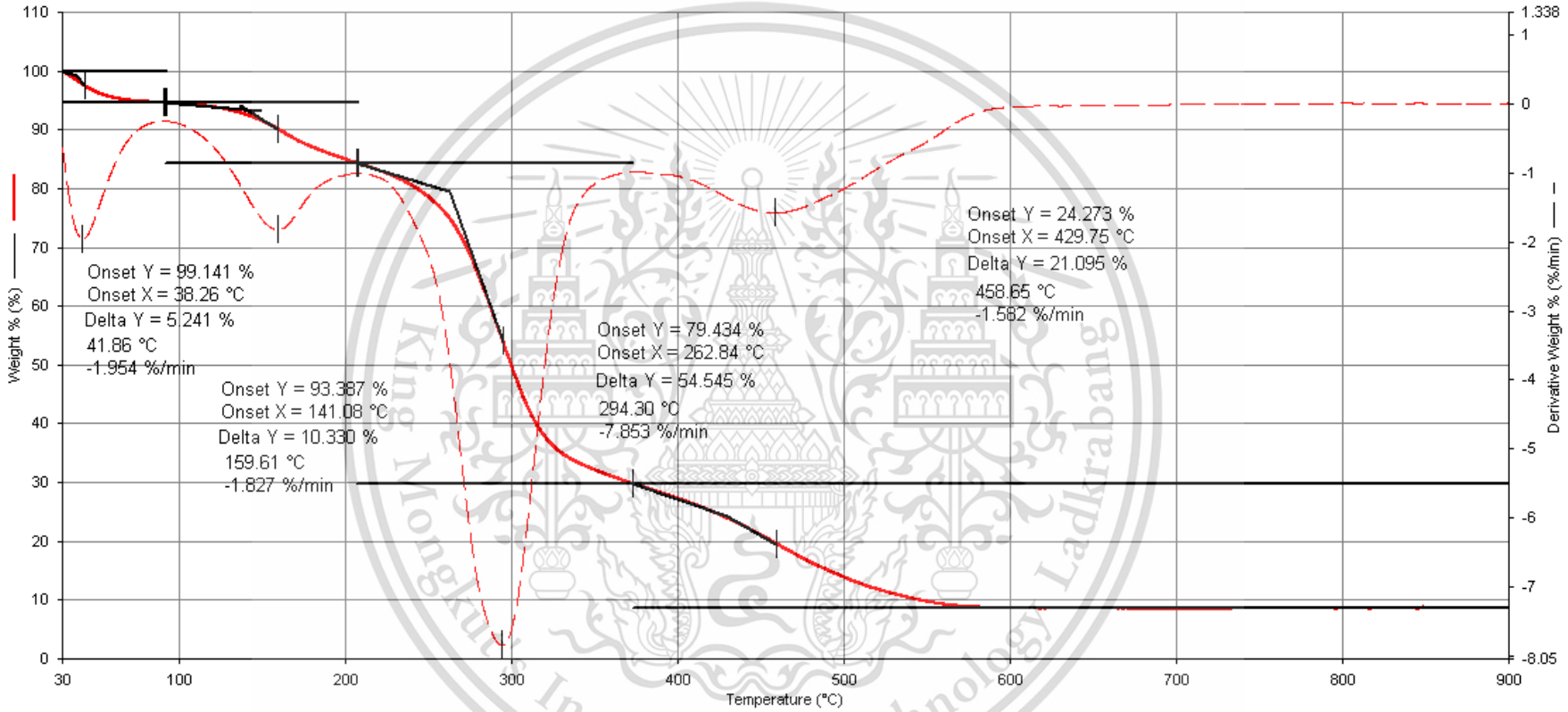

Figure D10. TGA and DTG thermograms of BSM hydrogel sponge crosslinked with 5%wt of STMP/STPP

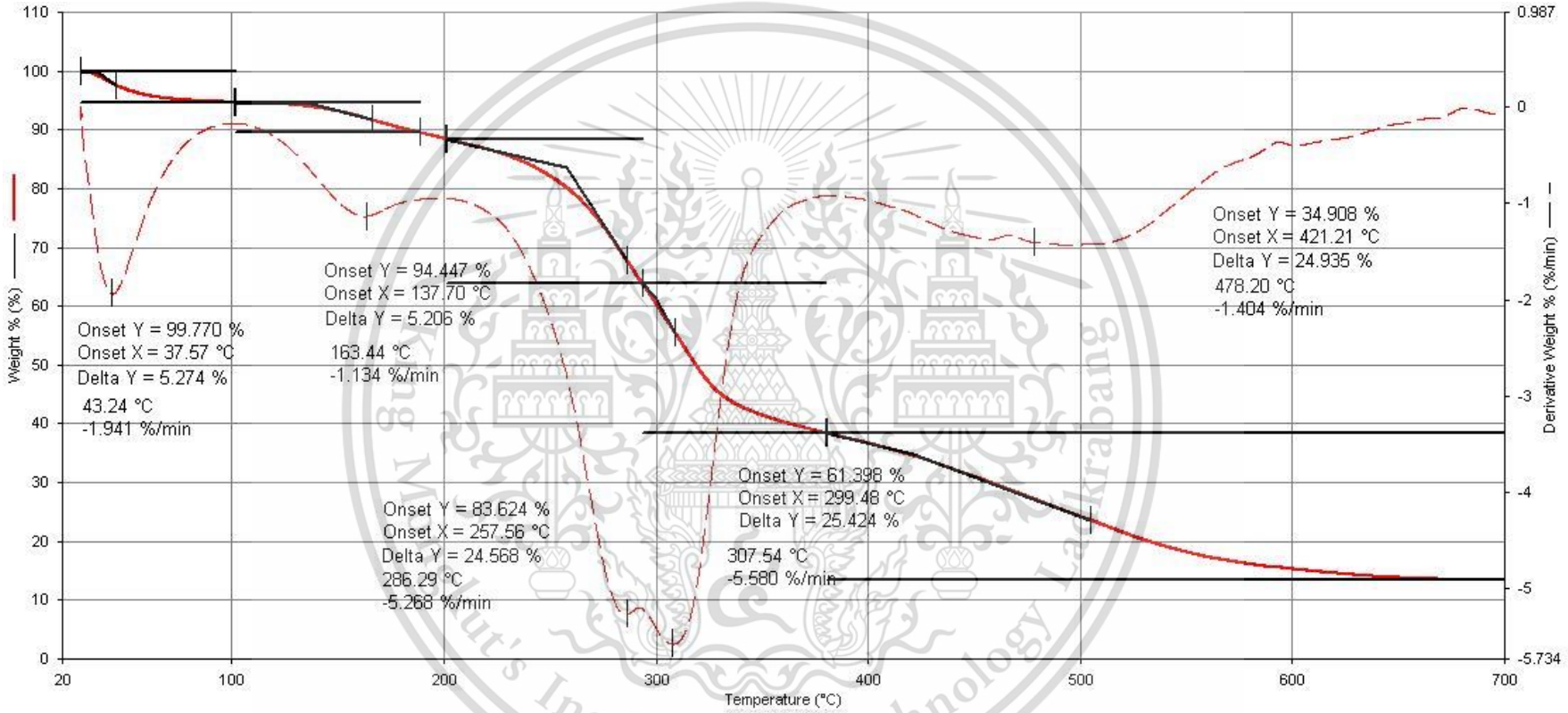

Figure D11. TGA and DTG thermograms of BSM hydrogel sponge crosslinked with 10%wt of STMP/STPP

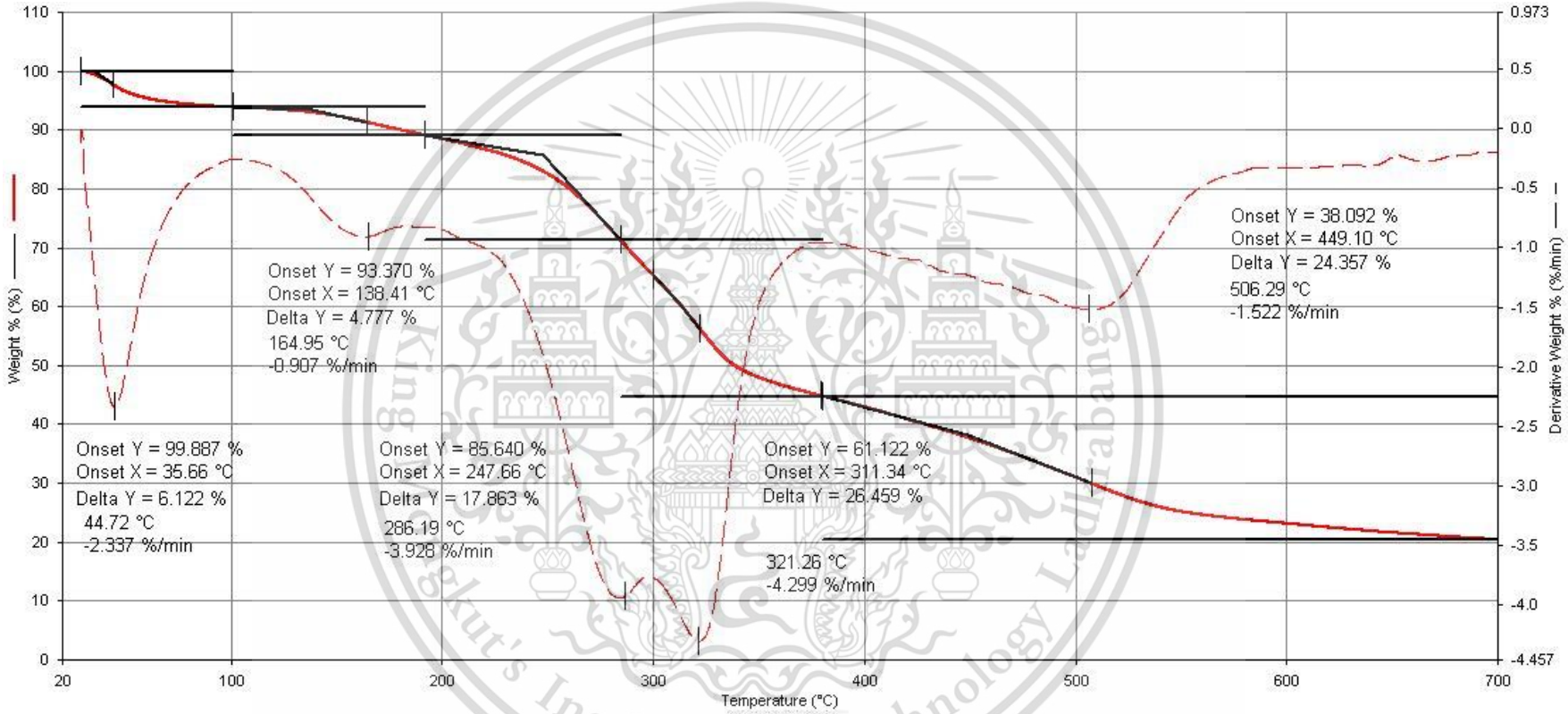

Figure D12. TGA and DTG thermograms of BSM hydrogel sponge crosslinked with 20%wt of STMP/STPP

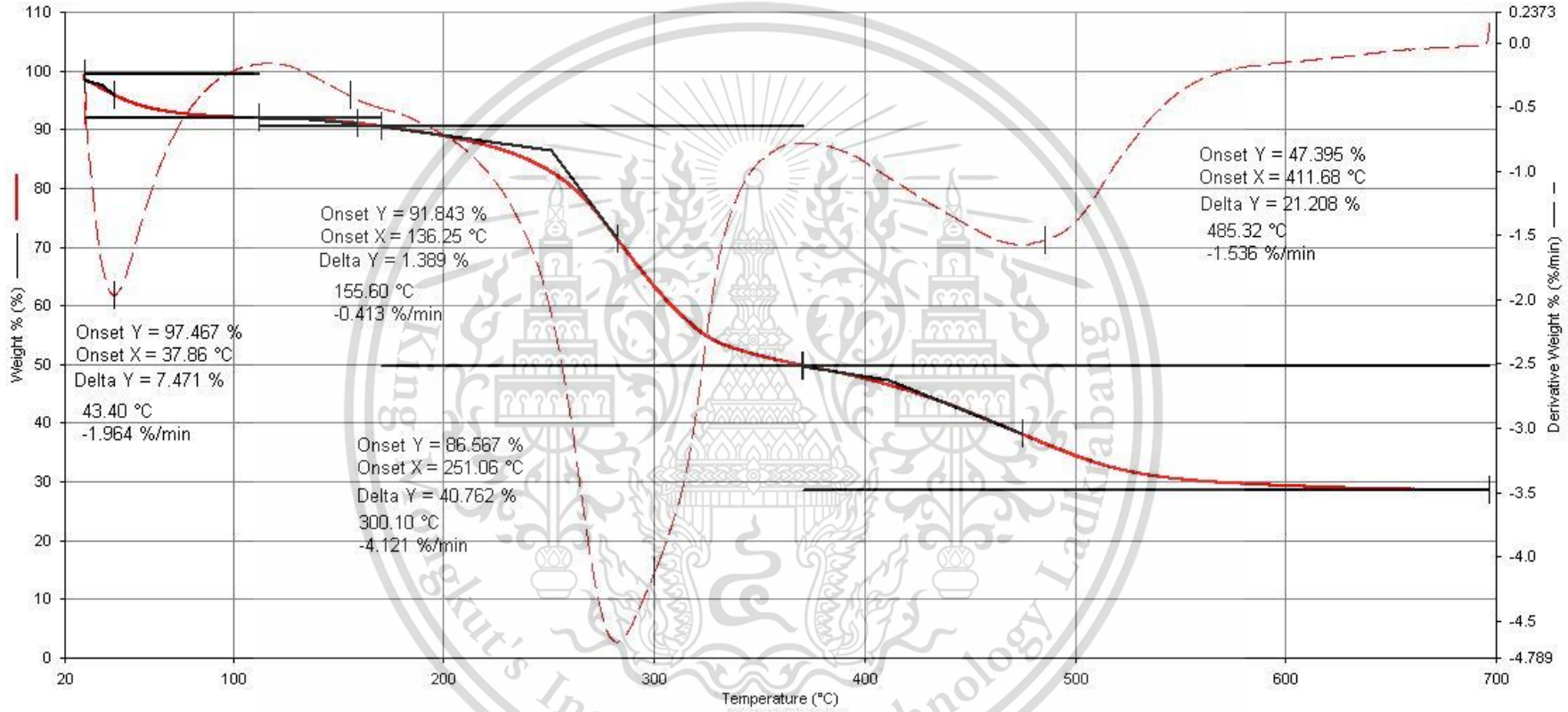

Figure D13. TGA and DTG thermograms of BSM hydrogel sponge crosslinked with 20%wt of STMP/STPP and incorporated with 30 wt% of ZnONP

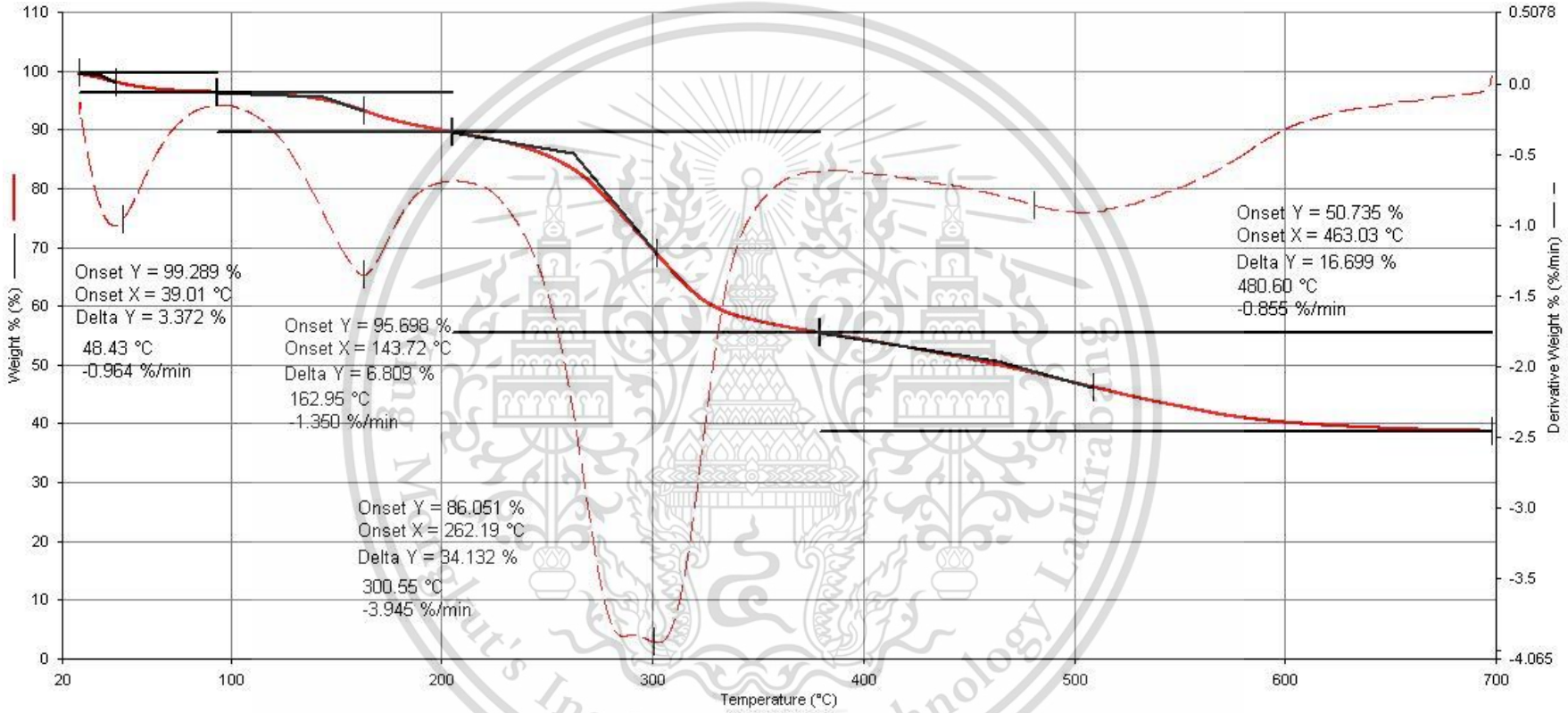

Figure D14. TGA and DTG thermograms of BSM hydrogel sponge crosslinked with 20%wt of STMP/STPP and incorporated with 50 wt% of ZnONP

Academic publications

Carbohydrate Polymers 227 (2020) 115360

Contents lists available at ScienceDirect

Carbohydrate Polymers

journal homepage: www.elsevier.com/locate/carbpol

Property improvement of antibacterial wound dressing from basil seed (*O. basilicum* L.) mucilage- ZnO nanocomposite by borax crosslinking

Siriporn Tantiwatcharothai[a], Jutarat Prachayawarakorn[a,b,*]

[a] Department of Chemistry, Faculty of Science, King Mongkut's Institute of Technology Ladkrabang (KMITL), Bangkok, 10520, Thailand
[b] Advanced Materials Research Unit, Faculty of Science, King Mongkut's Institute of Technology Ladkrabang (KMITL), Bangkok, 10520, Thailand

ARTICLE INFO

Keywords:
Antibacterial activity
Basil seed mucilage
Crosslinking
Hydrogel
ZnO nanoparticles

ABSTRACT

Some applications, in particular, wound dressings, require significant water holding capability: hydrogels formed from Basil seed mucilage (BSM) are non-toxic natural substances and exhibit the needed water holding capacity. However, the sponges have low dimensional stability and easily degrade in aqueous media. We overcame this drawback by crosslinking with borax. To provide antibacterial activity, zinc oxide nanoparticles (ZnO-NP) were added. With 10–20 wt% added borax and ZnO-NP, all key properties improved: dimensional stability, water retention capacity (31 to 41%), stress at maximum load (2.6 to 6.6 MPa), Young's modulus (74 to 113 MPa) and strain (28 to 54%). An interconnecting system of pores with well distributed ZnO-NP was observed from scanning electron microscope. In addition, higher borax and ZnO-NP loadings slightly decreased porosity (92% to 73%) and swelling (109 to 56). Moreover, antibacterial activity and cytotoxicity of BSM hydrogel sponge were also examined.

1. Introduction

In water, the outer pericarp of seeds of the basil plant (*Ocimum basilicum* L.), a well-known aromatic herb, swells into a mucilaginous layer - Basil Seed Mucilage (BSM) or basil seed gum. BSM is a hydrophilic hydrogel formed from polysaccharides (Tabashi & Razavi, 2017). The major polysaccharide in BSM is glucomannan (43%), with minor amount of xylan (24%) and cellulosic polysaccharides, along with 7% uronic acid (Tabashi & Razavi, 2017). BSM can absorb significant amount of water since many hydroxyl groups of the mucilage can form hydrogen bonds with water (Rana, Kamboj, Sharma, & Singh, 2015). As a result of the large water holding capacity, it becomes a potential source of safe, natural materials to produce polymers for wound dressings.

Dressing a wound to protect it from bacterial infection is essential to allow the wound to heal quickly (Xie et al., 2018). Ideally, a dressing should also absorb exudates from a wound and ensure a moist environment at the wound interface, as well as protecting it from microorganisms (Raguvaran et al., 2017; Xie et al., 2018). The large surface areas of porous hydrogel sponge dressings make them eff ;ective, allowing them to absorb and retain good exudate volumes (Autissier, Visage, Pouzet, Chaubet, & Letourneur, 2010). Freeze-drying is ordinarily used to fabricate three-dimensional spongy materials (Kamoun, Kenawy, & Chen, 2017). It was mentioned that hydrogel sponge from gelatin with gum kondagogu was porous (40–70%) and swelled substantially (30–65) (Rathore et al., 2016). Tavakoli reported that gelatin-starch sponge showed good swelling behavior but poor mechanical properties (Tavakoli, 2017).

Addition of inorganic antibacterial nanoparticles, such as ZnO nanoparticles (ZnO-NP), in a matrix of the wound dressing, brings another important property to a wound dressing, antibacterial activity. In general, ZnO-NP is also inexpensive and nontoxic to human cells (Gutierrez, Seligra, Jaramillo, Fama, & Goyanes, 2017; Nosar & Zyta, 2018). Bio-based materials, for example chitosan, xanthan gum and bacterial cellulose, incorporating ZnO-NP, have been shown to be effective antagonists for *Staphylococcus aureus* (*S. aureus*) and *Escherichia coli* (*E. coli*), and have suitable thermal and mechanical properties, high fluid absorption and water retention (Khalid, Khan, Ul-Islam, Khan, & Wahid, 2017; Mohandas, Deepthi, Biswas, & Jayakumar, 2018; Raafat, El-Sawy, Badawy, Mousa, & Mohamed, 2018).

From our previous study, BSM hydrogel sponge wound dressings, with ZnO-NP, showed high porosity, good swelling and effective antibacterial activity. However, its strong hydrophilic character leads to low dimensional stability and easy degradation in aqueous media during swelling (Tantiwatcharothai & Prachayawarakorn, 2019). Therefore, BSM hydrogel sponge wound dressings, for long term applications, need to be improved. One effective method to overcome its drawbacks is crosslinking. Crosslinking was widely used to improve

* Corresponding author at: Department of Chemistry, Faculty of Science, King Mongkut's Institute of Technology Ladkrabang (KMITL), Bangkok, 10520, Thailand.
E-mail address: jutarat.si@kmitl.ac.th (J. Prachayawarakorn).

https://doi.org/10.1016/j.carbpol.2019.115360
Received 17 July 2019; Received in revised form 19 September 2019; Accepted 20 September 2019
Available online 23 September 2019

water resistantance and also mechanical and thermal properties of many hydrophilic materials, such as, starch (Ghanbarzadeh, Almasi, & Entezami, 2011; Reddy & Yang, 2010; Seligra, Jaramillo, Famá, & Goyanes, 2016). Among various crosslinking agents, borax (di-sodium tetraborate, decahydrate) has potential, since it is non-toxic, inexpensive and readily available. Moreover, Tavakoli reported that water soluble borax, $Na_2[B_4O_5(OH)_4].8H_2O$, was successfully crosslinked in a starch-gelatin sponge, with good dimensional stability, swelling behavior and mechanical properties (Tavakoli, 2017). Borax crosslinked guar gum hydrogel was found to decrease swelling (Thombare, Jha, Mishra, & Siddiqui, 2017). It has also been reported that starch-poly(vinyl alcohol) blend, crosslinked with borax, showed improved thermal stability (Sreedhar, Sairam, Chattopadhyay, Syamala Rathnam, & Mohan Rao, 2005).

We aimed to improve several properties of BSM sponges, including dimensional stability, thermal and mechanical properties by crosslinking, using borax. The effect of borax loading (0–20 wt% of dry BSM) was investigated on the morphology, porosity, swelling, dimension stability, water retention capacity and mechanical and thermal properties. ZnO-NP was also supplement to improve antibacterial property of BSM sponge. Moreover, the effect of ZnO-NP on the properties of BSM sponge was also observed.

2. Experimental details

2.1. Materials

Basil seeds were purchased from Thai Baan Rai Co., Ltd. (Bangkok, Thailand). Borax was obtained from Chemipan. Co., Ltd. (Bangkok, Thailand). ZnO nanoparticles (20–40 nm) were purchased from Nanomaterials Technology, Co. Ltd. (Chonburi, Thailand). Glycerol was obtained from Lab System Co., Ltd. (Bangkok, Thailand).

2.2. BSM preparation

To form BSM, basil seeds were immersed in distilled water (1 h, ~30 °C). Each gram of seeds was covered in 30 g of water. The mucilage was scraped from the swollen seed surface with a blender for 1 min; then, filtered through a cheese cloth in order to remove the seeds and followed by centrifuging (5000 rpm, 5 min) to eliminate traces of seeds. The mucilage was refrigerated (24 h, −40 °C), then, lyophilized (24 h, −100 °C) in a freeze dryer (Coolsafe 110-4, Scan Vac, Denmark) to extract dried BSM.

2.3. Preparation of BSM hydrogel sponge

Dried BSM (1 wt%), plus a plasticizer (glycerol - 15 wt% of BSM), was dissolved in distilled water. Different amount of borax crosslinker (0, 5, 10, 20 wt% of dried BSM) was separately dissolved in 20 ml of distilled water; and, then added to the BSM solution (labelled as 0BO, 5BO, 10BO and 20BO). To study of the effect of ZnO-NP, ZnO-NP was added to 20BO formula solution (the optimum borax formula) at 30 and 50 wt%, based on the weight of dried BSM, (labelled as 20BO30ZnO-NP and 20BO50ZnO-NP). The solution was magnetically stirred (2 h, 40 °C). Next, 30 ml of the solution was placed in a petri dish (100 mm∅) to control the sample thickness, refrigerated (24 h, −40 °C) and, finally, lyophilized in a freeze dryer (24 h, −100 °C).

2.4. Morphology

Sample morphology was examined in images taken by a scanning electron microscope (SEM), (LEO 1455VP, ZEISS, Germany) using an acceleration voltage of 15 kV and magnification levels of 200 and 10,000 ×. Liquid N_2 was used to fracture the sample, after that, a thin Au layer was sputtered onto it.

2.5. Thickness

Sample thickness was measured with a micrometer (Model G, Peacock, Japan) on a 40 × 40 mm^2 sample. Eight measurements were made and the mean values were reported.

2.6. Porosity

Sample porosity was calculated from displacement. The sample was immersed for 10 min in a measured ethanol volume (V_1) in a graduated cylinder. Ethanol volumes were recorded, after immersion (V_2) and the remaining volume, after the sample was removed from the cylinder, (V_3). Porosity was computed from:

$$\text{Porosity}\ (\%) = \frac{V_1 - V_3}{V_2 - V_3} \times 100. \quad (1)$$

2.7. Water retention

A 20 × 20 mm^2 sample in distilled water was allowed to swell until it attained equilibrium. Excess water was removed from the sample by gently blotting with filter paper. After that, the sample was left for 24 h at ambient temperature and then weighed. Water retention was computed from:

$$\text{Water retention capacity}\ (\%) = \frac{W_T}{W_0} \times 100 \quad (2)$$

where W_0 was the initial mass and W_T was the mass after left for 24 h.

2.8. Swelling

A weighed 20 × 20 mm^2 dried sample was soaked in distilled water (~25 °C). After 48 h soaking, swelling was measured. The swollen sample was taken from the water, excess surface water was wiped off with a filter paper, and weighed immediately. Swelling was calculated as:

$$\text{Swelling} = \frac{M_w - M_0}{M_0} \quad (3)$$

where M_0 was the sample mass before immersion and M_w was the mass after immersion.

2.9. Dimensional stability

Dimensional stability was determined following Tavakoli (2017). A 20 × 20 mm^2 sample was soaked in distilled water for 48 h. A digital vernier caliper measured width, length and thickness (Super caliper, Mitutoyo, Japan) at 24 and 48 h. A mean from eight measurements was used.

2.10. Mechanical properties

A Lloyd universal testing machine (LR 5 K) (100 N load cell, 50 mm/min crosshead speed), was used to determine mechanical properties. Following the ASTM D-882 standard, 15 × 100 mm^2 rectangular pieces of the sample were kept at and relative humidity 58 ± 2% for 24 h, before each test. Means of 10 replicates were computed.

2.11. Thermal properties

Thermograms from 30 to 900 °C were recorded at 10 °C/min, under N_2 atmosphere, with a Perkin Elmer thermogravimetric analyzer (Pyris I TGA HT), from which Thermogravimetric (TGA) and derivative (DTG) properties were derived.

2.12. Antibacterial activity

The inhibition zones observed in agar discs were measured to assess activity against *S. aureas* (Gram-positive) and *E. coli* (Gram-negative). 10 mm ∅ circular discs were placed on an agar plate loaded with a bacterial lawn and incubated (24 h at 37 °C). The diameter of the resulting inhibition zone was measured. Means from 3 replicates were recorded.

2.13. In vitro cytotoxicity

3-(4, 5-dimethylthiazol-2 yl)-2, 5-diphenyl tetrazolium bromide or MTT assay with and human keratinocytes (HaCat) cells was used for cytotoxicity testing. After sterilization, a sample was soaked in phosphate buffered saline (24 h at 37 °C). After soaking, the sample was filtered and Dulbecco's Modified Eagle Medium (DMEM) was added to the filtrate: this mixture was incubated in a DMEM medium, supplemented with 10% fetal bovine serum. Then, 100 µl HaCat cells (1×10^5 cells/ml) were seeded and incubated (24 h, 37 °C) in the wells of a 96-well plate. After that, 100 ml of incubated filtrate mixture were added to the well, 10 µl of MTT solution (5 mg/mL) was added to the well and again incubated at 37 °C for 4 h. Next, formazan crystals were dissolved in 100 µl of 100% dimethyl sulfoxide: 10% sodium dodecyl sulfate solution and 100 µl of the resulting solution was transferred to the well. The final mixture absorbance at 570 nm of was measured using a Biochome (UK) microtiter plate reader (EZ read 2000). Optical microscope images were obtained to observe cell morphology.

2.14. Statistical analysis

Statistical analysis was performed using the analysis of variance (ANOVA) procedure with IBM SPSS statistics 25 software. Tukey's test was used to determine differences among the means ($p < 0.05$).

3. Results and discussion

A diagram showing the synthesis of BSM hydrogel sponge crosslinked with borax is shown in Fig. 1. Borax dissociates to boric acid and borate in aqueous medium, as suggested by Sarika, Kuriakose, Jayakrishnan, Anilkumar, and James (2014):

$$B_4O_7^{2-} + 7H_2O \leftrightharpoons 2B(OH)_3 + 2B(OH)^{4-} \quad (4)$$

Borate can crosslink with hydroxyl groups at C-2 and C-3 of polysaccharides in BSM, *i.e.* glucomannan, the major component in BSM and form coordinate covalent bond between boron and oxygen atoms (Fig. 1). The mechanism was also reported for other polysaccharides crosslinked with borax, *i.e.* starch (Sarika et al., 2014) and guar gum (Thombare et al., 2017). Furthermore, Fig. 1 shows the BSM and ZnO-NP interaction in the system. ZnO-NP could form electrostatic interaction with BSM molecules since ZnO-NP contained a polar structure from O^{2-} and Zn^{2+} in its tetrahedral structure, so the polar segments lead to the electrostatic interactions with oppositely charged of polymer segments in the system. Moreover, It could be occurred hydrogen bond between BSM and ZnO-NP could form as seen in Fig. 1. These observation were also found in PVA/chitosan incorporated with Zn-ONP and gum acacia- ZnO-NP hydrogel (Mohammad, Alireza, Armaghan, Hamidreza, & Zohreh, 2018; Sunil, Mamta, & Seema, 2016).

3.1. Morphology

The porous structure of the sponges was formed by ice sublimation with a freeze-dryer after freezing at −40 °C in the freezer. In the SEM images (Fig. 2), it is clear that all sponges showed a uniform interconnected opened-cell structure. The effect, on the sponge microstructure, of crosslinking with various borax loadings is shown in Fig. 2(b–d). It was seen that the higher borax loading created smaller cells and a more compact pore structure. This was attributed to the effect of crosslinking between hydroxyl groups of BSM and borax (Fig. 1), resulting in a decrease in free volume and mobility of polysaccharide chains in the BSM. A similar change in morphology after crosslinking has also been reported for crosslinked starch-borax sponge (Tavakoli, 2017) and crosslinked starch-citric acid foam (Pornsuksomboon, Holló, Szécsényi, & Kaewtatip, 2016). Moreover, it was observed that, the pore structure became a slightly tighter network after adding ZnO-NP. This was caused by electrostatic forces and hydrogen bonding, between polar segments (hydroxyl and carboxyl groups) of BSM and ZnO-NP (Fig. 1), led to the decrease of free hydroxyl and carboxyl groups able to interact with water. (Lu et al., 2017; Nafchi, Alias, Mahmud, & Robal, 2012).

Fig. 3 shows 10,000 × SEM cross section images of the sponges prepared with various borax and ZnO-NP loadings. A rougher surface is evident for sponges crosslinked with higher borax loading (Fig. 3(a–d)). This is a consequnce of a decrease in chain mobility of BSM after crosslinking. Additionally, ZnO-NP was seen to distribute evenly over BSM matrix for the 20BO30ZnO-NP and also the 20BO50ZnO-NP (Fig. 3(e) and (f)).

3.2. Thickness and porosity

The compact structure of the pores after crosslinking and the addition of ZnO-NP also affected thickness and porosity of the sponge as seen in Table 1. It was observed that the sponge prepared without borax and ZnO-NP was thicker and more porous. The borax and ZnO-NP loading decreased the thickness (1.53 mm–1.34 mm) and porosity (92% to 73%). Although the porosity was lower, it was higher than that of gum kondagogu sponge (60–70%) (Rathore et al., 2016). High porosity is an advantage for wound dressing because it helps to absorb large volumes of wound exudates.

3.3. Water retention

Water retention capacity is an ability of a hydrogel sponge to hold water molecules within their structures. It is another key property for a wound dressing, which should keep the environment at the wound surface moist (Zahedi, Rezaeian, Ranaei, Jafari, & Supaphol, 2010). Water retention capacity of BSM hydrogel sponge is shown in Table 1. Unmodified sponge (0BO) showed 31% water retention. It was comparable to water retention of hydrogels formed from xanthan gum with embedded ZnO-NP (8–30%) (Raafat et al., 2018). Water retention of the sponges increased slightly from 31 to 40% after crosslinking. Also, adding ZnO-NP further increased water retention capacity slightly. This was attributed to the tighter pore structure of the sponges after crosslinking and addition of ZnO-NP, which made it difficult to lose water from the sponge structure, as shown in Fig. 2.

3.4. Swelling and dimensional stability

Swelling and dimensional stability of hydrogel sponge are important parameters for wound dressing. The swelling of sponges fabricated with various borax and ZnO-NP loading is shown in Table 2. It can be seen that unmodified sponge (0BO) showed the highest swelling value. This was due to the hydrophilic nature of BSM molecules which contains the main composition of glucomamnan. Glucomannan is composed of many hydroxyl groups, which can interact strongly with water. In spite of the highest degree of swelling of unmodified BSM hydrogel sponge, it showed the lowest dimensional stability which is not appropriate property for wound dressing (Table 2). The dimensions of unmodified sponge (0BO) could not be measured accurately after 24 h, because some edges and outer surfaces were partially dissolved by water. As expected, after crosslinking, the increased borax loading resulted in decreased swelling (109–65) and also improved dimensional stability (Table 2). This was caused by crosslinking between hydroxyl groups of

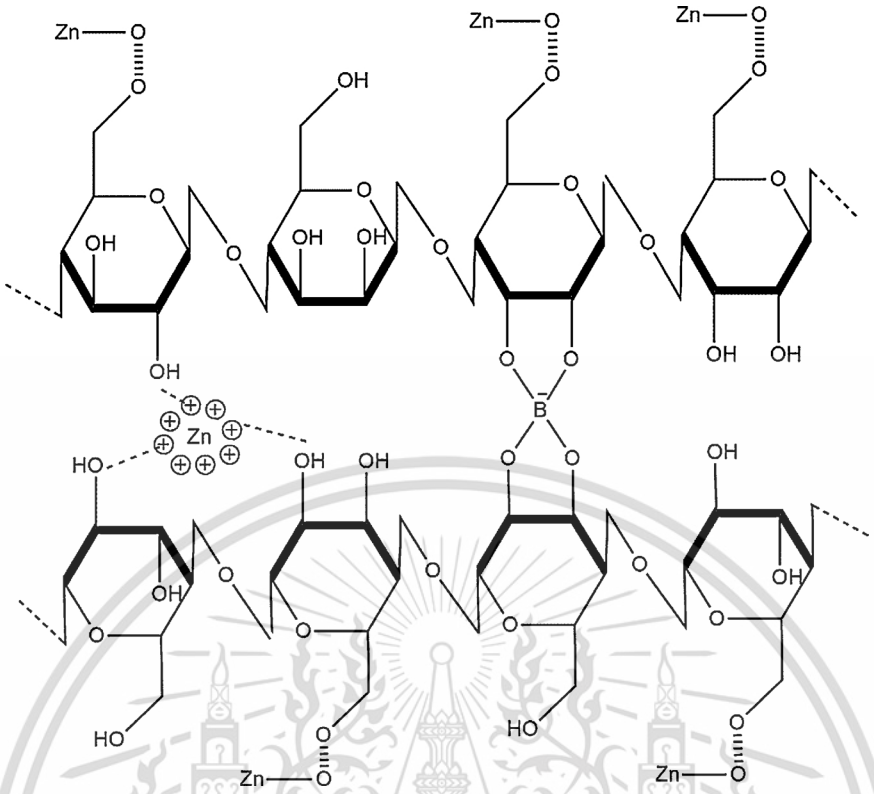

Fig. 1. The schematic representation for synthesis of BSM hydrogel sponge crosslinked with borax and incorporated with ZnO-NP.

polysaccharide molecules in BSM and borax leading to a decrease in hydroxyl groups available to interact with water. Moreover, the crosslinking reaction also enhanced the stabilization of BSM molecules. Further, the decrease in porosity, after crosslinking and the incorporation of ZnO-NP, contributed to lower swelling (Fig. 2 and Table 1.)

The effect of ZnO-NP on swelling and dimensional stability after 24 h and 48 h immersion in water is also shown in Table 2. It was observed that the increase of ZnO-NP loading resulted in slightly decreased swelling of the sponge. This was caused by hydrogen bonding and electrostatic interaction between BSM molecules and ZnO-NP (Fig. 1). Further, more ZnO-NP could fill some voids in BSM network, and restrict the network expansion and hinder water penetration. Similar observation was founded in xanthan gum- ZnO-NP (Raafat et al., 2018). Although the incorporation of borax and ZnO-NP caused lower swelling, the crosslinked BSM hydrogel sponge could swelled significantly more than that obtained from chitosan-Ag/ZnO dressing (20–25). In addition, the swelling of modified BSM was comparable to porous sponge from gum kondagogu (30–65) (Kanimozhi, Basha, & Kumari, 2016; Rathore et al., 2016). Moreover, Table 2 shows the effect of ZnO-NP content on dimensional stability of BSM hydrogel sponges. No significant difference of swelling and dimensional stability between

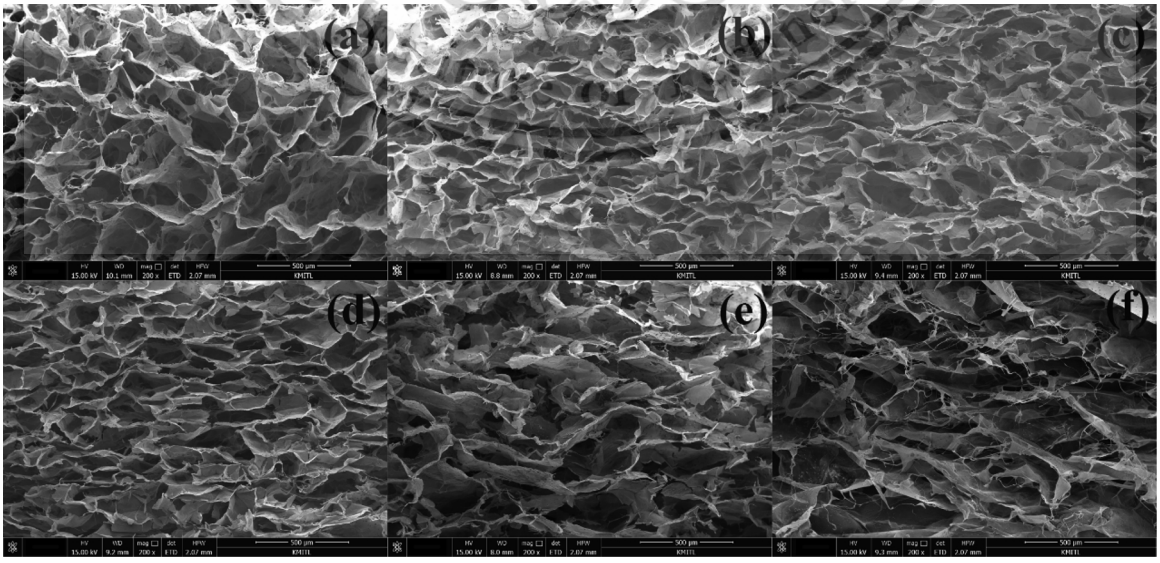

Fig. 2. SEM cross section images (200 × magnification) of BSM hydrogel sponges with varying borax and ZnO-NP loadings: (a) 0BO, (b) 5BO, (c) 10BO, (d) 20BO, (e) 20BO30ZnO-NP and (f) 20BO50ZnO-NP.

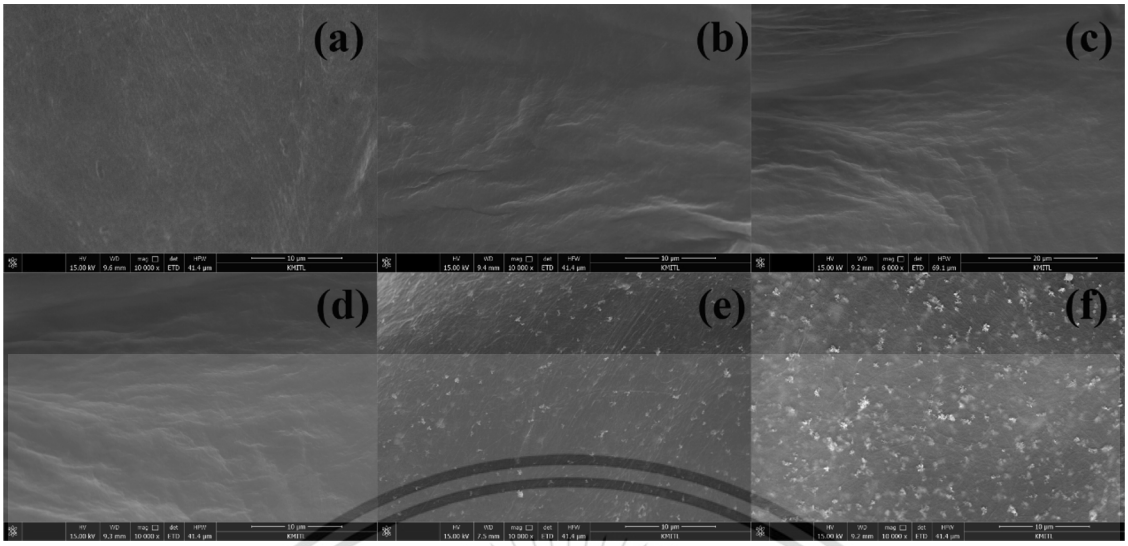

Fig. 3. SEM cross section images (10,000 × magnification) of BSM hydrogel sponges with varying borax and ZnO-NP loadings: (a) 0BO, (b) 5BO, (c) 10BO, (d) 20BO, (e) 20BO30ZnO-NP and (f) 20BO50ZnO-NP.

Table 1
Key properties of BSM hydrogel sponge *vs* borax and ZnO-NP loading.

Sample	Thickness (mm)	Porosity (%)	Water retention capacity (%)
0BO	1.53 ± 0.23^{a}	92.1^{a}	31.2^{a}
5BO	1.44 ± 0.11^{b}	89.1^{b}	38.7^{b}
10BO	1.41 ± 0.03^{c}	85.8^{c}	39.2^{b,c}
20BO	1.42 ± 0.06^{c}	82.3^{d}	39.9^{c}
20BO30ZnO-NP	1.39 ± 0.07^{c}	76.5^{e}	40.7^{c,d}
20BO50ZnO-NP	1.34 ± 0.05^{d}	73.3^{f}	41.3^{d}

Different superscript letters in the same column are significantly different ($p < 0.05$), based on Tukey's test.

Table 3
Mechanical properties of BSM hydrogel sponges *vs* borax and ZnO-NP loading.

Sample	Mechanical properties		
	Stress at maximum load (MPa)	Young's modulus (MPa)	Strain at maximum load (%)
0BO	2.6 ± 0.42^{a}	74 ± 5.2^{a}	28 ± 4.1^{a}
5BO	3.8 ± 0.37^{b}	92 ± 7.3$^{a, b}$	39 ± 3.5^{b}
10BO	4.9 ± 0.48^{b}	101 ± 6.6^{b}	47 ± 4.2^{b,c}
20BO	6.6 ± 0.36^{c}	113 ± 7.2^{b}	54 ± 3.6^{c,d}
20BO30ZnO-NP	9.8 ± 0.53^{d}	146 ± 9.4^{c}	57 ± 3.2^{d}
20BO50ZnO-NP	11.4 ± 0.6^{e}	173 ± 10.3^{d}	58 ± 2.7^{d}

Different superscript letters in the same column are significantly different ($p < 0.05$), based on Tukey's test.

Table 2
Swelling and dimensional stability of BSM hydrogel sponge *vs* borax and ZnO-NP loading in distilled water.

Sample	Swelling	Swelling time (h)	Dimension variation (mm)		
			Width	Length	Thickness
0BO	109 ± 2^{a}	0	0	0	0
		24	2.4 ± 0.61^{a}	2.6 ± 0.43^{a}	N/A*
		48	N/A*	N/A*	N/A*
5BO	82 ± 3^{b}	0	0	0	0
		24	1.2 ± 0.1^{b,A}	1.1 ± 0.15^{b,A}	0.7 ± 0.13^{b,A}
		48	1.6 ± 0.41^{A}	1.4 ± 0.21^{A}	0.8 ± 0.22^{A}
10BO	74 ± 2^{c}	0	0	0	0
		24	0.9 ± 0.19^{b,A}	0.8 ± 0.22^{b,A}	0.6 ± 0.14^{b,A}
		48	1.2 ± 0.34^{A}	1.1 ± 0.43^{A}	0.7 ± 0.18^{A}
20BO	65 ± 4^{d}	0	0	0	0
		24	0.3 ± 0.06^{c,A}	0.3 ± 0.12^{c,A}	0.2 ± 0.04^{c,A}
		48	0.4 ± 0.09^{A}	0.3 ± 0.07^{A}	0.3 ± 0.11^{A}
20BO30ZnO-NP	60 ± 1^{e}	0	0	0	0
		24	0.4 ± 0.11^{c,A}	0.3 ± 0.13^{c,A}	0.2 ± 0.11^{c,A}
		48	0.4 ± 0.05^{A}	0.4 ± 0.07^{A}	0.3 ± 0.05^{A}
20BO50ZnO-NP	56 ± 2^{e}	0	0	0	0
		24	0.3 ± 0.12^{c,A}	0.3 ± 0.15^{c,A}	0.2 ± 0.11^{c,A}
		48	0.3 ± 0.06^{A}	0.4 ± 0.05^{A}	0.3 ± 0.02^{A}

Reported values are mean ± standard deviation. Different superscript letters (a–d) in the same column are significantly different ($p < 0.05$) between each sample, different letters (A–B) are significantly different ($p < 0.05$) between the same sample at different swelling times, based on Tukey's test.

* N/A: not available.

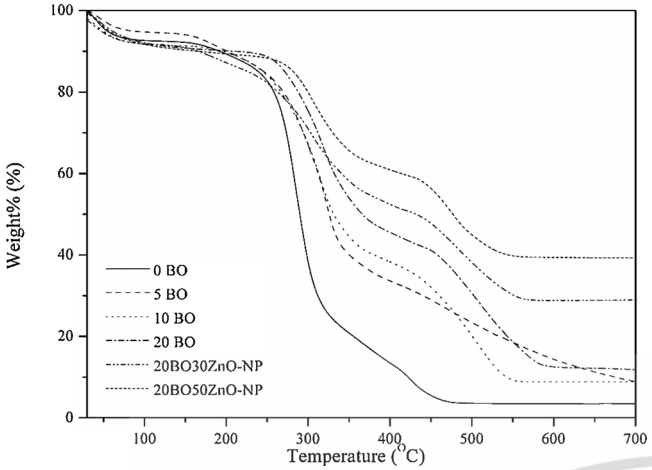

Fig. 4. TGA curves of BSM hydrogel sponges with various borax and ZnO-NP loadings.

Table 4
E. coli and *S. aureus* inhibition zones for BSM hydrogel sponges *vs* borax and ZnO-NP loadings.

Sample	Zone of inhibition (mm)	
	S. aureus	*E. coli*
0BO	Inactive	Inactive
5BO	Inactive	Inactive
10BO	Inactive	Inactive
20BO	Inactive	Inactive
20BO30ZnO-NP	15.2	14.2
20BO50ZnO-NP	16.7	14.8

20BO30ZnO-NP and 20BO50ZnO-NP could be observed.

3.5. Mechanical properties

Mechanical properties of sponges prepared with different borax and ZnO-NP contents are shown in Table 3. Increasing the borax loading resulted in the increased stress at maximum load (2.6–6.6 MPa), Young's modulus (74–113 MPa) and also strain at maximum load (28–54%). These mechanical properties improved because of increased crosslinking density between borate and hydroxyl group at C-2 and C-3 of polysaccharide molecules in BSM as shown in Fig. 1. Moreover, the decreased distance between the BSM layers and the tight network structure after crosslinking is clear in the SEM images (Fig. 2), leading to stronger layer to layer interactions. The improved mechanical properties with borax crosslinking was also observed by Tavakoli in crosslinked starch-borax sponge (Tavakoli, 2017). Furthermore, we observed an increased stress at maximum load, Young's modulus and strain at maximum load of the sponge with the incorporation of ZnO-NP. ZnO-NP's high strength and large surface area clearly reinforced the sponge, and Fig. 2 shows that the nanoparticles were evenly distributed. Further, the hydrogen bonds and electrostatic interaction between ZnO-NP and the BSM matrix resulted in load transfer between matrix and nanoparticles.

3.6. Thermal properties

Fig. 4 shows TGA curves of BSM sponges with increased borax and ZnO-NP loadings. For the unmodified sponge, four thermal degradation stages were found. The initial step between 35 and100 °C was due to the loss of moisture. The second step at 120–210 °C was caused by the decomposition of glycerol in the sponge. The main degradation step at 255-340 °C was the decomposition of the polysaccharides (glucomannan, xylan, *etc*) of hemicellulose in BSM (Azwa, Yousif, Manalo, & Karunasena, 2013; Kurd, Fathi, & Shekarchizadeh, 2017; Pinpueng & Hongsriphan, 2015). Finally, cellulose and lignin decomposition in BSM caused the fourth step (410–460 °C) (Azwa et al., 2013; Pinpueng & Hongsriphan, 2015). It should be mentioned that BSM molecules decomposition temperature shifted significantly to higher temperature and the residual weight percentage increased when borax loading increased. This was attributed to crosslinking between borax and numerous hydroxyl groups of the polysaccharides in BSM, leading to the strong linkages and stronger BSM backbone chains.

With the addition of ZnO-NP, all degradation steps were shifted to higher temperatures and the residual weight percentage increased. This may be attributed to electrostatic interaction and hydrogen bond between polar segment of BSM and ZnO-NP. These results indicated that the borax crosslinking and the adding of ZnO-NP could improve thermal stability of BSM hydrogel sponges. The shift of thermal degradation temperature towards higher temperature was found for agar/carrageenan/CMC blended films with added ZnO-NP (Kanmani & Whan Rhim, 2014) and starch–poly(vinyl alcohol) film crosslinked with borax (Sheehar, Sairam, Chattopadhyay, Rathnam and Rao, 2004).

3.7. Antibacterial activity

We assessed the effectiveness of BSM hydrogel sponges as wound dressings by measuring antibacterial activity against two bacteria commonly found in wounds - *S. aureus* and *E.coli* (Table 4). As expected, the incorporation of different borax content did not affect antibacterial activity of BSM sponge. However, ZnO-NP loading resulted in better antibacterial activity against both of *S. aureus* and *E.coli*. Moreover, greater activity was observed against *S. aureus* than *E.coli*. This is

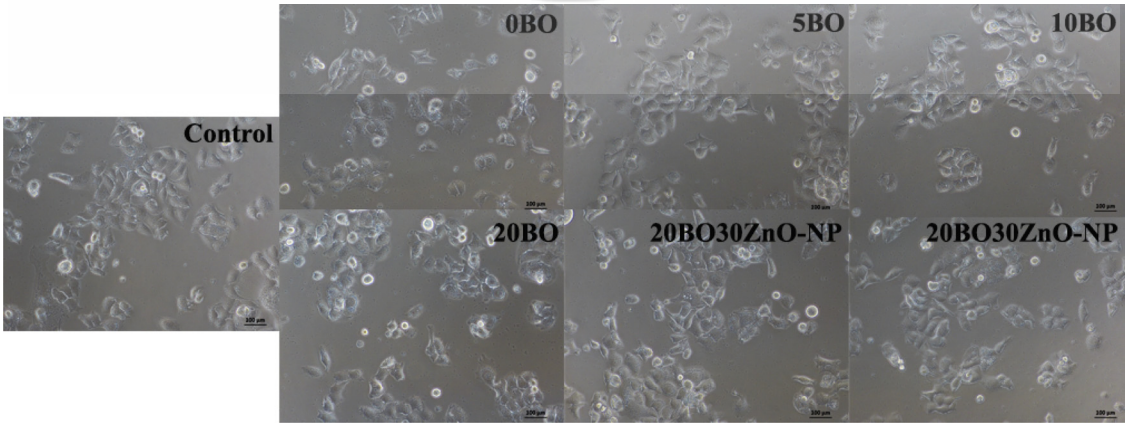

Fig. 5. Optical microscopy images (200× magnification) of the control and BSM hydrogel sponges with several borax and ZnO-NP loadings.

possibly due to differences in cell wall structures: Gram-positive bacteria possess thick cell walls of peptidoglycan; whereas, Gram-negative cell wall structures are more complex, and, thus, more resistant to attack by any antimicrobial agent (Gutierrez et al., 2017). Several biologically sourced materials, loaded with ZnO-NP, have shown similar behaviour: xanthan gum-based hydrogels and agar/carrageenan/CMC films (Kanmani & Whan Rhim, 2014; Raafat et al., 2018).

3.8. In vitro cytotoxicity

As the amount of borax and ZnO-NP in the sponge may be toxic to humans, we assessed cytotoxicity of the various BSM sponges by comparing to that of a control (with no borax or ZnO-NP), by MTT assay with HaCat cells. Fig. 5 shows that there were no significant differences between the control cells and all of BSM hydrogel sponge. There was no morphological hallmark, for example, chromatin condensation, chromatin fragmentation or nuclear fragmentation. Thus, the crosslinked BSM sponges were not toxic to human cells.

4. Conclusion

Antibacterial dressings from Basil Seed Mucilage (BSM) with ZnO-NP were improved after crosslinking with borax. The crosslinked sponges showed better dimensional stability, water retention capacity, mechanical and thermal properties than unmodified sponges. Moreover, increase in borax and ZnO-NP loading resulted in a slight decrease in sponge thickness, porosity and swelling. From morphology, ZnO-NP was evenly distributed on the BSM surface and the increase of borax and ZnO-NP loadings led to a tighter network structure. Finally, all crosslinked sponges were not toxic to HaCat cells, examined by cytotoxicity evaluation.

Acknowledgements

The authors would like to express our appreciation to the KMITL Research Fund (KREF 046108) for financial support and the Department of Chemistry and faculty of science of KMITL for facility support. The authors also thank John Morris for proof reading this article.

References

Autissier, A., Visage, C. L., Pouzet, C., Chaubet, F., & Letourneur, D. (2010). Fabrication of porous polysaccharide-based scaffolds using a combined freeze-drying/cross-linking process. *Acta Biomaterialia, 6*, 3640–3648.

Azwa, Z. N., Yousif, B. F., Manalo, A. C., & Karunasena, W. (2013). A reiew on the degradability of polymeric composites based on nateral fibres. *Materials & Design, 47*, 424–442.

Ghanbarzadeh, B., Almasi, H., & Entezami, A. A. (2011). Improving the barrier and mechanical properties of corn starch-based edibble films: Effect of citric acid and carboxymethyl cellose. *Industrial Crops and Products, 33*, 229–235.

Gutierrez, T. J., Seligra, P. G., Jaramillo, C. M., Fama, L., & Goyanes, S. (2017). Effect of filler properties on the antioxidant response of thermoplastic starch composites. In K. M. Vijay, K. T. Manju, & R. K. Michael (Eds.). *Handbook of composites from renewable materials* (pp. 337–370). Argentina: Scrivener Publishing LLC.

Kamoun, E. A., Kenawy, E. S., & Chen, X. (2017). A review on polymeric hydrogel membranes for wound dressing applications: PVA-based hydrogel dressings. *Journal of Advanced Research, 8*, 217–233.

Kanimozhi, K., Basha, S. K., & Kumari, V. S. (2016). Processing and characterization of chitosan/PVA and methylcellulose porous scaffolds for tissue engineering. *Materials Science and Engineering C, 61*, 484–491.

Kanmani, P., & Whan Rhim, J. (2014). Properties and characterization of bionanocomposite films prepared with various biopolymers and ZnO nanoparticles. *Carbohydrate Polymers, 106*, 190–199.

Khalid, A., Khan, R., Ul-Islam, M., Khan, T., & Wahid, F. (2017). Bacterial cellulose-zinc oxide nanocomposites as a novel dressing system for burn wounds. *Carbohydrate Polymers, 164*, 214–221.

Kurd, K., Fathi, M., & Shekarchizadeh, H. (2017). Basil seed mucilage as a new source for electrospinning: Production and physicochemical characterization. *International Journal of Biological Macromolecules, 95*, 689–695.

Lu, Z., Gao, J., He, Q., Wu, J., Liang, D., Yang, H., et al. (2017). Enhanced antibacterial and wound healing activities of microporous chitosan-Ag/ZnO composite dressing. *Carbohydrate Polymers, 156*, 460–469.

Mohandas, A., Deepthi, S., Biswas, R., & Jayakumar, R. (2018). Chitosan based metallic nanocomposite scaffolds as antimicrobial wound dressings. *Bioactive Materials, 3*, 267–277.

Mohammad, T. K., Alireza, J., Armaghan, M., Hamidreza, S., & Zohreh, M. (2018). Incorporation of ZnO nanoparticles into heparinised polyvinyl alcohol/chitosan hydrogels for wound dressing application. *International Journal of Biological Macromolecules, 114*, 1203–1215.

Nafchi, A. M., Alias, A. K., Mahmud, S., & Robal, M. (2012). Antimicrobial, rheological, and physicochemical properties of sago starch films filled with nanorod-rich zinc oxide. *Journal of Food Engineering, 113*, 511–519.

Nosar, M. N., & Zyta, Z. M. (2018). Wound dressings from naturally-occurring polymers: A review on homopolysaccharide-based composites. *Carbohydrate Polymers, 189*, 378–389.

Pinpueng, A., & Hongsriphan, N. (2015). *Study of water adsorption and fertilizer release of poly (butylene succinate) blended with natural absorbent for using in agriculture application.* Thesis of department of materials science and engineering, Silapakorn university.

Pornsuksomboon, K., Holló, B. B., Szécsényi, K. S., & Kaewtatip, K. (2016). Properties of baked foams from citric acid modified cassava starch and native assava starch blends. *Carbohydrate Polymers, 136*, 107–112.

Raafat, A. I., El-Sawy, N. M., Badawy, N. A., Mousa, E. A., & Mohamed, A. M. (2018). Radiation fabrication of Xanthan-based wound dressing hydrogels embedded ZnO nanoparticles: In vitro evaluation. *International Journal of Biological Macromolecules, 118*, 1892–1902.

Raguvaran, R., Balvinder, K. M., Meenu, C., Rajesh, T., Taruna, A., Anu, K., et al. (2017). Sodium alginate and gum acacia hydrogels of ZnO nanoparticles show wound healing effect on fibroblast cells. *International Journal of Bioloical Macromolecules, 96*, 185–191.

Rana, V., Kamboj, S., Sharma, R., & Singh, K. (2015). Modification of gums: Synthesis techniques and pharmaceutical benefits. In K. T. Vijay, & K. T. Manju (Eds.). *Handbook of polymer for pharmaceutical technologies* (pp. 299–364). Massachusetts: Scrivener Publishing LLC.

Rathore, H. S., Sarubala, M., Ramanathan, G., Singaravelu, S., Raja, M. D., Gupta, S., et al. (2016). Fabrication of biomimetic porous novel sponge from gum kondagogu for wound dressing. *Materials Letters, 177*, 108–111.

Reddy, N., & Yang, Y. (2010). Citric acid cross-linking of starch films. *Food Chemistry, 118*, 702–711.

Sarika, P. R., Kuriakose, C., Jayakrishnan, A., Anilkumar, P. R., & James, N. R. (2014). Modified gum arabic cross-linked gelatin scaffold for biomedical applications. *Materials Science and Engineering C, 43*, 272–279.

Seligra, P. G., Jaramillo, C. M., Famá, L., & Goyanes, S. (2016). Biodegradable and non-retrogradable eco-films based on starch-glycero with citric acid as crosslinkinh agent. *Carbohydrate Polymers, 138*, 66–74.

Sreedhar, B., Sairam, M., Chattopadhyay, D. K., Syamala Rathnam, P. A., & Mohan Rao, D. V. (2005). Thermal, Mechanical, and Surface Characterization of starch–poly(vinyl alcohol) blends and borax-crosslinked films. *Journal of Applied Polymer Science, 96*, 1313–1322.

Sunil, K. B., Mamta, J., & Seema, T. (2016). Synthesis, characterization and antimicrobial applications of zinc oxide nanoparticles loaded gum acacia/poly(SA) hydrogels. *Carbohydrate Polymers, 114*, 60–65.

Tabashi, S. N., & Razavi, S. M. (2017). Functional properties and applications of basil seed gum: An overview. *Food Hydrocolloids, 73*, 313–325.

Tantiwatcharothai, S., & Prachayawarakorn, J. (2019). Characterization of an antibacterial wound dressing from basil seed (*Ocimum basilicum* L.) mucilage-ZnO nanocomposite. *International Journal of Bioloical Macromolecules, 135*, 133–140.

Tavakoli, J. (2017). Physico-mechanical, morphological and biomedical properties of a novel natural wound dressing material. *Journal of the Mechanical Behavior of Biomedical Materials, 65*, 373–382.

Thombare, N., Jha, U., Mishra, S., & Siddiqui, M. Z. (2017). Borax cross-linked guar gum hydrogels as potential adsorbents for water purification. *Carbohydrate Polymers, 188*, 274–281.

Xie, H., Chen, X., Shen, X., He, Y., Chen, W., Luo, Q., et al. (2018). Preparation of chitosan-collagen-alginate composite dressing and its promoting effects on wound healing. *International Journal of Bioloical Macromolecules, 107*, 93–104.

Zahedi, P., Rezaeian, I., Ranaei, S., Jafari, S., & Supaphol, P. (2010). A review on wound dressings with an emphasis on electrospun nanofibrous polymeric bandages. *Polymers for Advanced Technologies, 21*, 77–95.

International Journal of Biological Macromolecules 135 (2019) 133–140

Contents lists available at ScienceDirect

International Journal of Biological Macromolecules

journal homepage: http://www.elsevier.com/locate/ijbiomac

Characterization of an antibacterial wound dressing from basil seed (*Ocimum basilicum* L.) mucilage-ZnO nanocomposite

Siriporn Tantiwatcharothai [a], Jutarat Prachayawarakorn [a,b,*]

[a] Department of Chemistry, Faculty of Science, King Mongkut's Institute of Technology Ladkrabang (KMITL), Bangkok 10520, Thailand
[b] Advanced Materials Research Unit, Faculty of Science, King Mongkut's Institute of Technology Ladkrabang (KMITL), Bangkok 10520, Thailand

ARTICLE INFO

Article history:
Received 28 March 2019
Received in revised form 3 May 2019
Accepted 19 May 2019
Available online 21 May 2019

Keywords:
Basil seed mucilage
ZnO nanoparticles
Wound dressing

ABSTRACT

The large water holding capacity of Basil Seed (*Ocimum basilicum* L.) Mucilage (BSM) gives it potential to produce a valuable polymer for water holding applications such as wound dressing. The objective of this research was to prepare a natural-based antibacterial wound dressing from BSM by freeze-drying. Various contents of zinc oxide nanoparticles (ZnO-NP) were incorporated as an antibacterial agent. BSM hydrogel sponge showed considerable porosity and degree of swelling. From FTIR analysis, hydrogen bond and electrostatic interaction between BSM molecules and ZnO-NP were confirmed. SEM images revealed an interconnecting open-cell structure of pores in the BSM hydrogel sponge with a good distribution of ZnO-NP. Moreover, increase in ZnO-NP content improved the mechanical properties (stress at maximum load 8.9 MPa, Young's modulus 151 MPa and strain at maximum load 51%), thermal properties, water retention capacity and antibacterial activity. Cytotoxicity and cell adhesion studies of BSM hydrogel sponge indicated non-cytotoxicity and non-adherent nature of the sponge.

1. Introduction

There has been considerable interest in natural polymers to replace traditional synthetic polymers. Many natural materials, including mucilages, have been successfully used for pharmaceutical applications due to their biocompatibility, biodegradability and non-toxicity [1,2]. Natural mucilages consist of polysaccharides with numerous sugar units, connected together to form large molecules. Many natural mucilages form three-dimensional interconnected networks called "gels" [3].

Basil Seed (*Ocimum basilicum* L.) Mucilage (BSM), commonly known as 'basil seed gum', is the outer pericarp of basil seeds and is composed of starch, sugar, hemicellulose, cellulose and lignin [4]. BSM is a high molecular weight polysaccharide (~2300–6000 kDa) [4]. The mucilaginous layer of the swollen seeds has two major components: glucomannan (43%) and (1, 4)-linked xylan (24%) along with 6% of uronic acid [4]. The applications of BSM include emulsifying, foaming, thickening, gelling and stabilizing agents in food and pharmaceutical industries. BSM can produce edible films, with good mechanical properties and appearance by casting [5]. Additionally, BSM/Polyvinyl alcohol can produce thermostable ultra-thin nanofibers, for different applications in the food sector such as bioactive encapsulation [6].

BSM has a large water holding capacity; it can entrap large amounts of water to form a mucilaginous cluster, since it has numerous hydroxyl groups, which form hydrogen bonds with water molecules [6]. This makes it an interesting source of polysaccharides, to form polymers where water holding is required, such as wound dressings. Wound dressings are designed to cover a wound bed and protect it from factors that may delay its healing. The important requirements of an ideal wound dressing are high fluid absorption and retention [7]. The porous hydrogel sponge applied in wound dressing is effective, because it could absorb and retain large amounts of wound exudates [8]. The most common technique for producing three-dimensional porous material is freeze-drying [9,10]. Gum kondagogu with gelatin has been fabricated into a porous hydrogel sponge with a high degree of swelling (30–65%), porosity (40–70%) and excellent biocompatibility [11]. Gelatin-starch sponge has also shown good swelling behavior, but low mechanical strength [12]. Domestic silk worms in China, Japan and Thailand produce "Eri silk", which has been used in fiber based sponges and showed a high degree of swelling and suitable mechanical properties for tissue engineering applications [13].

Another key requirement of a wound dressing is antibacterial activity. Bionanocomposite wound dressing is an incorporation of biopolymer and inorganic antibacterial materials, for example, Ag, TiO_2 and ZnO nanoparticles [14]. Among the nanoparticles used in wound dressing, ZnO nanoparticles (ZnO-NP) have excellent antibacterial activity, are inexpensive and nontoxic to human cells [15,16]. Chitosan hydrogel, incorporating ZnO-NP, showed high antibacterial activity toward *E. coli* and *S. aureus* [17]. Bacterial cellulose fibers, modified with ZnO-NP, possessed good antibacterial activity and ZnO-NP was shown to improve thermal and mechanical properties of the bacterial cellulose-ZnO

* Corresponding author at: Department of Chemistry, Faculty of Science, King Mongkut's Institute of Technology Ladkrabang (KMITL), Bangkok 10520, Thailand.
E-mail address: jutarat.si@kmitl.ac.th (J. Prachayawarakorn).

https://doi.org/10.1016/j.ijbiomac.2019.05.118
0141-8130/

nanocomposites [18]. Also, xanthan-based wound dressing hydrogels, with embedded ZnO-NP, formed by casting, showed useful antimicrobial activity, high fluid uptake ability and water retention [19].

BSM has effective swelling and water holding properties, but there is no published data on the use of BSM as a material for wound dressing. So, the objective of this research was to prepare a new natural antibacterial hydrogel sponge from basil seed (*Ocimum basilicum* L.) mucilage by freeze drying. ZnO-NP was added to improve antibacterial activity of BSM hydrogel sponge. Functional group analysis, morphology, porosity, mechanical properties, thermal properties, degree of swelling and water retention capacity of BSM hydrogel sponge were measured. Antibacterial activity, cytotoxicity and cell adhesion of BSM hydrogel sponge were also measured.

2. Materials and methods

2.1. Materials

Basil seeds were obtained from Thai Baan Rai Co., Ltd. (Bangkok, Thailand). Glycerol was purchased from Lab System Co., Ltd. (Bangkok, Thailand). ZnO nanoparticles (20–40 nm) were obtained from Nanomaterials Technology, Co. Ltd. (Chonburi, Thailand).

2.2. Basil seed mucilage (BSM) preparation

BSM was prepared by hydration: the basil seeds were soaked in distilled water at a seed:water ratio of 1:30 for 1 h at ambient temperatures (typically 30 °C in Thailand). Then, the mucilage was scraped off the surface of the swollen seeds in a blender for 1 min. Next, the mucilage was separated from the swollen seeds by filtering the mixture with a cheese cloth and centrifuged at 5000 rpm for 5 min to remove seed residue. The resulting mucilage was refrigerated at −40 °C for 24 h in a freezer (DW-40L92, Haier, China), followed by lyophilization at −100 °C for 24 h with a freeze dryer (Coolsafe 110-4, Scan Vac, Denmark) to obtain dried BSM.

2.3. Hydrogel sponge preparation

The dried BSM (1 wt% of distilled water) was dissolved in distilled water using glycerol as a plasticizer (15 wt% of BSM). Various contents of ZnO-NP, from 0 to 50 wt% of dry BSM, were added to the solution. Then, the solution was mechanically stirred using a magnetic stirrer (IKA, Germany) at 40 °C for 45 min. After that, 30 ml of the solution was poured into a 100 mm ∅ circular petri dish to control the thickness of the sample and then refrigerated at −40 °C for 24 h in a freezer and lyophilized at −100 °C for 24 h using a freeze dryer.

2.4. Fourier transform infrared spectroscopy (FTIR)

The functional groups of a sample were analyzed with a transmission FTIR, Spectrum 2000 GX spectrometer (Perkin Elmer, USA) in a range of 4000–350 cm^{-1} at 4 cm^{-1} resolution. Each spectrum was obtained from 10 scans.

2.5. Morphology

The morphology of a sample was examined in images taken by a scanning electron microscope (SEM), (LEO 1455VP, ZEISS, Germany). The sample was fractured in liquid nitrogen and then covered with a thin layer of gold for electrical conduction before imaging.

2.6. Thickness

For measuring the thickness of a sample, a micrometer (Model G, Peacock, Japan) was applied to a 40 × 40 mm^2 piece of the sample. The thickness was reported as an average of 8 measurements.

2.7. Porosity

Porosity was measured by a displacement liquid method using ethanol. The sample was immersed in a known volume (V_1) of ethanol in a graduated cylinder for 10 min. The total volume of ethanol after sample immersion was recoded as V_2. Then, the sample was removed from the cylinder, and the volume of the remaining ethanol was recorded as V_3. The percent porosity was calculated as:

$$\text{Porosity}\ (\%) = \frac{V_1 - V_3}{V_2 - V_3} \times 100. \quad (1)$$

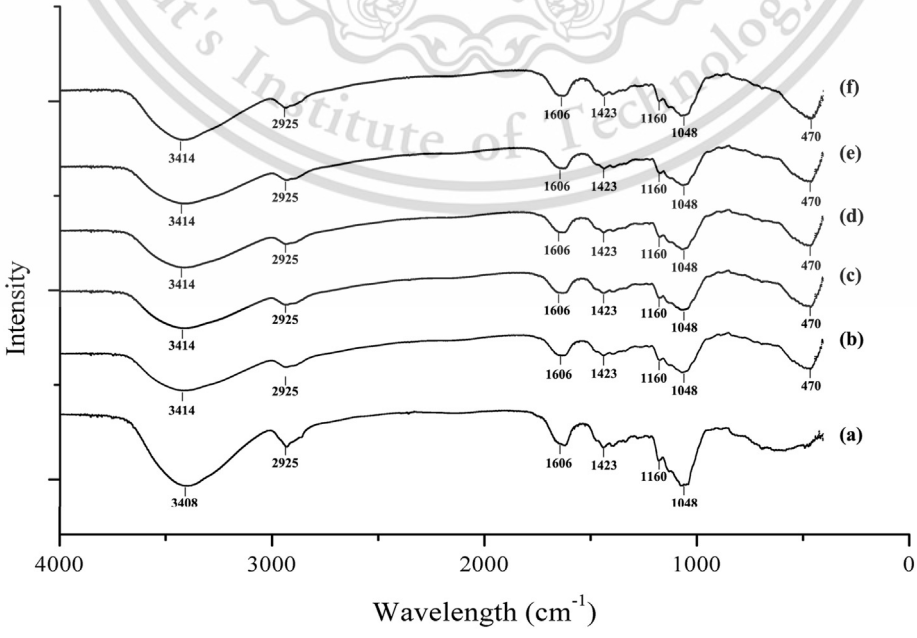

Fig. 1. FT-IR spectra of BSM hydrogel sponges with various levels of ZnONP: (a) 0 wt%, (b) 10 wt%, (c) 20 wt%, (d) 30 wt%, (e) 40 wt% and (f) 50 wt%.

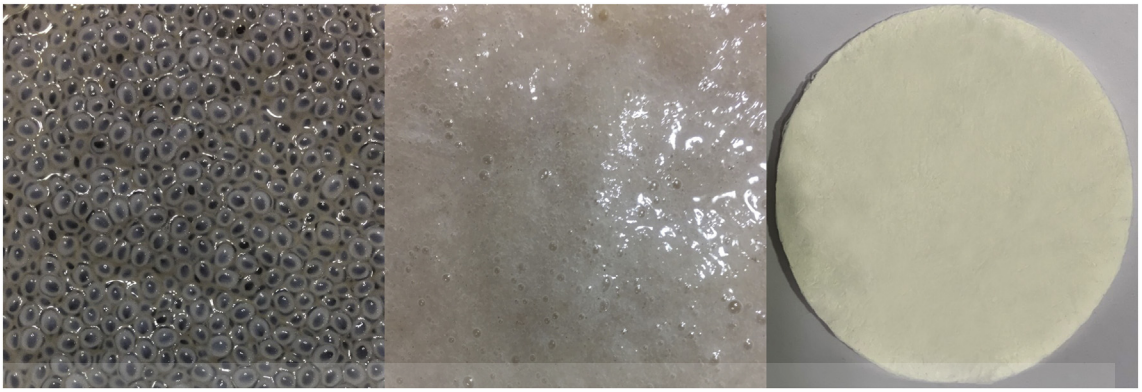

Fig. 2. Basil seed in different forms (a) swollen basil seed, (b) mucilage extracted from outer pericarp of the seeds and (c) BSM hydrogel sponge.

2.8. Mechanical properties

Mechanical properties were measured with a universal testing machine (Lloyd Instrument, LR 5 K, West Sussex, UK) with a 100 N load cell at a crosshead speed of 50 mm/min, following the ASTM D-638-2010 standard [20]. The sample was cut into 15×100 mm^2 rectangular pieces and kept at ambient temperature (~25 °C) and relative humidity (RH) 58 ± 2% for 24 h before testing. Data was reported as an average from 10 replicates.

2.9. Degree of swelling

A dried sample (20×20 mm^2) was weighed and immersed in distilled water at ambient temperature. The degree of swelling of the sample was measured after 48 h. The swollen sample was taken out of the water, water that adhered on its surface was removed by gentle blotting with filter paper and immediately weighed. The degree of swelling was calculated as:

$$\text{Degree of swelling} = \frac{M_w - M_0}{M_0}, \tag{2}$$

where M_0 and M_w are the weights of the sample before and after immersion, respectively.

2.10. Water retention capacity

A sample (20×20 mm^2) was allowed to swell in distilled water until it reached equilibrium. After excess water was wiped off the sample with a filter paper, it was left at ambient temperature for 24 h, then weighed. The water retention capacity was calculated as:

$$\text{Water retention capacity } (\%) = \frac{W_T}{W_0} \times 100, \tag{3}$$

where W_0 and W_T are the initial weight and the weight after 24 h, respectively.

2.11. Thermal properties

The thermogravimetric (TGA) and derivative thermal gravimetric (DTG) properties were determined from thermograms in the temperature range of 30 to 900 °C at a heating rate of 10 °C/min under a nitrogen atmosphere with a thermogravimetric analyzer (Pyris I TGA HT, Perkin Elmer, USA).

2.12. Antibacterial activity

The antibacterial activity against *Escherichia coli* (Gram-negative) and *Staphylococcus aureas* (Gram-positive) was assessed from the size

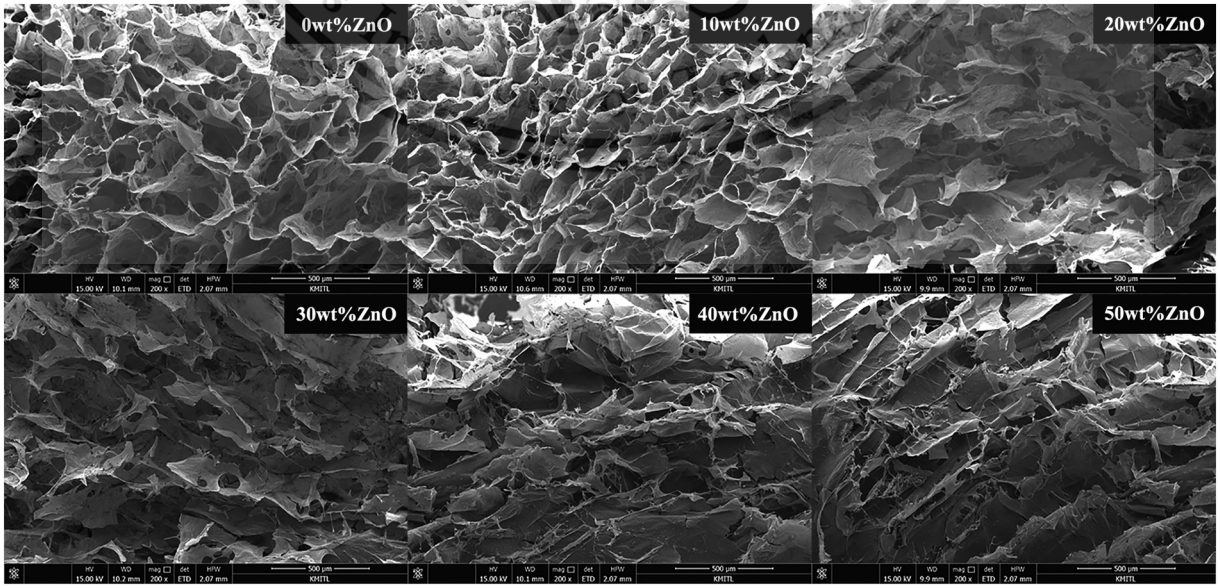

Fig. 3. SEM images of BSM hydrogel sponges prepared with various ZnONP contents; 200 × magnification.

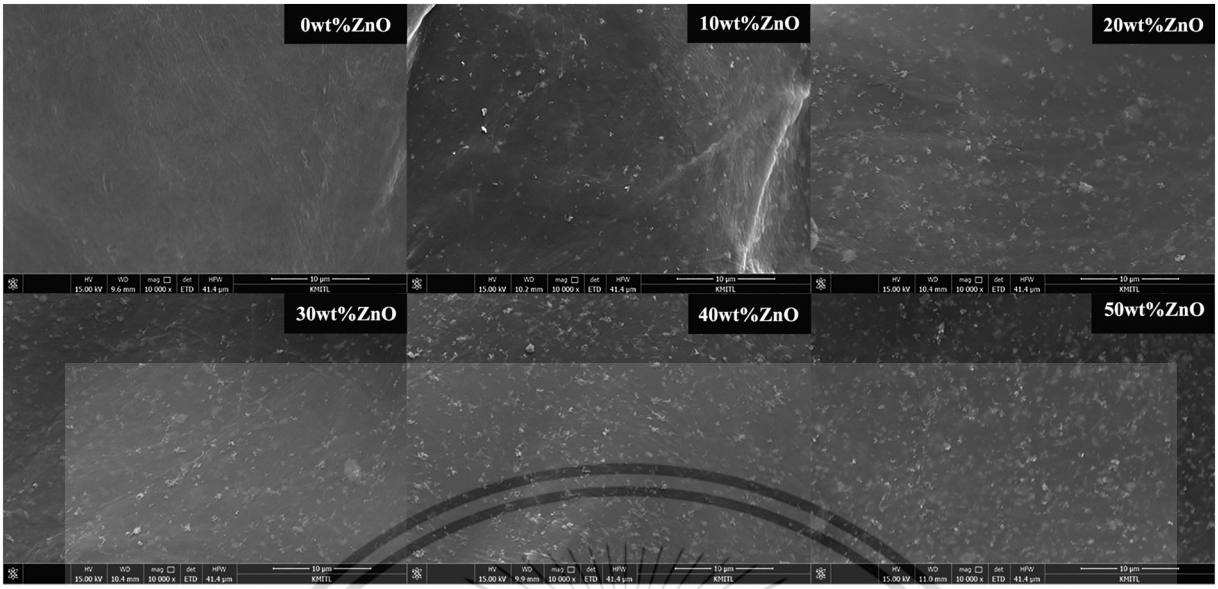

Fig. 4. SEM images of BSM hydrogel sponges prepared with various contents of ZnONP; 10,000× magnification.

of the inhibition zone in agar discs. Samples were cut into 10 mm ∅ circular discs with a sharp metal cutter. The disc was placed on an agar plate containing a bacterial lawn and incubated at 37 °C for 24 h. After that, the diameter of the zone of inhibition was measured to estimate the antibacterial activity. Data was reported as an average from 3 replicates.

2.13. In vitro cytotoxicity study

Cytotoxicity was assessed by 3-(4, 5-dimethylthiazol-2yl)-2, 5-diphenyl tetrazolium bromide (MTT) assay with human keratinocytes (HaCat) cells. Each sample was sterilized and then soaked in PBS at 37 °C for 24 h. The soaked sample was filtered and Dulbecco's Modified Eagle Medium (DMEM) was added to the filtrate. The mixture was then incubated in a medium of DMEM, supplemented with 10% Fetal Bovine Serum. Next, 100 μl of HaCat cells (1×10^5 cells/ml) were seeded and incubated at 37 °C for 24 h in wells of a 96-well plate. After that, 100 ml of the incubated filtrate mixture were added into the well, 10 μL of MTT solution (5 mg/mL) was added into the well and further incubated at 37 °C for another 4 h. Next, formazan crystals were dissolved in 100 μl of 100% DMSO: 10% SDS solution and 100 μl of the resulting solution was added to the well. Finally, the absorbance of the final mixture was measured at 570 nm with a microtiter plate reader (EZ read 2000, Biochome, UK). The samples were checked with an optical microscope to observe cell morphology. Three replicates of each sample were measured and averaged. Percentage cytotoxicity was calculated from

$$\text{Cytotoxicity}\ (\%) = \frac{A-B}{A} \times 100, \tag{4}$$

where A is the absorbance of the control and B is the absorbance of the sample.

2.14. Cell adhesion test

A cell adhesion test was also use to confirm viability of cells adhered to a sample. Firstly, a piece of sample was placed in a well of a 96-well plate. Then, 1 ml of Hacat cells (1×10^5 cells/ml) were seeded and allowed to grow and adhere to the hydrogel at 37 °C in a 5% CO_2 atmosphere for 24 h. Next, the hydrogel piece was rinsed twice with 1 ml phosphate buffer saline (PBS) and the cells fixed with a pre-fixative solution for 1 h. Then, the sample was dehydrated and sputter-coated with gold. The cell morphology was observed with a scanning electron microscope (JSM-IT500HR, JEOL, Japan). $\frac{W_T}{W_0} \times 100$.

3. Results and discussion

3.1. FTIR spectroscopy analysis

Fig. 1 shows FTIR spectra of BSM hydrogel sponges prepared with various ZnO-NP levels. All spectra had similar characteristic peaks. A broad peak around 3400–3000 cm^{-1} was due to the complex vibrational stretching associated with free, inter- and intra-molecular hydroxyl groups on BSM molecules. A peak at 2925 cm^{-1} was assigned to C—H stretching. The peaks at 1606 cm^{-1} and 1423 cm^{-1} were caused by C-OO asymmetric stretching and C-OO symmetric stretching of free carboxylate of uronic acid, respectively, in the BSM sample. The stretching peaks at 1160 cm^{-1} were assigned to C—O and at 1048 cm^{-1} to C—O—C [5].

Table 1
Thickness, porosity, degree of swelling and water retention capacity of BSM hydrogel sponge *vs* ZnONP content.

Sample % ZnONP	Thickness (mm)	Porosity (%)	Degree of swelling	Water retention capacity (%)
0	1.53 ± 0.11	92.1	109.0 ± 2.2	31.2
10	1.31 ± 0.06	89.3	98.7 ± 1.7	35.3
20	1.18 ± 0.04	86.4	92.1 ± 2.8	36.7
30	1.06 ± 0.05	82.7	88.8 ± 2.4	40.1
40	0.93 ± 0.05	79.2	84.4 ± 1.3	42.0
50	0.82 ± 0.04	76.1	80.5 ± 2.1	44.8

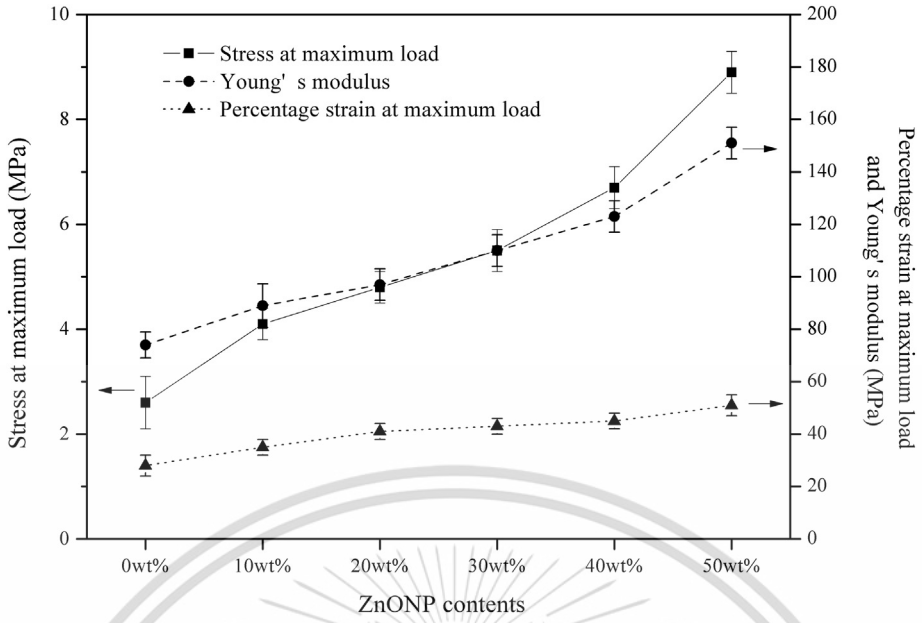

Fig. 5. Stress at maximum load, Young's modulus and % strain at maximum load for BSM hydrogel sponges *vs* ZnONP content.

FTIR spectra of BSM hydrogel sponges, prepared with ZnO-NP, see Fig. 1(b)–(f), exhibited a new peak at 470 cm^{-1} which is assigned to Zn—O stretching in ZnO-NP [18,21]. The O—H stretching peak at 3408 cm^{-1} of the BSM hydrogel sponge without ZnO-NP shifted to a higher frequency after ZnO-NP was added. The shift of those broad spectra indicated the existence of hydrogen bonding and electrostatic interaction between hydroxy and carboxyl groups of BSM and ZnO-NP [22]. The shift of broad spectra was also observed from PVA/chitosan hydrogels prepared with ZnO-NP [23]. It was also reported that ZnO-NP could form electrostatic interaction with gum acacia, since ZnO-NP contained a O^2-Zn^2 dipole in its tetrahedral structure, leading to electrostatic interactions with dipoles in the polymer segments [24,25].

3.2. Morphology

Fig. 2 shows swollen basil seed, mucilage extracted from the outer pericarp of basil seeds and BSM hydrogel sponge images. The microstucture of the cross-sections of BSM hydrogel sponges prepared with various ZnO-NP contents is shown in Fig. 3. After pre-freezing and freeze-drying, water molecules in the BSM solution formed ice and sublimed, leaving empty pores. The interconnected open-cell structure of the pores can be seen in the images. BSM hydrogel sponges with various ZnO-NP contents showed a change in the morphology. The round open-pored structures changed to a tighter network structure as the ZnO-NP content increased. This was due to hydrogen bonding and electrostatic interaction between the hydroxyl and carboxyl groups of BSM and the dipoles of ZnO-NP. A similar change in morphology has also been reported for ZnO-NP loaded gum acacia/polyacrylate [25]. Further, the electrostatic interaction between these two components led to reduced numbers of BSM hydroxyl and carboxyl groups available to interact with water [24]. These observations showed that ZnO-NP content played an important role in changing the pore shape of samples obtained by freeze drying.

Fig. 4 shows high magnification images of cross-section of BSM hydrogel sponge prepared with various contents of ZnO-NP. It is evident that small ZnO-NPs were distributed uniformly over the BSM matrix and strongly attached to the sponge surface.

3.3. Thickness and porosity

Table 1 shows the thickness and porosity of BSM hydrogel sponges *vs* ZnO-NP content. The unmodified BSM hydrogel sponge had a thickness of 1.53 mm and a high porosity of 92.1%. A hydrogel sponge with high porosity can absorb a large volume of exudate from a wound surface. As expected, increasing the ZnO-NP content led to decreases in thickness (1.53 to 0.82 mm) and porosity (92.1 to 76.1%). Despite the decrease in porosity, it was still comparable to that of chitosan-

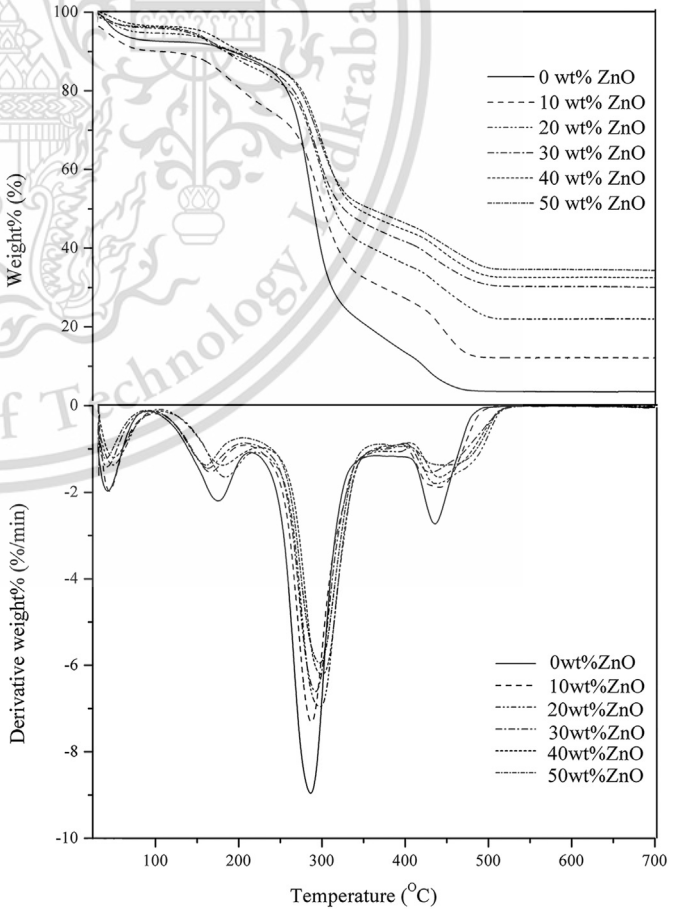

Fig. 6. TGA and DTG curves of BSM hydrogel sponges for different ZnONP contents.

Table 2
Zone of inhibition and %cytotoxicity for BSM hydrogel sponges *vs* ZnONP content for *E. coli* and *S. aureus*.

Sample (wt%ZnONP)	Zone of inhibition (mm)		%Cytotoxicity
	Escherichia coli	*Staphylococcus aureus*	
0	Inactive	Inactive	−5.99 ± 0.87
10	Inactive	14.4 ± 0.07	−4.64 ± 0.33
20	Inactive	15.7 ± 0.05	−2.26 ± 0.54
30	15.3 ± 0.04	15.9 ± 0.08	0.62 ± 0.33
40	15.5 ± 0.03	16.2 ± 0.04	1.42 ± 0.17
50	15.9 ± 0.03	16.7 ± 0.06	10.47 ± 0.31

Ag/ZnO composite dressing (83–91%) and chitosan/PVA porous scaffolds (82–87%) [20,26] and even higher than that of gum kondagogu sponge (60–70%) [11].

3.4. Mechanical properties

Stress at maximum load, Young's modulus and percentage strain at maximum load of BSM hydrogel sponges *vs* ZnO-NP content are shown in Fig. 5. It was observed that stress at maximum load, Young's modulus and percentage strain of BSM hydrogel sponge were 2.6 MPa, 74 MPa and 28%, respectively. These values are slightly higher than those reported for gelatin/starch sponge, which showed 0.25 MPa stress at maximum load and 22% strain at maximum load [12] but lower than those of chitosan/PVA porous scaffolds (55.8 MPa stress at maximum load and 36% strain at maximum load) [20].

Clearly, the mechanical properties of BSM hydrogel sponges were greatly improved by increasing ZnO-NP content. BSM hydrogel sponge with 50 wt% ZnO-NP content showed stress at maximum load 8.9 MPa, Young's modulus 151 MPa and strain at maximum load 51%. This may be attributed to the shorter distance between BSM layers and the tighter network structure seen in the SEM image (Fig. 3), resulting in a stronger interaction between layers. Furthermore, ZnO-NP also acted as a good reinforcing element due to its high strength and high surface area, as well as its uniform distribution in the BSM hydrogel sponge. Additionally, the electrostatic interaction and hydrogen bonding between ZnO-NP and BSM resulted in a greater transfer of the nanoparticles' mechanical properties to the matrix.

3.5. Degree of swelling and water retention capacity

Table 1 shows the degree of swelling after 48 h of immersion in distilled water of BSM hydrogel sponges prepared with different ZnO-NP content. All of the BSM hydrogel sponges showed a considerable degree of swelling (80.5–109), which was significantly higher than those shown by gum kondagogu (30–65) and chitosan-Ag/ZnO dressing (20–25) [11,20]. This was caused by the hydrophilic nature of BSM molecules that have a high number of hydroxyl and carboxyl groups interacting strongly with water. The high porosity of the sponge, facilitating water diffusion into BSM porous structure, also contributes to the swelling. As expected, the highest degree of swelling was found in sponge prepared without ZnO-NP.

Furthermore, the degree of swelling decreased with increase of ZnO-NP content, as seen in Table 1 and Fig. 3. The porosity of BSM hydrogel sponge with ZnO-NP decreased. Electrostatic interaction and hydrogen bonding between ZnO-NP and the BSM matrix led to fewer hydroxyl and carboxyl groups of the hydrogel available to interact with water. Moreover, ZnO-NP may occupy some vacancies in the hydrogel network, restricting its expansion and hindering water penetration. Similar observations were reported in xanthan-based hydrogel embedded with ZnO-NP and chitosan-Ag/ZnO wound dressing [19,20]. Marvizadeh et al. also reported that an incorporation of ZnO-NP increased the hydrophobicity behavior of the starch/gelatin bionanocomposite film [27]. In spite of the slight decrease in swelling for sponges with added ZnO-NP, the degree of swelling was still higher than that of xanthan-based hydrogel embedded ZnO-NP and chitosan-Ag/ZnO wound dressing [19,20]. This excellent swelling property of the BSM hydrogel sponge indicated that it is suitable for wound dressing applications.

Water retention capacity, one of the important properties of wound dressing, is the ability of a dressing material to hold water molecules within its structure. The water retention capacity of sponges, with various ZnO-NP contents, after exposure to air, at room temperature for 24 h, is shown in Table 1. Sponge without ZnO-NP showed 30.6% water retention capacity. This is comparable to that of xanthan-based hydrogel embedded ZnO-NP (8–30%) [19]. Moreover, the water retention capacity of BSM sponge slightly increased from 30.6 to 44.8% when the ZnO-NP content increased from 0 to 50 wt%. The tighter pore structure of BSM sponges, when ZnO-NP content was increased, shown in Fig. 3, made it more difficult for the hydrogel to release water from its structure. Similar behavior was found in xanthan-based hydrogel embedded ZnO-NP [19].

3.6. Thermal properties

Fig. 6 shows TGA and DTG thermograms of BSM hydrogel sponges prepared with various ZnO-NP contents. There were four thermal degradation steps. The first step, between 35 and 100 °C, was related to moisture vaporization. The second step, at 120–210 °C, was caused by thermal degradation of glycerol in the sponge. The third step, at 255–340 °C, was due to thermal degradation of glucomannan, xylan and other polysaccharides in the hemicellulose in BSM molecules [5,28,29]. The forth step, at 410–460 °C, was due to the thermal decomposition of cellulose and lignin in BSM [28,29]. The decomposition temperature of BSM molecules

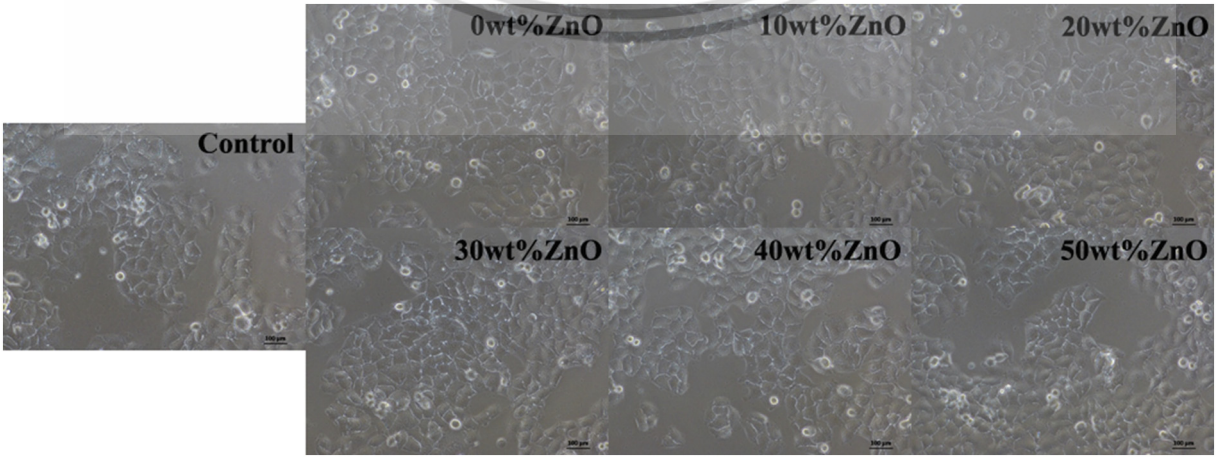

Fig. 7. Optical microscopy images of the negative control and sponges prepared with various ZnONP content; 200× magnification.

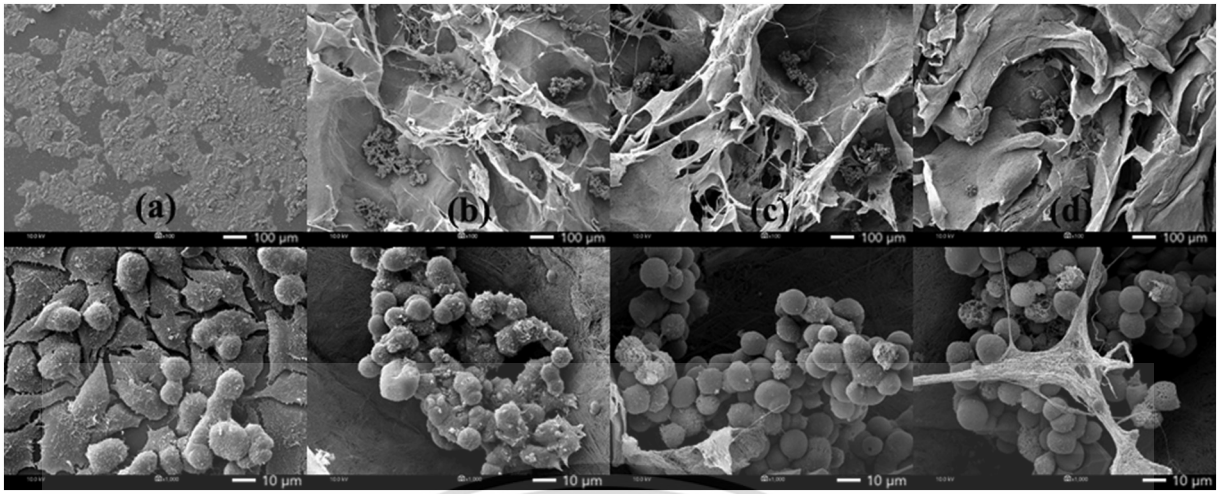

Fig. 8. Viability confirmation for adhered cells (a) negative control, (b-d) HaCat cells cultured on BSM hydrogel sponge with 0 wt%, 20 wt% and 50 wt% ZnONP; magnification −100× (Top) and 1000× (Bottom).

significantly shifted to a higher temperature, when ZnO-NP was incorporated in the sponge. This is due to hydrogen bonding and electrostatic interaction between hydroxy and carboxyl groups of BSM with polar segments of ZnO-NP. Incorporation of ZnO-NP improved the thermal stability of the BSM hydrogel sponges. Similar observations were made in agar, carrageenan and CMC films with added ZnO-NP [22].

3.7. Antibacterial activity

The potential of BSM nanocomposite hydrogel sponge as an effective wound dressing was assessed by an agar disc diffusion method against *S. aureus* (Gram-positive) and *E.coli* (Gram-negative) as representatives of bacteria commonly found in a wound. The results are shown in Table 2. Sponge, without ZnO-NP, exhibited no antibacterial activity. However, with added ZnO-NP, the sponge showed effective antibacterial activity against both *S. aureus* and *E.coli*. The diameter of the inhibition zone for *S. aureus* was 14.4 mm. for a sponge with 10 wt% ZnO-NP and increased to 16.7 mm for a sponge with 50 wt% ZnO-NP. For *E.coli*, the inhibition zone was initially measured at 15.5 mm for 30 wt% ZnO-NP and slightly increased to 15.9 mm with 50 wt% ZnO-NP. The higher antibacterial activity against *S. aureus vs E. coli* is likely due to the difference in Gram-positive and Gram-negative bacteria cell wall structures. Generally, Gram-positive bacteria have a thick cell wall structure with multiple layers of peptidoglycan, while Gram-negative bacteria have a more complex cell wall structure, making them more resistant to an external attack of any antibacterial agent [16]. Similar observations were also made for xanthan-based hydrogel embedded ZnO-NP and agar, carrageenan and CMC films with ZnO-NP [19,22].

3.8. In vitro cytotoxicity study

Since the amount of ZnO-NP in the BSM hydrogel sponge may cause a toxic effect, the cytotoxicity of the sponge prepared with various ZnO-NP contents was evaluated and compared to that of a negative control by MTT assay [26]. It can be seen in Fig. 7 and Table 2 that, at 0–20 wt % of ZnO-NP, the sponge even promoted the growth of Hacat cells slightly, compared to the control. However, the cytotoxicity of all sponges with different ZnO-NP contents was very low. It can be concluded that the hydrogel sponges were not toxic to HaCat cells.

3.9. Cell adhesion

Fig. 8 confirms viability of adhered cells cultured on a BSM hydrogel sponge prepared with 0, 20, 50 wt% of ZnO-NP compared with the negative control. It can be seen that all BSM hydrogel sponges prepared with various contents of ZnO-NP retained cell viability and were non-toxic to the human keratinocytes (HaCat) cells. Moreover, an increase in ZnO-NP content resulted in a trend of less cell spreading and a characteristic spindle morphology. These results substantiated the non-cytotoxicity and non-adherence properties of the BSM hydrogel sponge prepared with a high content of ZnO-NP.

4. Conclusion

A new natural-based antibacterial wound dressing from Basil Seed Mucilage (BSM) with ZnO-NP was successfully prepared by freeze-drying. BSM hydrogel sponges showed considerable porosity and degree of swelling. FTIR analysis confirmed hydrogen bond and electrostatic interaction between BSM molecules and ZnO-NP. Good distribution of ZnO-NP on the BSM surface was observed and the increasing ZnO-NP content caused tighter network structure. Furthermore, increase in ZnO-NP content resulted in the slightly decrease in thickness, porosity, water uptake and degree of swelling of the sponges. Moreover, mechanical, thermal properties and antibacterial activity were improved by adding ZnO-NP into sponge. Cytotoxicity evaluation and cell adhesion studies demonstrated non-cytotoxicity and non-adherent nature of the sponge.

Acknowledgements

The authors thank the KMITL Research Fund (KREF 046108) for financial support and the Department of Chemistry, Faculty of Science of KMITL for facility support. The authors thank John Morris for proof reading the article.

References

[1] V.D. Prajapati, G.K. Jani, N.G. Moradiya, N.P. Randeria, Pharmaceutical applications of various natural gums, mucilages and their modified forms, Carbohydr. Polym. 92 (2013) 1685–1699.
[2] G.D. MMogosanu, A.M. Grumezescu, Natural and synthetic polymers for wounds and burns dressing, Int. J. Pharm. 463 (2014) 127–136.
[3] V. Rana, S. Kamboj, R. Sharma, K. Singh, Modification of gums: synthesis techniques and pharmaceutical benefits, in: K.T. Vijay, K.T. Manju (Eds.), Handbook of Polymer for Pharmaceutical Technologies, Scrivener Publishing LLC, Massachusetts 2015, pp. 299–364.
[4] S.N. Tabashi, S.M. Razavi, Functional properties and applications of basil seed gum: an overview, Food Hydrocoll. 73 (2017) 313–325.
[5] N. Khazaei, M. Esmaiili, Z.E. Djomeh, M. Ghasemlou, M. Jouki, Characterization of new biodegradable edible film made from basil seed (Ocimum basilicum L.) gum, Carbohydr. Polym. 102 (2014) 199–206.

[6] F. Kurd, M. Fathi, H. Shekarchzadeh, Basil seed mucilage as a new source for electrospinning: production and physicochemical characterization, Int. J. Biol. Macromol. 95 (2017) 689–695.
[7] P. Zahedi, I. Rezaeian, S.R. Siadat, S. Jafari, P. Supaphol, A review on wound dressings with an emphasis on electrospun nanofibrous polymeric bandages, Polym. Adv. Technol. 21 (2010) 77–95.
[8] A. Autissier, C.L. Visage, C. Pouzet, F. Chaubet, D. Letourneur, Fabrication of porous polysaccharide-based scaffolds using a combined freeze-drying/cross-linking process, Acta Biomater. 6 (2010) 3640–3648.
[9] E.A. Kamoun, E.S. Kenawy, X. Chen, A review on polymeric hydrogel membranes for wound dressing applications: PVA-based hydrogel dressings, J. Adv. Res. 8 (2017) 217–233.
[10] Z. Fereshteh, Freeze-drying technologies for 3D scaffold engineering, in: D. Ying, K. Jordan (Eds.), Functional 3D Tissue Engineering Scaffolds: Materials, Technologies and Applications, Woodhead Publishing Inc 2018, pp. 151–174.
[11] H.S. Rathore, M. Sarubala, G. Ramanathan, S. Singaravelu, M.D. Raja, S. Gupta, U.T. Sivagnanam, Fabrication of biomimetic porous novel sponge from gum kondagogu for wound dressing, Mater. Lett. 177 (2016) 108–111.
[12] J. Tavakoli, Physico-mechanical, morphological and biomedical properties of a novel natural wound dressing material, J. Mech. Behav. Biomed. Mater. 65 (2017) 373–382.
[13] S.S. Silva, N.M. Oliveira, M.B. Oliveira, D.P. Soares da Costa, D. Naskar, J.F. Mano, S.C. Kundu, R.L. Reis, Fabrication and characterization of Eri silk fibers-based sponges for biomedical application, Acta Biomater. 32 (2016) 178–189.
[14] D. Simões, S.P. Miguel, M.P. Ribeiro, P. Coutinho, A.G. Mendonça, I.J. Correia, Recent advances on antimicrobial wound dressing: a review, Eur. J. Pharm. Biopharm. 127 (2018) 130–141.
[15] M. Naseri-Nosar, Z.M. Ziora, Wound dressings from naturally-occurring polymers: a review on homopolysaccharide-based composites, Carbohydr. Polym. 189 (2018) 378–389.
[16] T.J. Gutiérrez, P.G. Seligra, C.M. Jaramillo, L. Famá, S. Goyanes, Effect of filler properties on the antioxidant response of thermoplastic starch composites, in: K.M. Vijay, K.T. Manju, R.K. Michael (Eds.), Handbook of Composites from Renewable Materials, Scrivener Publishing LLC, Argentina 2017, pp. 337–370.
[17] A. Mohandas, S. Deepthi, R. Biswas, R. Jayakumar, Chitosan based metallic nanocomposite scaffolds as antimicrobial wound dressings, Bioact. Mater. 3 (2018) 267–277.
[18] A. Khalid, R. Khan, M. Ul-Islam, T. Khan, F. Wahid, Bacterial cellulose-zinc oxide nanocomposites as a novel dressing system for burn wounds, Carbohydr. Polym. 164 (2017) 214–221.
[19] A.I. Raafat, N.M. El-Sawy, N.A. Badawy, E.A. Mousa, A.M. Mohamed, Radiation fabrication of xanthan-based wound dressing hydrogels embedded ZnO nanoparticles: in vitro evaluation, Int. J. Biol. Macromol. 118 (2018) 1892–1902.
[20] K. Kanimozhi, S.K. Basha, V.S. Kumari, Processing and characterization of chitosan/PVA and methylcellulose porous scaffolds for tissue engineering, Mater. Sci. Eng. C 61 (2016) 484–491.
[21] G. Yuvaraja, J.L. Pathak, Z. Weijiang, Z. Yaping, X. Jiao, Antibacterial and wound healing properties of chitosan/poly(vinyl alcohol)/zinc oxide beads (CS/PVA/ZnO), Int. J. Biol. Macromol. 103 (2017) 234–241.
[22] P. Kanmani, J. Rhim, Properties and characterization of bionanocomposite films prepared with various biopolymers and ZnO nanoparticles, Carbohydr. Polym. 106 (2014) 190–199.
[23] M.T. Khorasani, A. Joorabloo, A. Moghaddam, H. Shamsi, Z. Mansoorimoghadam, Incorporation of ZnO nanoparticles into heparinised polyvinyl alcohol/chitosan hydrogels for wound dressing application, Int. J. Biol. Macromol. 114 (2018) 1203–1215.
[24] A.M. Nafchi, A.K. Alias, S. Mahmud, M. Robal, Antimicrobial, rheological, and physicochemical properties of sago starch films filled with nanorod-rich zinc oxide, J. Food Eng. 113 (2012) 511–519.
[25] S.K. Bajpai, M. Jadaun, S. Tiwari, Synthesis, characterization and antimicrobial applications of zinc oxide nanoparticles loaded gum acacia/poly(SA) hydrogels, Carbohydr. Polym. 114 (2016) 60–65.
[26] Z. Lu, J. Gao, Q. He, J. Wu, D. Liang, H. Yang, R. Chen, Enhanced antibacterial and wound healing activities of microporous chitosan-Ag/ZnO composite dressing, Carbohydr. Polym. 156 (2017) 460–469.
[27] M.M. Marvizadeh, N. Oladzadabbasabadi, A.M. Nafchi, M. Jokar, Preparation and characterization of bionanocomposite film based on tapioca starch/bovine gelatin/nanorod zinc oxide, Int. J. Biol. Macromol. 99 (2017) 1–7.
[28] P. Arak, H. Nattakarn, Study of Water Adsorption and Fertilizer Release of Poly (Butylene Succinate) Blended with Natural Absorbent for Using in Agriculture Application, Thesis of department of materials science and engineering Silapakorn university, 2015.
[29] Z.N. Azwa, B.F. Yousif, A.C. Manalo, W. Karunasena, A review on the degradability of polymeric composites based on natural fibres, Mater. Des. 47 (2013) 424–442.

PCT-8

The International Polymer Conference of Thailand

PROCEEDINGS BOOK

June 14th-15th, 2018

Amari Watergate Bangkok Hotel,
Bangkok, Thailand

PST
Organized by Polymer Society of Thailand

Effect of Glycerol Contents on Properties of Hydrogel Sponge from Basil Seed Mucilage

Siriporn Tantiwatcharothai [1] and Jutarat Prachayawarakorn[1,2*]

[1] Department of Chemistry, Faculty of Science, King Mongkut's Institute of Technology Ladkrabang, Bangkok 10520

[2] Advanced Materials Research Unit, Faculty of Science, King Mongkut's Institute of Technology Ladkrabang, Bangkok 10520

Phone +66 2329 8400, Fax +66 2329 8428, *E-Mail: jutarat.si@kmitl.ac.th

Abstract

Due to a large capacity for hydration of basil seed mucilage (BSM), the objectives of this research were to prepare hydrogel sponge from BSM and investigate the effect of glycerol contents on properties of BSM hydrogel sponge. Different BSM hydrogel sponges were prepared by freeze-drying technique using various contents of glycerol i.e. 0 wt%, 15 wt% and 30 wt%, as a plasticizer. It was found that FTIR spectra showed a shift to lower wavenumber of O-H stretching peak by the addition of glycerol, indicating of new hydrogen bond formation between glycerol and BSM phases. SEM image also revealed interconnecting open-cell structure of pores in unplasticized BSM hydrogel sponge. BSM hydrogel sponges plasticized with glycerol presented tight network structure and narrow transport pores with the increase of glycerol content. Furthermore, the increase in glycerol contents clearly resulted in the increase of hardness but the decrease of thickness of BSM hydrogel sponges. In addition, the increase in glycerol content also resulted in a considerable increase in degree of swelling of BSM hydrogel sponges. Moreover, thermal decomposition temperature of BSM hydrogel sponge improved by the use of glycerol plasticizer.

Keywords: basil seed mucilage, freeze-drying, glycerol, hydrogel sponge

1. Introduction

Worldwide consumption of bioplastics has increased more than 600% in the past decades. This remarkable growth is resulted from the global trend of environmental awareness [1]. Hydrogels are physical or chemical cross-linked macromolecules forming a three dimensional network capable of retaining water without disintegrating. The use of natural polymers in hydrogels is advantageous due to their biodegradability and non-toxicity. Basil (*Ocimum americanum L.*) seed is one of an interesting product of Thailand. Basil seed mucilage (BSM) is high molecular weight heteropolysaccharide. It composes of D-glucose, D-galactose, D-mannose, L-arabinose, D-xylose, and L-rhamnose in the approximate proportions of 25:25:10:15:15:5, along with uronic acid [2, 3]. Basil seed offers a great potential for use as an emulsifying, foaming, thickening and gelling stabilizing agents in food and pharmaceutical industries. There was a few reports for the use of BSM. It was mentioned that BSM showed a good potential to be used for edible films in various food applications and coatings. BSM film was transparent and presented good tensile strength and excellent barrier properties [4]. Additionally, thermostable ultra-thin BSM/PVA nanofibers was reported to be used for different applications in food sector such as bioactive encapsulation [5]. As a result of BSM water holding capacity, BSM is a novel natural source of polysaccharides and could potentially generate interesting polymer for water holding application such as hydrogel sponge. However, there is no report for the use of BSM as a material for hydrogel sponge.

The aim of this study was to prepare a new natural hydrogel sponge based on BSM and to examine physical, mechanical, thermal and microstructural properties of the hydrogel sponge as a function of varying concentration of glycerol as plasticizer (0, 15 and 30 wt% of BSM).

2. Experimental Methods

2.1 Hydrogel sponge preparation

BSM was obtained with hydration process. The basil seeds were soaked in distilled water at the ratio of seed: water at 1:30 for 1 h at room temperature. Then, the swollen seed was stirred with a blender for 1 min to scrape the mucilage layer off the seed surface. Separation of the mucilage from the swollen seeds was achieved by filtration with muslin cloth. The resulting mucilage was frozen at -40°C for 24 h in a deep freezer (DW-40L92, Haier, China), followed by lyophilization at -100°C for 24 h using a freeze dryer (Coolsafe 110-4, Scan Vac, Denmark) to obtain the dried BSM. For the preparation of hydrogel sponge from BSM with various concentration of glycerol, BSM was dissolved in distilled water (1%w/w) using glycerol as a plasticizer (0, 15, 30 wt% of BSM). The solutions were mechanically stirred using a magnetic stirrer at 40°C for 45 min. After that, the solution was refrigerated and lyophilization at the same condition as mentioned.

2.2 Hydrogel sponge characterization

2.2.1 Fourier Transform Infrared Spectroscopy (FT-IR)

Functional groups of different hydrogel sponges were analyzed by using Fourier-Transform Infrared (FTIR) Spectroscopy, (Perkin Elmer Model Spectrum GX, USA). The sample was tested by the transmission method in the range of 4000-600 cm^{-1}.

2.2.2 Hardness testing

Hardness testing was carried out according to technical standard method ASTM, D 2240 using type OO durometer, (Teclock, Japan). All the measurements were carried out at 50% relative humidity. The thickness of specimens was approximately 6 mm. 5 specimens were tested to obtain the average values.

2.2.3 Morphology

The morphology of BSM hydrogel sponge was observed using a scanning electron microscope (SEM), (LEO 1455VP, ZEISS, Germany). BSM hydrogel sponge was fractured in liquid nitrogen before the examination. Prior the tests, the sample was covered with a thin layer of gold for thermal and electrical conduction.

2.2.4 Degree of swelling

BSM hydrogel sponge (20×20 mm^2) was weighted and immersed in deionized water at room temperature for 48 h. The degree of swelling of hydrogel sponges were measured after immersing the sample for different periods of time, i.e. 0.5 , 1 , 2 , 3 , 4 , 5 , 6 , 24 and 48 h. After swelling, the hydrogel sponge were taken out of water and removed water that adhered on the surface by gently blotting with tissue paper and immediately weighted. The degree of swelling (DS) was calculated by Eq.1

$$DS=\frac{m_w-m_0}{m_0}\times 100 \quad (1)$$

where m_0 and m_w were the weight of the hydrogel sponge before and after immersion.

2.2.5 Thermal properties

Derivative thermal gravimetric (DTG) analyses of a specimen was scanned within a temperature range of 30 to 600°C at the heating rate of 10°C/min under nitrogen atmosphere using thermogravimetric analyzer (Pyris I TGA HT, Perkin Elmer, USA).

3. Results and Discussion

3.1 Functional group analysis

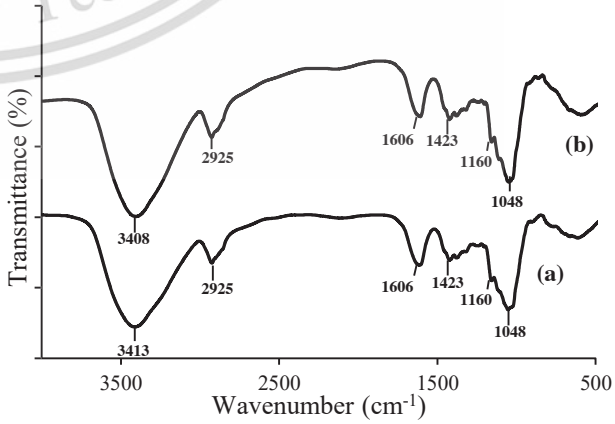

Figure 1 FT-IR spectra of different BSM hydrogel sponges (a) unplasticized (b) plasticized with 15%w/w of glycerol

Figure 1 shows FT-IR spectra of unplasticized and plasticized BSM hydrogel sponges. Two spectra presented similar characteristic peaks. The broad peak around 3400-3000 cm^{-1} was attributed to the complex vibrational stretching associated with free, inter- and intra-molecular hydroxyl groups. The peak position at 2925 cm^{-1} were arisen from the characteristic of C–H stretching. The wave numbers at 1606 cm^{-1} and 1423 cm^{-1} were caused by C=O asymmetric and symmetric stretching of free carboxylate, respectively. The presence of both peak positions confirmed the existance of uronic acid in BSM. In addition, the peaks at 1160 cm^{-1} and 1048 cm^{-1} were attributed to C-O and C-O-C stretching, respectively [3]. It should be noted that, a shift of the broad absorption band due to O-H stretching from 3413 to 3308 cm^{-1} was observed, indicating that hydrogen bonding occurred between BSM and glycerol molecules.

3.2 Scanning electron microscopy

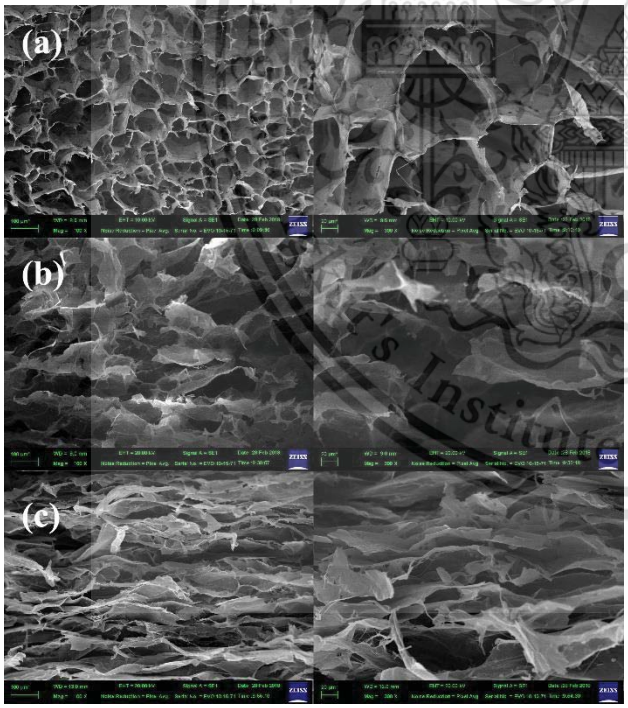

Figure 2 SEM images of different BSM hydrogel sponges (a) unplasticized (b) plasticized with 15%w/w of glycerol (c) plasticized with 30 wt% of glycerol; magnification of 100X (left) and 300X (right)

Figure 2 presents the microstucture of cross-section BSM hydrogel sponges at various contents of glycerol. After prefreezing and freeze-drying, water in BSM solution became ice and, then, sublimed to be pores. It can be seen that, BSM hydrogel sponges represented interconnecting open-cell structures of pores. Unplasticized BSM hydrogel sponge (Figure 2(a)) showed many large round pores; on the other hand, BSM hydrogel sponges plasticized with glycerol (Figures 2(b) and 2(c)) presented different morphology. The round pores turned to be transported pores and tight network structure with increasing glycerol content. This could be caused by a plasticizing effect brought about better distribution of water in BSM during the mixing method. As a result, the pores were connected with each other after freeze-drying and turned to be transported pores.

3.3 Hardness properties

Thickness and hardness (shore OO) of different BSM hydrogel sponges are shown in Table 1. It can be observed that the thickness of BSM hydrogel sponges decreased with increasing glycerol contents. This is may be due to the plasticizing effect of glycerol which corresponded to SEM image (Figure 2). The pores were narrower and the network structure was tighter when glycerol content increased.

For hardness (shore OO) testing, it was found that hardness increased with increasing of glycerol contents. The increase of hardness could be due to the decrease of distance between BSM layers and tighter network as seen in SEM images (Figure 2).

Table 1 Thickness and Hardness of different BSM hydrogel sponges

Sample	Thickness (mm)	Hardness (shore OO)
BSM/0%Gly	3.09 ± 0.43	13.20 ± 1.52
BSM/15%Gly	1.53 ± 0.26	33.17 ± 3.04
BSM/30%Gly	0.80 ± 0.14	49.33 ± 5.71

3.4 Swelling property

The degree of swelling of unplasticized and plasticized BSM hydrogel sponges is shown in Figure 3.

It can be seen that BSM hydrogel sponges show very high degree of swelling. Hydrogel sponges rapidly adsorbed water within 1 h; after that, lower amount of water was adsorbed and reached a plateau indicating that they became equilibrated. This result was higher than several reports [6-7]. Aloe vera and acacia gum hydrogel sponge were achieved a degree of swelling about 3,000% and 4,700%, respectively [6-7]. High degree of swelling of BSM hydrogel sponge could be due to hydrophilicity of –COOH group of uronic acid in BSM molecules. In addition, there was significant difference between the degree of swelling of hydrogel sponges made from different glycerol contents. The degree of swelling increased significantly with an increase in glycerol content. This could be due to the plasticizing effect of glycerol. The glycerol diminished interactions between BSM molecules and a consequent increase of free volume and segmental motions, allowing water molecules to diffuse more easily and giving higher degree of swelling which suitable for hydrogel applications.

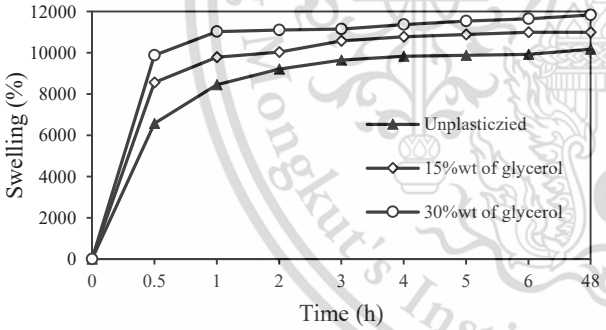

Figure 3 Degree of swelling of unplasticized and plasticized BSM hydrogel sponges.

3.5 Thermogravimetric analysis

DTG thermograms of unplasticized and plasticized BSM hydrogel sponges are shown in Figure 4. DTG analysis showed three thermal degradation steps for unplasticized BSM hydrogel sponge. The first step was related to an initial weight loss due to moisture vaporization between 35- 100˚C. The main degradation step at 255-340˚C was due to thermal degradation of BSM. The third step at 410-460˚C was due to continuous decomposition of BSM. These results corresponded to the results reported by Khazaei N. *et al*. who reported thermal degradation temperature of BSM casted film [4]. For BSM hydrogel sponges plasticized with 15%w/w of glycerol, the additional degradation step at 120-210˚C was observed. This step was caused by the thermal decomposition of glycerol in BSM hydrogel sponge.

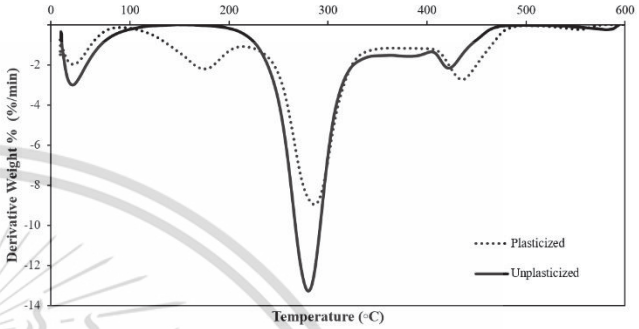

Figure 4. DTG thermograms of unplasticized and plasticized BSM hydrogel sponges

It should be mentioned that BSM hydrogel sponges plasticized with glycerol showed higher degradation temperature than unplasticized BSM hydrogel sponge. This should be due to the presence of hydrogen bonding between glycerol and BSM as confirmed by the shift of IR wavenumber (Figure 1).

4. Conclusion

BSM hydrogel sponges were successfully prepared by freeze-drying technique. For the results, FTIR spectra showed new hydrogen bond formation between BSM and glycerol, as a result from IR shift. SEM image presented interconnecting open-cell structure of pores in unplasticized BSM hydrogel sponge. BSM hydrogel sponges plasticized with glycerol revealed tight network structure and narrow transport pores with the increase of glycerol content. Moreover, the increment of glycerol content resulted in the decrease of thickness and the increase of hardness, caused by the plasticizing effect of glycerol. Furthermore, degree of swelling substantially increased with increasing in glycerol content. For thermal

analysis, BSM hydrogel sponges plasticized with glycerol represented the improved decomposition temperatures, compared with unplasticized BSM hydrogel sponge.

Acknowledgment

This work was financially supported by KMITL Research Fund, King Mongkut's Institute of Technology Ladkrabang.

References

[1] Ceresana Consulting; Worldwide consumption of biodegradable plastics from 2000-2008

[2] Dick, M., Costa, T. M. and Gomaa, A., "Edible film production from chia seed mucilage: Effect of glycerol concentration on its physicochemical and mechanical properties", Carbohydrate Polymers : 198-205 (2015).

[3] Tabashi, A. J. and Razavi, S. M., "Functional properties and applications of basil seed gum: An overview", Food Hydrocolloids : 313-325 (2017)

[4] Khazaei, N., Jouki, M. and Esmaiili, M., "Characterization of new biodegradable edible film made from basil seed (Ocimum basilicum L.) gum", Carbohydrate Polymers : 199-206 (2014).

[5] Kurd, F., Fathi, M. and Shekarchizadeh, H., "Basil seed mucilage as a new source for electrospinning: Production and physicochemical characterization", International Journal of Biological Macromolecules : 689-695 (2017)

[6] Silva, S., Oliveira, M. and Mano, J., "Bio-inspired Aloe vera sponges for biomedical applications", Carbohydrate Polymers : 264-270 (2014)

[7] Singh, B., Sharma, S. and Dhiman, A., "Acacia gum polysaccharide based hydrogel wound dressings: Synthesis, characterization, drug delivery and biomedical properties", Carbohydrate Polymers: 294-303 (2017)

The 7th International TIChE Conference (ITIChE 2017)
"Innovative Chemical Engineering and Technology toward Sustainable Future"
Shangri-La Hotel, Bangkok, Thailand, October 18-20, 2017

PREPARATION AND PROPERTIES OF BIODEGRADABLE MUNG BEAN STARCH- MUNG BEAN PROTEIN BLENDED FILMS

Siriporn Tantiwatcharothai[1], Jutarat Prachayawarakorn[1,2*]
[1]*Department of Chemistry, Faculty of Science, King Mongkut's Institute of Technology Ladkrabang, Bangkok 10520*
[2]*Advanced Materials Research Unit, Faculty of Science, King Mongkut's Institute of Technology Ladkrabang, Bangkok 10520*
**E-mail: jutarat.si@kmitl.ac.th*

Abstract: Mung bean is one interesting source for biodegradable film production since it is generally available in the market and mung bean protein is a by-product, obtained from glass noodle. Due to low tensile strength and high water uptake of mung bean protein film, mung bean starch (MS) - mung bean protein (MP) blended films were produced. Different MS- MP blended films were prepared by casting of 8% (w/v) film forming solution with various MS: MP weight ratio (%), i.e. 0:100, 25:75, 50:50, 75:25 and 100:0. Glycerol (30%w/w of total solid) was used as a plasticizer. It was found that FTIR spectra showed good compatibility between both polymer components. Furthermore, the increase of MS content of the blended films clearly resulted in the significant increase in tensile strength and Young's modulus of the blended films. Moreover, the increase of MS content caused in the decrease in water uptake due to more hydrophobicity of MS component.

Keywords: biodegradable film, mung bean protein, mung bean starch, properties

INTRODUCTION

There is a growing interest to develop new biodegradable materials based on renewable and natural polymers such as protein and starch [1]. There are many types of protein which can be used for biodegradable films such as collagen, gelatin, soy protein, wheat gluten and mung bean protein. Mung bean protein is a by-product from glass noodle or transparent bean vermicelli manufacture. Few information on mung bean protein film preparation and physicochemical properties has been reported. Although protein films show good gas barrier properties, they tend to have high water uptake and low mechanical properties [2]. One interesting method to improve properties of mung bean protein films is to combine with mung bean starch. Mung bean starch has been extensively used to produce edible films as it exhibits appropriate physical characteristics. It is odorless, tasteless, colorless, impermeable to oxygen and has high amylose content. Mung bean starch film had good tensile properties and heat sealability comparable to polyolefins [3]. From literatures, soybean protein concentrate and cassava starch blended films have been studied properties at low content of protein (0-30%wt). The results showed that high cassava starch content resulted in the improvement of tensile properties of the films [4]. Furthermore, peanut protein isolate and pea starch have also been used to prepare blended film at low content of protein (0-50%wt). The results showed that pea starch could improve tensile strength of films which in accordance with the results of soybean protein concentrate and cassava starch blended films [5].

The aim of this study was to improve properties of mung bean protein (MP) films by incorporation with mung bean starch (MS). In this research, the effect of MS contents at various ratios of MS: MP, i.e. 0:100, 25:75, 50:50, 75:25 and 100:0, on properties of MS- MP blended film was investigated.

EXPERIMENTAL

MS-MP blended film was prepared by casting of 8 % (w/v) film forming solution with various MS: MP weight ratio (%) 0:100, 25:75, 50:50, 75:25 and 100:0. The mixture of MS and MP was prepared by following steps. Firstly, MP solution was prepared by dissolving MP powder in distilled water, then pH was adjusted to 8.0 with 1 N sodium hydroxide solution with continuous stirring at room temperature for 4 hours. The MP solution was centrifuged at 4000 rpm for 3 minutes to remove undissolved protein and impurities. Then, MS powder was added at various

weight ratios. Glycerol was used as a plasticizer at 30%wt of total solid content. After that, the solution was stirred at 80°C for 20 minutes. Finally, the mixture was casted onto a plate and dried at 55°C for 48 hours.

FOURIER-TRANSFORM INFRARED SPECTROSCOPY (FT-IR)

Functional groups of a sample was analyzed by using Fourier-transform infrared spectroscopy (FTIR), Perkin Elmer Model Spectrum GX. Films were tested by the transmission method in the range of 4000-600 cm^{-1}.

MECHANICAL PROPERTY TESTING

A film was cut into rectangular piece of 15 mm × 100 mm to test tensile properties. The tensile testing was carried out using Universal Testing Machine (LLOYD Instrument, LR 5K, UK) with 100 N load cell and at a crosshead speed of 50 mm/min according to ASTM D-882. The sample was conditioned at the room temperature and relative humidity of 60±5% before testing.

WATER UPTAKE

For water uptake, a sample was dried at 105°C for 2 hours and then weighted. After that, it was stored at 100% relative humidity (RH) in room temperature and weighted every day until the constant weight was reached. The water uptake (M_t) was calculated as follows:

$$M_t(\%) = \frac{(W_W - W_d)}{W_d} \times 100 \qquad (1)$$

where Mt was the percentage of water uptake, W_d and W_w were the weights of the film before and after stored at 100% RH, respectively.

RESULTS AND DISCUSSION

FUNCTIONAL GROUP ANALYSIS

Figure 1 shows FT-IR spectra of MS- MP blended films at various weight ratios. For protein film spectra (Figure 1(a)), the characteristic peak around 3390 cm^{-1} was found. The peak is indicative of N-H stretching. A peak at 1646 cm^{-1} was caused by C-O stretching of amide I functional group in protein component. A peak at 1524 cm^{-1}, attributed to N-H bending of amide II and 1400 cm^{-1}, was caused by a carboxylic group in protein structure. A peak at 1238 cm^{-1} was C-N stretching of amide III in protein component [6]. The characteristic absorption peaks observed for MS were shown in Figure 1(e): the main peak around 3400-3000 cm^{-1} (broad band) was attributed to the complex vibrational stretching associated with free, inter- and intra-molecular hydroxyl groups. The band at 2924 cm^{-1} was arisen from the characteristic of C–H stretching. The peak at 1638 cm^{-1} was caused by stretching of O-H group in starch molecules. The peaks at 1155 cm^{-1} and 1019 cm^{-1} were attributed to C-O-H bending and C-O-C stretching of starch molecule, respectively [7].

When MS was added to MP (Figures 1(b)-1(d)), a shift of the broad absorption band due to the shift of O-H vibration from 3427 to 3391 cm^{-1} was found, indicating that the hydrogen bonding occurred between protein chain and hydroxyl group of starch [6]. In addition, different MS- MP blended films spectra showed a shift of absorption band from 1646-1652 cm^{-1} for amide I band, compared with MP film (Figure 1(a)). This result pointed out that the main interaction between MP and MS in blended films would be through the formation of hydrogen bonds as suggested by L.E. Abugoch and E. Tapia who studied the physicochemical characteristic of quinoa protein and chitosan blended films [8].

MECHANICAL PROPERTIES

Mechanical properties of MS- MP blended films with various weight ratios are shown in Table 1. It was found that the increase of MS content in the blended films resulted in a significant increase of tensile strength. The tensile strength value of various MP- MS blended films are in the range of 2.4 to 8.7 MPa. Moreover, the increase in MS content led to the considerable increase in Young's modulus from 24.4 to 254.6 MPa. Thus, the presence of MS in the MS-MP blended films yielded an increase in tensile strength and Young's modulus. As a result, the increase of MS content in the blended films caused the decrease in elongation at break from 108.1 to 58.4%. This is the result

of higher crystallinity of MS than MP duo to high amylose content of MS [3]. The linear structure of the amylose encourages interchain hydrogen bonding in starch stucture. Futhermore, closer proximity of the starch chains with high amylose content promotes the formation of cohesive force in the starch film [3]. On the other hand, protein structure in MP is in random coil conformation which result in low crystallinity [9]. Consequently, MS-MP blended films are denser and stronger than MP films.

On the other hand, increasing MP contents affected the decrease of tensile strength but the increase of elongation at break. The change in elongation at break of the blended films suggests plasticizing effect by MP in the blended films. The result of tensile strength, Young' s modulus and elongation at break of the MS- MP blended films also suggest that MP would act as a plasticizer of starch network. A similar effect was also observed for other biopolymeric films such as pea starch and peanut protein [5]. It was reported that additional of peanut protein isolate decreased the tensile strength and increase elongation at break of pea starch film. These might be attributed by the interaction between swollen pea starch granules and pea protein isolate, which led to the formation of flexible network [5]. In this case, MP may act as two functions; (1) MP contains lots of amino acid residues which can form hydrogen bond and interact with water. The water can act as a plasticizer for starch network, (2) protein molecule is capable of forming hydrogen bonds; thus, interacting with starch molecule by interrupting starch-starch bonding and resulting the further distance between polymer chains.

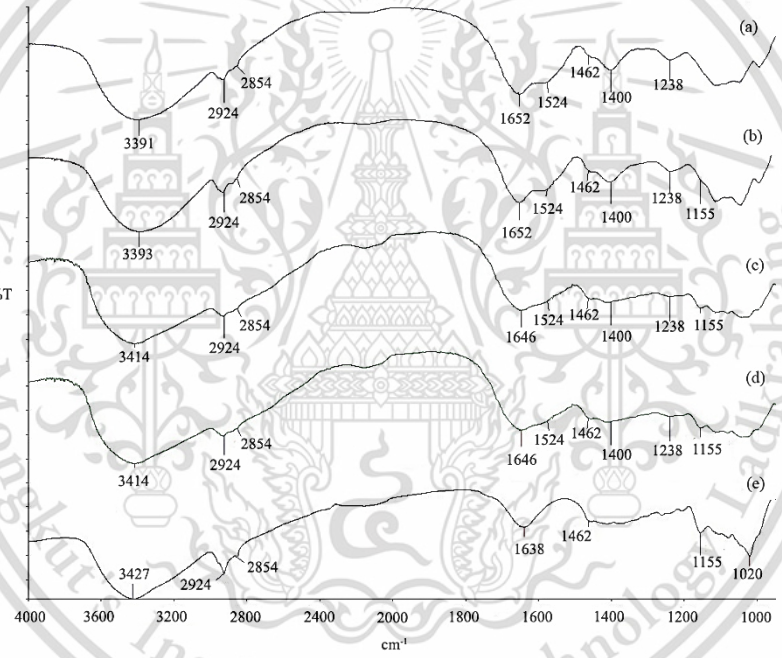

Figure 1. FT-IR spectra of MS- MP blended film at various ratio of MS:MP (a) 0:100 (b) 25:75 (c) 50:50 (d) 75:25 and (e) 100:0

Table 1. Tensile strength, Young's modulus and elongation at break, of MS- MP blended film with various ratio of MS: MP

Sample MS: MP	Tensile strength (MPa)	Young's modulus (MPa)	Elongation at break (%)
0:100	N/A*	N/A*	N/A*
25:75	2.4 ± 0.37	24.4 ± 7.13	108.1 ± 10.63
50:50	4.2 ± 0.75	126.6 ± 18.24	92.4 ± 5.25
75:25	8.7 ± 1.04	176.4 ± 27.71	88.0 ± 3.13
100:0	13.9 ± 1.82	254.6 ± 32.04	58.4 ± 10.21

*The film cound not be prepared.

WATER UPTAKE

From Figure 2, it was found that increasing MS contents caused the decrease of water uptake of different MS-MP blended films. This may due to higher cystallinity of MS than MP resulted in lower free volume in MS structure to retain water molecules. In addition, MS molecules show more hydrophobicity than MP molecules. More hydrophilic character of protein molucules in MP such as OH, COOH and NH_3 or amide group can, therefore interact with large amounts of water to retain more water molecules compare with starch molecules [5]. As shown in Figure 2, the water uptake of different MS-MP blended films were lower than MP film (0:100).

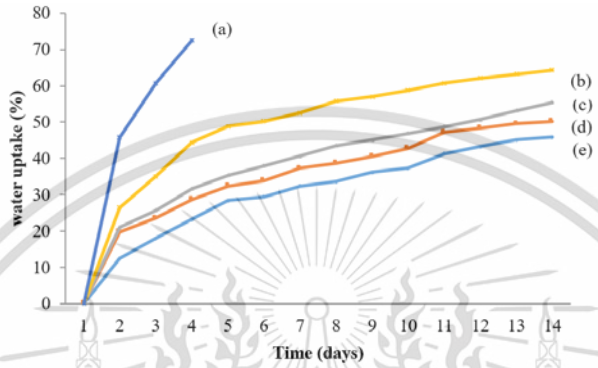

Figure 2. Water uptake of MS- MP blended film at various ratio of MS:MP (a) 0:100 (b) 25:75 (c) 50:50 (d) 75:25 and (e) 100:0

CONCLUSIONS

Mung bean protein-starch blended films were successfully prepared by casting solution of MP and MS. FTIR spectra showed good compatibility between both MP and MS polymers. The main interaction was hydrogen bond between MP chain and hydroxyl group of MS. The addition of MS into MS- MP blended films could significantly increase tensile strength and modulus of the blended films and decrease elongation at break of the blended films. In addition, the increase in MS proportion resulted in the decrease in water uptake of the blended films.

ACKNOWLEDGEMENT

The authors express their sincere appreciation to KMITL Research Fund for supporting the study financially.

REFERENCES

[1] X. Ma, P. R. Chang and J. Yu, Carbohydr Polym., 72 (2008) 369.
[2] T. Bourtoom, Inter Food Res J., 15 (2008), 167.
[3] O. Rompothi, P. Pradipasena, K. Tananuwong and A. Somwangthanoroj, Carbohydr Polym., 157 (2017) 748.
[4] C. E. Chinma, C. C. Ariahu and J. O. Abu, Food Sci Tech., 47 (2012) 383.
[5] R.E. Cian, P.R. Salgado, S.R. Drago, R.J. Gonzalez and A.N. Mauri, Food Chem., 146 (2014) 6.
[6] A. Gonzalez and A. Igarzabal, Food Hydrocoll., 33 (2013) 289.
[7] S. Somboonsub and S. Thawornchinsombut, Food Sci Tech., 1 (2015) 62.
[8] L.E. Abugoch and E. Tapia, Food Hydrocoll., 25 (2011) 879.
[9] T. Bourtoom, Inter Food Res J., 16 (2009), 1

Author Biography

Name	Miss. Siriporn Tantiwatcharothai
Date of Birth	25 January 1989
Address	94/688 Suwintawong road, Lamphukchee, Nongjok, Bangkok 10530
Education	(2010) Bachelor of science in Petrochemical technology, King Mongkut's Institute of Technology Ladkrabang) (2014) Master of science in polymer technology, King Mongkut's Institute of Technology Ladkrabang

Academic Publications

1. S.Tantiwatcharothai and J.Prachayawarakorn. 2017. “Preparation and properties of biodegradable mung bean starch-mung bean protein blended films.” 382-385. in the inietnational Thai institute of chemical engineering and applied chemistry conference 2017 (ITiche 2017), Bangkok.
2. S.Tantiwatcharothai and J.Prachayawarakorn. 2018. “Effect of Glycerol Contents on Properties of Hydrogel Sponge from Basil Seed Mucilage.” 100-104 in International Polymer Conference of Thailand 2018 (PCT-8). Bangkok.
3. S.Tantiwatcharothai and J.Prachayawarakorn. 2019, “Characterization of an antibacterial wound dressing from basil seed *(Ocimum basilicum L.)* mucilage-ZnO nanocomposite.” International journal of biological macromolecules. 135:133-140
4. S.Tantiwatcharothai and J.Prachayawarakorn. 2019, “Property improvement of antibacterial wound dressing from basil seed (*O. basilicum L.*) mucilage- ZnO nanocomposite by borax crosslinking.” Carbohydrate polymer. 227:11536